Significance of light polarization in solar panels, *Ephoron virgo* mayflies and Viking navigation

Ph.D. Thesis

Dénes Száz

Doctoral School of Physics

Programme of Statistical Physics, Biological Physics and Physics of Quantum Systems

Physical Institute

Faculty of Natural Sciences

Eötvös University

Head of Doctoral School: Prof. Tamás Tél

Head of Doctoral Programme: Prof. Jenő Kürti

Supervisors: D.Sc. habil. Gábor Horváth, associate professor

Dr. habil. György Kriska, associate professor

Environmental Optics Laboratory

Department of Biological Physics

Physical Institute

Faculty of Natural Sciences

Eötvös University

Budapest, 2018

Table of contents

Introduction

Astronomical light pollution and ecological light pollution has been known and studied for a long time, but the concept of polarized light pollution was introduced less than a decade ago (Horváth et al. 2009). Dark and shiny artificial surfaces (e.g. solar panels) can reflect highly and horizontally polarized light which deceive water-seeking polarotactic aquatic insects. These insects land and oviposit on these polarizing surfaces, which causes maladaptive behaviour of the concerned species and can leads to the failure of their reproduction. One way to reduce the degree of polarization of the surfaces is to make them matte, but this is not always enough to reduce the polarized light pollution. In Chapter 1, I show the measurements of the polarized light pollution of matte solar panels in two field experiments performed with polarotactic tabanids, mayflies and non-biting midges.

Closely related to polarized light pollution is the formation a complex ecological trap, where the effect of a strongly polarizing surface and high intensity illumination strengthen each other. In Chapter 2, I describe the complex ecological trap formed at illuminated bridges affecting the compensatory flight of the night-swarming mayfly, *Ephoron virgo*. I show that *Ephoron virgo* is polarotactic, that is strongly attracted to horizontally polarized light and normally detects water by means of the horizontally polarized light reflected from the water surface. This species also has phototaxis, thus the dual trap formed at the bridge attracts and keeps the individuals above the bridge surface, where they oviposit instead of the water, which is lethal for them and their laid eggs. Based on our observations and measurements, I introduce a method, with which *Ephoron virgo* mayflies can be prevented from flying up to the bridge-lamps and can be kept above the water surface, so that they oviposit into the water, thus the offspring generation can be saved.

Some animals use polarization in nature to detect water bodies, while others perceive the polarization patterns of the sky to orient themselves. These animals recognise the very typical direction pattern of skylight polarization that refers to the location of the Sun, even when it is covered by clouds or fog. According to the famous hypothesis of Ramskou (1967), the ancient Vikings used a very similar method to navigate on the open ocean. With birefringent or dichroic crystals, called sunstones, they measured the polarization of sky, based on which they could locate the Sun's position when it was hidden behind clouds or fog. Archeological findings suggest that in clear weather they used a sun-compass, with which they measured the geographical North. With the help of sunstones, the sun-compass could be

used even when the Sun was not visible, but the degree of polarization of the sky high enough to detect intensity changes of the light transmitted through the crystals. This hypothesis has been accepted and cited for decades without knowing its actual accuracy in different weather situations. Chapter 3 focuses on studying the accuracy of the sky-polarimetric Viking navigation. I show the measurements of the error functions of the individual steps of this method in psychophysical experiments and then, the determination of the resulting net North error in an error propagation process for 1080 weather situations, 3 sunstone crystals (calcite, cordierite, tourmaline), 2 specific dates (spring equinox and summer solstice). Then, I analyze, which situations are the best and worst for navigation.

The chapters of my thesis are based on the following publications:

Chapter 1:

Száz D, Mihályi D, Farkas A, Egri Á, Barta A, Kriska Gy, Robertson B, Horváth G. 2016. Polarized light pollution of matte solar panels: Anti-reflective photovoltaics reduce polarized light pollution but benefit only some aquatic insects. *Journal of Insect Conservation* 20 (4): 663-675 (doi: 10.1007/s10841-016-9897-3)

Chapter 2:

Száz D, Horváth G, Barta A, Robertson B, Farkas A, Egri Á, Tarjányi N, Rácz G, Kriska Gy. 2015. Lamp-lit bridges as dual light-traps for the night-swarming mayfly, Ephoron virgo: Interaction of polarized and unpolarized light pollution. *Public Library of Science ONE* 10 (3): e0121194 (doi: 10.1371/journal.pone.0121194)

Chapter 3:

Száz D, Farkas A, Blahó M, Barta A, Egri Á, Kretzer B, Hegedüs T, Jäger Z, Horváth G. 2016. Adjustment errors of sunstones in the first step of sky-polarimetric Viking navigation: Studies with dichroic cordierite/tourmaline and birefringent calcite crystals. *Royal Society Open Science* 3: 150406 (doi: 10.1098/rsos.150406)

Száz D, Farkas A, Barta A, Kretzer B, Egri Á, Horváth G. 2016. North error estimation based on solar elevation errors in the third step of sky-polarimetric Viking navigation. *Proceedings of the Royal Society A* 472: 20160171 (pp. 1-15, doi: 10.1098/rspa.2016.0171)

Száz D, Farkas A, Barta A, Kretzer B, Blahó M, Egri Á, Szabó Gy, Horváth G. 2017. Accuracy of the hypothetical sky-polarimetric Viking navigation versus sky conditions: revealing solar elevations and cloudinesses favourable for this navigation method. *Proceedings of the Royal Society A* 473: 20170358 (18 pages, doi: 10.1098/rspa.2017.0358)

Chapter 1.

Polarized Light Pollution of Matte Solar Panels

1.1. Introduction

1.1.1. Polarized light pollution

The term of light pollution may sound familiar to many people and can be categorized according to different fields of application. By astronomical light pollution we mean the phenomenon when the city light sources hinder the astronomical observations. That is the reason, why most of the observatories are built in scarcely populated areas, like mountain tops. Ecological light pollution refers to all kinds of photopollution that disrupt the natural patterns of light and dark experienced by organisms in ecosystems (Longcore and Rich 2004). The most well-known forms of ecological light pollution include direct glare like the night traffic lights of cities, temporary, unexpected fluctuations of light emitted from illuminated structures (e.g. buildings, towers, bridges) and vehicles. These light sources can attract or repulse living organisms in nature, inducing a maladaptive migration behaviour, distracting them from their natural habitats. According to Longcore and Rich (2004), animals around the ecologically photopolluting light sources tend to select inferior nest sites or mates, collide with artificial structures, the predator-prey relationship can be disrupted, and foraging times are reduced. All of these altered behavioral patterns can change the community structure. This reflex-based migration behaviour (called phototaxis) is elicited by the intensity and/or colour of the light sources which has been considered as the major visual phenomenon underlying ecological light pollution.

In the last decades it has become clear, that other cues of light can affect the behaviour of animals. Many animal species are able to perceive the linear polarization of light and use it for various purposes like orientation, looking for habitat to mate and oviposit or finding host animals for blood sucking (von Frisch 1967; Lythgoe and Hemmings 1967; Schwind 1985, 1991, 1995; Danthanarayana and Dashper 1986; Shashar et al. 1998; Wildermuth 1998; Marshall et al. 1999; Novales Flamarique and Browman 2001; Wehner 2001; Labhart and Meyer 2002; Dacke et al. 2003; Horváth and Varjú 2004; Waterman 2006; Wehner and Labhart 2006; Henze and Labhart 2007; Kriska et al. 2009; Horváth et al. 2011b;

Egri et al. 2012a; Bernáth et al. 2012; Boda et al. 2014). Horváth et al. (2009) have shown that the highly and horizontally polarized light reflected from artificial surfaces can disrupt the natural patterns of polarized light experienced by organisms in nature that alters the behaviour of polarization-sensitive animals eliciting similar behavioural patterns to the ecological light pollution. The phenomenon is an alternative form of ecological light pollution, called polarized light pollution. The reflex-based migration elicited by polarized light in animals is called polarotaxis.

1.1.2. Natural and artificial sources of polarized light

Light coming from natural light sources, like the Sun, is unpolarized. It consists of electromagnetic waves vibrating at all possible planes perpendicular to the direction of propagation. We talk about totally linearly polarized light when the electromagnetic waves oscillate only in a single plane. In most cases, polarized light in our environment is partially linearly polarized that can be characterized by the following parameters: intensity I, degree of linear polarization d and angle of polarization α, meaning the direction of the oscillation of the electric field vector with respect to a reference direction. The mathematics of light polarization and the method of its measurement is described in detail by Horváth and Varjú (2004).

Polarized or partially polarized light can arise from two primary sources in our natural environment. These are (1) the scattering of sunlight and moonlight within the atmosphere and hydrosphere and (2) the reflection of light from the surface of water bodies and other non-metallic surfaces (rocks, soil, vegetation, etc.). Water is the primary natural source of horizontal polarization by reflection, however, its depth, turbidity, transparency, composition and illumination can influence the reflection-polarization characteristics of its surface (Horváth and Varjú 2004).

Reflections from artificial objects can also cause the polarization of reflected light. The extent to which an object polarizes light depends on the angle of reflection and the material of the surface. The darker and smoother (shinier) the surface is, the higher degree of linear polarization d it can produce (Umow 1905). From rough surfaces the reflection is usually diffuse, resulting in depolarization (d decreases), because the reflected electromagnetic waves vibrate in many planes. The net d originating from an object is determined by the relative intensities of (i) the light reflected from the object's surface and (ii) the light scattered back from the object's material and refracted at its surface. The two

components are polarized parallel and perpendicular to the surface of the object, respectively. Therefore, they have a mutual depolarizing effect to each other. Thus, in the case of darker and smoother objects the first component has higher intensity, while the intensity of the second component is lower in the specific part of the spectrum that the polarization-sensitive animals perceive, consequently these surfaces have higher *d* and stronger effect on polarization-sensitive organisms (a stronger polarized light polluting effect). In the case of objects with lighter and rougher surface, the phenomenon and the effect is the opposite. This phenomenon is called the Umow effect (Können 1985).

1.1.3. Effects of polarized light pollution on animals and ecosystems

One of the most well-known effects of polarized light pollution is the alteration of animals' habitat-selecting and ovipositing behaviour. The horizontally polarized light reflected from water bodies is a guidance mechanism to find nesting, mating and oviposition sites, used by at least 300 species of dragonflies, mayflies, caddisflies, tabanid flies, diving beetles, water bugs, and other aquatic insects (Schwind 1991; Horváth and Kriska 2008). Dark and shiny artificial objects (e.g. asphalt roads, dark gravestones, cars, plastic sheetings, oil lakes, glass windows) can reflect strongly and horizontally polarized light that can deceive water-seeking polarotactic animals by mistakenly detecting them as water bodies (Horváth and Zeil 1996; Kriska et al. 1998, 2006a, 2007, 2008; Horváth et al. 2007, 2008). In some cases the *d* of light reflected from these surfaces is even higher than that of natural waters' that acts as a supernormal optical stimulus eliciting a stronger attraction to artificial surfaces than to water bodies (Horváth and Zeil 1996; Horváth et al. 1998; Kriska et al. 1998). The ecological consequences of such an abnormal behaviour can be very different and depend on the polarized-light-polluting source. In the case of dry surfaces, insects try to oviposit on the surface where the eggs dry out and perish. When the surface is heated by sunlight, the attracted insects can dry out and die, as well (Bernáth et al. 2001a; Kriska et al. 2007). Oil spills and pools are detected as 'superwaters' by water-seeking insects and lure large amounts of polarotactic animals. However, interactions with the sticky oil surface often have a mortal result, since animals get stuck in the oil and cannot escape. Large numbers of dragonflies, mayflies, caddisflies, water bugs, and water beetles can be trapped by waste oil pools and oil spills in spring, summer and autumn, during their annual swarming and migration. Certain waterbirds are also attracted to oil lakes either by mistakenly detected as water by polarization vision or attracted by the numerous died insects, meaning ideal sites for foraging

(Horváth and Zeil 1996; Bernáth et al. 2001b). Emerging *Hydropsyche pellucidula* caddisflies are attracted to the vertical glass surfaces of buildings on river banks as a result of their strong polarization signature (Kriska et al. 2008; Malik et al. 2008). Based on the observation that they copulate and remain attracted to the glass panes for hours, a new theory assumes that vertical glass buildings can serve as swarming markers, giving a well-visible linearly polarized signal to caddisflies.

Certain predators (cephalopods, trout, longfin squid and other aquatic predators) can also benefit from polarization sensitivity while looking for prey. Underwater, both the degree d and angle α of polarization of scattered light depend on the position of the Sun or the Moon. When scattered light transmits a transparent prey animal (e.g. jellyfish, ctenophores), its polarization characteristics are altered, increasing the visual contrast of the prey relative to its background (Lythgoe and Hemmings 1967; Shashar et al. 1998). As a result, transparent animal bodies repolarize transmitted, reflected or refracted light, increasing the prey-detecting success of polarization-sensitive predators. Plankton feeders are adept at detecting zooplankton in the water column that would otherwise be transparent (Shashar et al. 1998; Marshall et al. 1999; Novales Flamarque and Browman 2001). When these predators are deceived by the polarization signature of garbage, plastic bottles, plastic bags in the water, their foraging success is reduced and the energy resource of these animals may be depleted in such a way that can cause the death of the predator.

Polarized light pollution can also have an indirect secondary effect on the predation and foraging behaviour. The predators of insects trapped near artificial polarizing objects are lured to the site by the large amount of available food. Wagtails (*Motacilla alba* and *M. flava*) often hunt polarotactic insects attracted to dry asphalt roads and highly polarizing black plastic sheets laid on the ground, which function like a huge bird feeder (Kriska et al. 1998; Bernáth et al. 2008). Caddisflies attracted to vertical glass surfaces lure various predators, including birds, such as European magpies (*Pica pica*), white wagtails (*M. alba*), house sparrows (*Passer domesticus*), and great tits (*Parus major*). These predators systematically hunt and catch the caddisflies that have landed on glass panes or are swarming near windows. Spiders are also attracted in large numbers to feed on these caddisflies.

A more complex food chain has been observed by Bernáth et al. (2001b) at an open-air waste oil reservoir in Budapest, Hungary. The strongly and horizontally polarizing black surface of the oil attracted large numbers of polarotactic aquatic insects. These insects lured various insectivorous birds and bats, which then got stuck in the sticky oil where they died. The carcasses of these birds and bats in turn attracted other carnivorous birds (e.g. owls,

kestrels, hawks), which may also become trapped in the oil. In both the less lethal and more serious cases, the polarizing objects changed the predation behaviour of these animals that is a secondary effect of polarized light pollution.

1.1.4. Navigation and orientation

Numerous animal species navigate with the help of the polarization signature of skylight or light reflected from open water surface in order to find feeding, mating or ovipositing habitats (detailed review in Horváth and Varjú 2004). Certain insect species (e.g. bees, crickets, desert ants) use the skylight polarization as a cue for orientation, however, they can still be trapped by artificial point sources of polarized light (Kovarov and Monchadskiy 1963; Danthanarayana and Dashper 1986). The maximal degree of polarization of skylight, depending on the daytime and cloudiness, is ranging from 15-75 % (Coulson 1988), so highly polarizing artificial objects reflecting horizontally polarized light can act as supernormal stimulus towards which animals are attracted (Horváth and Pomozi 1997). Since the threshold of polarization perception in some species is relatively low (in field crickets, *Gryllus campestris*, 5-7 %, Henze and Labhart 2007) for navigaton under cloudy skies, *d* of light reflected from artificial objects may produce signals as high as 80-95 % (Horváth and Varjú 2004), that easily deceive polarization-sensitive orienting animals.

1.1.5. Human benefit from polarized light pollution

Horse and cattle farmers often confront with the problem in summertime that the livestock is disturbed and bitten by blood-sucking female tabanid flies. These polarization-sensitive insects not only disturb the animals, but also can spread various diseases. Horváth et al. (2010b) observed that more tabanids are attracted to dark coloured horses than to white ones and contributed the effect to the polarized light reflected from dark horses, the *d* of which is much higher than that reflected from white ones. Field experiments with sticky model horses proved that black and brown horses attracted more tabanids than white ones in an extent of two order of magnitudes (Horváth et al. 2010b). A naturally occurring continuation of this experiment was to answer how attractive the black and white striped zebras are to tabanids. On the contrary of what one may think that the attraction of such a striped surface being the result of strongly and weakly polarizing effects may fall between the attraction of white and black horses, the zebra striped coating turned out to be even less attractive to tabanids than

white horse coats. In addition, the denser the striping is, the less attractive is the surface (Egri et al. 2012b). Based on these experiences, one (however not only) evolutionary benefit of zebra stripes is to effectively prevent zebras from being bitten by polarotactic blood-sucking insects. The striped, spotted or otherwise inhomogeneous fur or coating of other animals may also have this tabanid-repellent benefit. Young individuals of many species possess similar integument that raises the possibility of juvenile survival (Száz and Herczeg 2013).

Since various tabanid taxa do great harm to human livestock-breeding, the artificial reduction of the number of tabanids has been an issue for several decades. The first man-made tabanid traps were developed in the 1930s. The principal of their upbuilt was similar and based on the false hypothesis that size, shape, movement, colour and light intensity are the main cues for the attraction of tabanids to a target (Malaise 1937; Catts 1970; Muirhead–Thomson 1991; Moore et al. 1996). However, the majority of these traps were not effective enough. The first real effective traps were designed to use up the polarotactic behavior of tabanids, that is the water seeking by reflected horizontally polarized light. Then, after the discovery of a new kind of polarotaxis in host-seeking tabanids, governed only by the degree of polarization of the host animal, alternative tabanid trap constructions could be applied, for example a black tray filled with dark coloured water and cooking oil (Egri et al. 2012a). Since oil is less dense than water, it remains on its surface and at contact with the tabanids, they get stuck and captured. With traps based on the water-seeking polarotactic mechanism, only tabanids with the motivation of water-seeking can be captured and host-seeking females may avoid these traps.

One of the most widespread traps, the Manitoba or H-trap, consists of a round, black, shiny target object placed under a tent which is open from upwards with a container at the opening so that the tabanids are trapped and captured in the container. This trap, in turn, uses only the polarotactic host-seeking mechanism of tabanids, thus, water-seeking individuals avoid it. With the trap construction of Egri et al. (2013), consisting of a black horizontal and a black vertical surface covered with sticky plastic sheets, tabanids with both kinds of motivation could be captured. All the above examples are based on the polarized-light-polluting effect of polarized light reflected from different artificial objects which in these cases have benefits by helping humans to get rid of harmful horseflies.

1.1.6. Polarized light pollution of solar panels

Solar panels (photovoltaic cells and solar thermal collectors), that change the solar radiation to electric power or heat, are regarded as green technologies since they can be applied without carbon dioxide or other pollutant emission (Horváth and Kriska 2010). Note, however, that during the production of these devices, the amount of arising air-polluting material is not negligible (Boyle 2012). The efficiency of commercial solar panels is 17-18 %, but recently the maximum efficiency has reached 25 % under experimental circumstances (Paulescu et al. 2013). The theoretical maximum of efficiency is estimated up to 31 %. The actual efficiency greatly depends on proper positioning and orientation, and on the geology and climate of the application area (Foster et al. 2010; Tomar et al. 2013; Mihályi 2015). For the effective operation of solar panels, dark surfaces are required to absorb and utilize the most possible amount of sunlight. Amorphous silicon solar panels have a black shiny surface (Hough 2007) that are similarly polarized-light-polluting as waste oil lakes (Horváth and Zeil 1996), agricultural black plastic sheets or glass buildings (Kriska et al. 2008). Water-seeking insects tend to detect these surfaces as water where they oviposit and the laid eggs unavoidably dry out and perish. Horváth and Kriska (2010) and Horváth et al. (2014b) found in field experiments that polarotactic tabanids, mayflies and non-biting midges tend to land on solar panels onto which they oviposit, as well. In the case of protected species, solar panels can cause great ecological damages.

The effect of polarized light pollution of solar panels can be reduced if the panel surface is covered by a thin white grid as Horváth et al. (2010a) discovered by chance during a field experiment with polarotactic insects. In this study, thirty times less insects were attracted to black and shiny surfaces to which a white grid pattern was added than to homogeneous ones. The explanation of this phenomenon is that a flying water-seeking polarotactic insect perceives the white-gridded shiny black surface as a composition of individual small water surfaces due to the white grid, where the cell area is too small to oviposit into because the eggs would not develop properly. Mono- and polycrystalline solar panels include several individual solar cells that are separated by white metal lines, so a built-in white grid is formed due to this technology (Boxwell 2012).

Recently, a new efficiency-increasing production technique has appeared by covering the surface of solar panels with anti-reflective coating. This layer makes the surface matte and rough, rather than shiny and smooth. With a rough surface, superficial reflections can be reduced, thus more photons are absorbed making the energy production more effective. For

the production of the rough surface, the outer surface of the solar panel is covered with SiO_2 or TiO_2 nanotubes in several layers (Kang et al. 2009). The orientation of these nanotubes is disordered which helps to absorb up to 96 % of the incoming light (Kuo et al. 2008). Another technique is to itch small holes in a glass layer making the surface porous as applied by the Danish Sunarc company (http://sunarc.net). The solar panel is then covered by this matte, rough, porous glass. Besides the energetic benefits, as a byproduct, these rough surfaces reflect polarized light with lower degrees of polarization *d* than the shiny ones. Thus, this newly applied technique could be a solution for polarized light pollution of solar panels. To test this hypothesis, we performed field experiments using horizontal black papers covered either with an anti-reflective matte glass pane or a non-coated shiny glass pane, at two locations with polarotactic horseflies (Tabanidae), mayflies (Ephemeroptera) and non-biting midges (Chironomidea), to quantify the polarized light pollution by the number of attracted insects. These insects were selected because of their large abundance at our test sites, and their taxonomic diversity allowed us to study their taxon-dependent responses to anti-reflective coating. We also measured the reflection-polarization characteristics of the applied test surfaces. I present here the results of these field experiments, and answer the question whether matte solar panels are environmentally friendly with respect to polarized light pollution.

1.2. Materials and Methods

1.2.1. Test surfaces

For the field experiments, we created two kinds of test surfaces, shiny (smooth) black and matte (rough) black, that were exposed to flying aquatic insects. Each shiny surface was composed of two glass panes (smooth window glass, 400 mm x 400 mm x 3 mm) with a black cardboard underneath. This structure mimicked the optical properties of shiny (smooth) solar panels considering the polarization signature. The matte (rough) surfaces consisted of a glass pane with an anti-reflective porous upper and lower layer manufactured by the Danish company, Sunarc Technology for use in the solar industry (http://www.sunarc.net/index.php/ap-processing/argenerelt). In this solution, the anti-reflectiveness is secured by a random array of glass spheres interspersed with air bubbles (Fig. 1.1).

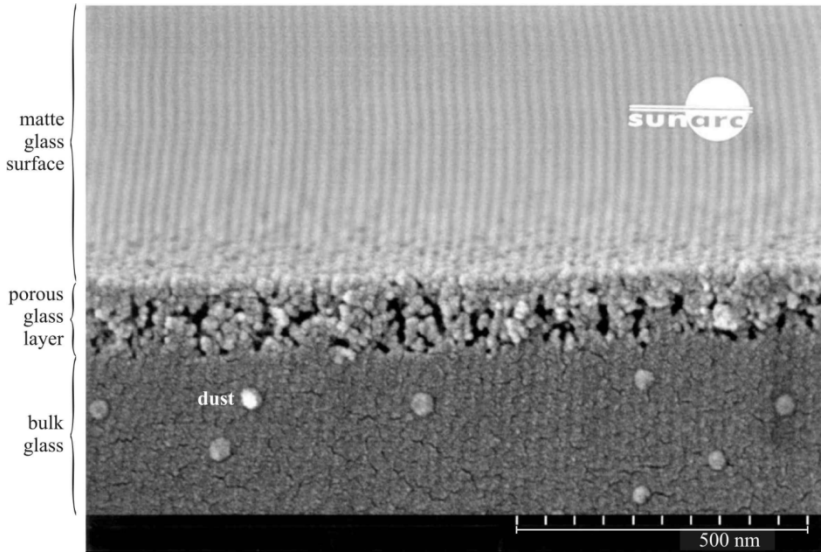

Figure 1.1: Scanning electron microscopic picture of the upper surface and the underlying substrate of the anti-reflective matte glass pane used in matte solar cells produced by the Danish Sunarc Ltd. and also used in our matte black test surface (photograph courtesy of Sunarc Ltd.). The pale approximately vertical lines in the picture are just scanning artefacts and bear no meaning. In the lowermost part of the picture, there are some spherical dust particles originating from the glass breakage and having no importance.

Under this pane a similar black cardboard was placed as in the case of the shiny one. The glass panes were held together with a 20 mm thick shiny, black wooden frame. A set of test surface consisted of a pair of the same quadratic (400 mm x 400 mm) shiny or matte black surface with the wooden frame that were placed on the ground next to each other, without a gap. The matte and shiny surface were placed in one row, along a straight line, 50 cm apart from each other. The positions of the surfaces were exchanged periodically in the field experiments to avoid site-specific bias.

1.2.2. Imaging polarimetry of the test surfaces

The indicator insect species (horseflies, mayflies and non-biting midges), occurred in our field experiments, have green-, blue- and UV-sensitive photoreceptors (Briscoe and Chittka 2001), however, we do not know in which spectral range they perceive polarization. Since polarization patterns depend on the illumination circumstances and the direction of view, we measured the reflection-polarization characteristics of our test surfaces for different viewing

directions from the solar median under various weather conditions (clear and cloudy skies). Flying insects could approach the test surfaces from any direction. The patterns of degree d and angle α of linear polarization were determined in the red (650 nm), green (550 nm), blue (450 nm) and UV (350 nm) spectral ranges. To perform the measurements, in the visible range, we used an imaging polarimeter, the hardware and software of which was described in detail by Horváth and Varjú (1997, 2004). In the UV range, we applied an UV-sensitive polarimeter composed of an UV-transmitting linearly polarizing filter (HNP'B), and an UV-transmitting lense (focal length = 60 mm, Jenoptik CoastalOpt UV-VIS-IR) and an UV-sensitive camera (Nikon D7100 UV mod). Both d and α of reflected light changed within the area of a given test surface caused by the alteration of the angle of reflection and the change of the optical variables of incoming sky- and sunlight. To quantify the polarizing ability of a given test surface, we computed the mean and standard deviation of d and α averaged through the surface area. From previous studies we know that polarotactic aquatic insects identify a surface as water body if the following conditions are fulfilled: (1) $d > d^*$ and (2) $|\alpha\text{-}90°| < \alpha^*$, where d^* and α^* are taxon-dependent thresholds. In these experiments, we used the following thresholds: $d^* = 15$ %, $\alpha^* = 10°$, that is typical for horseflies and mayflies (Kriska et al. 2009).

1.2.3. Experiment 1: horseflies

Previously, Horváth and Varjú (2004), Kriska et al. (2009), Blahó et al. (2013), Horváth (2014) and Herczeg et al. (2015) designed polarizing traps to capture tabanids touching the bait surface that was covered with an adhesive. Applying adhesive in this experiment was out of option, because (1) it would have changed the reflection-polarization characteristics of the surfaces by making them shiny and (2) with the application of adhesive, we could not have studied the motivation of arriving insects. Our main concern was to mimic the reflected optical cues of real solar panels.

The goal of this experiment was to test the relative attractiveness of the test surfaces on horseflies that were known to be more attracted to the more strongly polarizing sources (Horváth et al. 2008a; Krcmar 2013). The experiment was performed over 11 days between 5 July and 1 August 2014 under warm, sunny conditions and clear sky on a Hungarian horse farm in Szokolya (47° 52' N, 19° 00' E). The number of horseflies in this area is abundant, the following species occur: *Tabanus tergestinus, T. bromius, T. bovinus, T. autumnalis,*

Atylotus fulvus, A. loewianus, A. rusticus, Haematopota italica (Blahó et al. 2014; Herczeg et al. 2014).

The test surfaces were placed on the ground in a meadow, 50 cm apart from each other, 5 m far from a row of trees and bushes. Two observers sat 2 m far from the test surfaces to record the behaviour of the attracted insects. The experiment started in the morning and ended in the afternoon. The surfaces were exchanged every 30 minutes to eliminate site-specific bias. The time interval of the observation was adjusted to warm and sufficiently calm weather to avoid rapid temperature drops, since horseflies are active only in warm and calm weather.

The typical reactions, that horseflies usually perform near water bodies and host animals, were registered: (i) Aerial looping in any (horizontal, oblique or vertical) plane, during which the flying horsefly approached the test surface and performed at least 1 loop above it within a few decimeters; (ii) touch-down, during which the horsefly touched the test surface at least once and flew away within 3 seconds; (iii) landing, when a horsefly landed on the test surface and stayed on it for at least 3 seconds. Reactions (i) and (ii) are typical behaviours around water bodies while drinking or bathing, behaviour (iii) is usually performed while searching for suitable ovipositing site or blood source (Horváth et al. 2008a; Krcmar and Lajos 2011; Blahó et al. 2014).

The observers counted the reaction groups (the occurrence number a horsefly individual reacted to a given test surface with aerial looping, touching or landing, excluding repetitions by the same individual before flying away) and reaction items (the occurrence number a given reaction element - looping, touching, landing - was performed by a horsefly individual before it flew away, repetitions included). The advantage of recording reaction groups and reaction items parallel is that both variables are good measures of attractiveness: the former characterizes the frequency of the different behaviour types, while the latter gives their intensities. Former studies has shown that the numbers of reaction groups and items are positively correlated with abundance (Horváth et al. 2010a,b; Blahó et al. 2014; Herczeg et al. 2014, 2015).

1.2.4. Experiment 2: mayflies and non-biting midges

The above test surfaces were reapplied at a different location in the Hungarian Duna-Ipoly National Park at Dömörkapu (47°40’ N, 19°03’ E), where polarotactic mayflies and non-biting midges (chironomids) were abundant and were used as test species for Experiment 2,

which was conducted between 4 and 30 May 2015 on 8 warm days. An asphalt road, being a known polarized-light- polluting source (Kriska et al. 1998), was running in the immediate vicinity (within a few meters) of a mountain creek, from which several *Ephemeroptera* (Baetidae, Heptageniidae) and chironomid species emerged. These insects swarm above the road at dusk in every May and June (Kriska et al. 2009, Horváth et al. 2011b).

The previously applied matte and shiny black test surfaces were laid on the asphalt road in a straight line, parallel to the direction of the creek, 50 cm apart from each other. The experiment started each day at 19:00 h (GMT + 2 h) and ended 21:00 h. During the experiment the test surfaces were in the shade of the surrounding trees and bushes. Again, we altered the positions of the surfaces every 30 minutes to avoid site-specific bias in the number of attracted insects. Since these insects did not show such specific behaviour patterns as tabanids, we quantified the amount of attracted insects differently from Experiment 1. After each swap, a photograph was taken of both test surfaces with a digital camera in every 3 minutes to count the number of insects on or above them. The evaluation of the photos happened later in the laboratory with a self-written computer software, with which we counted the number of mayflies and chironomids in the pictures. We identified insects as belonging to order Ephemeroptera, families Baetidae and Heptageniidae and order Diptera, family Chironomidae exclusively. We did not find eggs lain on the test surfaces during the experiment. In previous field experiment with polarizing surfaces at the same site (Kriska et al. 1998, 2009; Horváth et al. 2010a, 2011; Blahó et al. 2014) the following species occurred: *Baetis rhodani*, *Epeorus sylvicola*, *Rhithrogena semicolorata* (mayflies), *Chironomus riparius*, *Micropsectra atrofasciata*, *M. notescens*, *Rheocricotopus atripes* (chironomids).

1.2.5. Statistical analysis

Since the distribution of our data was Poisson fashion rather than normal, we used non-parametric Mann-Whitney U test (Zar 2010) to compare differences between the attractiveness of matte (rough) and shiny (smooth) test surfaces to polarotactic insects (horseflies, mayflies and non-biting mindges) in our field experiments. We also applied Wilcoxon matched pair test and obtained the same results as for the non-parametric Mann-Whitney U test. Since the goal of our experiments was to examine the relative conservation benefit of anti-reflective solar panel coatings for polarotactic insects, we studied the consistent effect of this treatment over time and not a day-to-day variation of the responses that could be influenced by fine scale variations of environmental effects or ecological

conditions. The numbers of captures of two test surfaces of the same type (matte or shiny) were pooled, since they are not independent replicants. All statistical tests were performed with the statistical software package R and software Statistica 8.0 (Zar 2010).

1.3. Results

1.3.1. Reflection-polarization characteristics of test surfaces

In Fig. 1.2, polarization data of the applied test surfaces are visualized for all three (red, green, blue) parts of the visible spectrum. When the direction of measurement was facing the sun, the degree of polarization d of light reflected from the matte black test surface was about 10 % higher than that from the shiny one. The standard deviation of the angle of polarization α of light reflected from the matte black test surface was about twice as large as that from the shiny black test surface (Figs. 1.2, 1.3, 1.4, Table 1.1). In direct sunlight, the area of the test surfaces detected as water by polarotactic insects was much smaller for the matte black test surface than for the shiny one. This predicted, that the former was polarotactically less attractive to the examined insects.

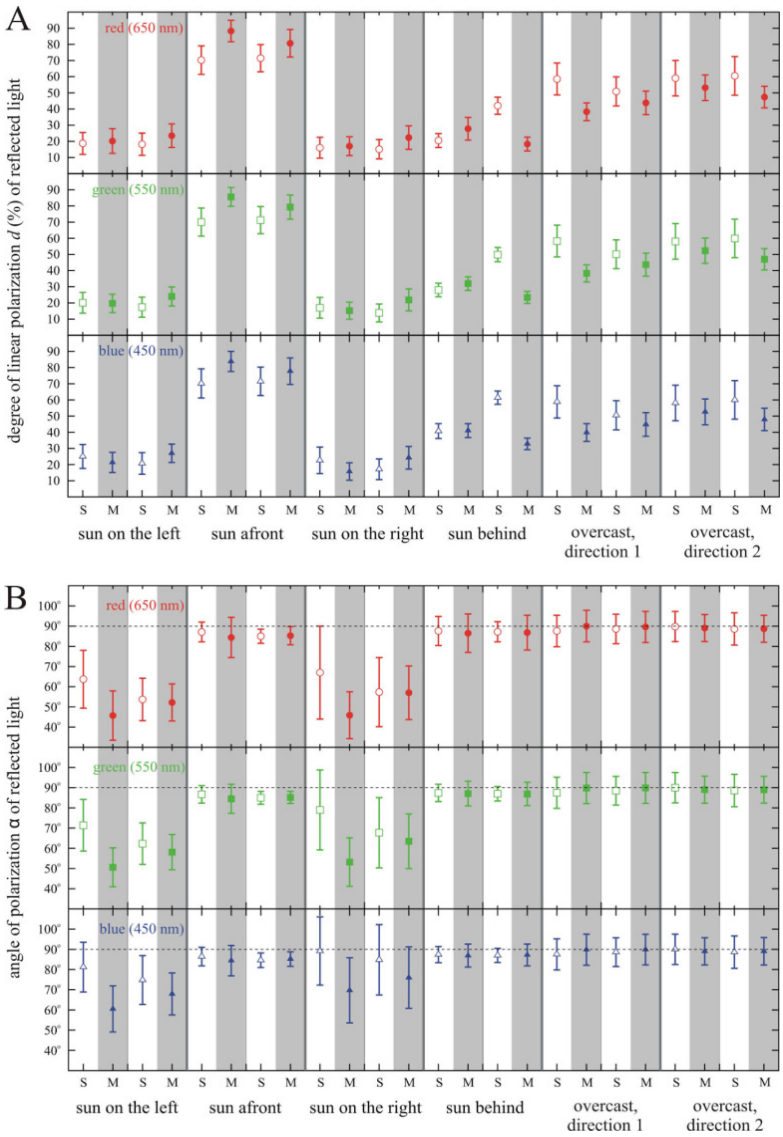

Figure 1.2: Means (dots, rectangles, triangles) and standard deviations (vertical I-shaped bars) of the degree of linear polarization d (%, A) and the angle of polarization α (°, B, measured clockwise from the vertical) of light reflected from the shiny (S, empty dots, rectangles and triangles, white columns) and matte (M, filled dots, rectangles and triangles, grey columns) horizontal black test surfaces used in our field experiments measured by imaging polarimetry in the red (650 nm), green (550 nm) and blue (450 nm) spectral ranges from different directions of view relative to the solar meridian (SM) under a clear and overcast sky. Sun on the left: the sun shone from the left, perpendicular to SM. Sun afront: the sun shone from afront. Sun on the right: the sun shone from the right, perpendicular to SM. Sun behind: the sun shone from behind. Direction 1: arbitrary relative to SM. Direction 2: perpendicular to direction 1. In B the horizontal dashed lines represent horizontal polarization (α = 90° from the vertical). The numerical values of the data displayed here are in Table 1.1.

illumination	shiny (smooth) test surface						matte (rough) test surface					
	d (%)			|α – 90°|			*d* (%)			|α – 90°|		
	R	G	B	R	G	B	R	G	B	R	G	B
sun on the left	18.7 ± 6.8	20.1 ± 6.4	25.9 ± 7.4	63.7 ± 14.3	71.4 ± 12.8	81.2 ± 12.3	20.2 ± 7.6	19.7 ± 5.7	21.3 ± 6.2	45.7 ± 12.2	50.6 ± 9.6	60.5 ± 11.4
sun on the left	18.2 ± 6.9	17.4 ± 6.2	20.7 ± 6.7	53.7 ± 10.5	62.3 ± 10.3	74.8 ± 12.1	23.5 ± 7.3	24.0 ± 5.9	27.0 ± 5.7	52.2 ± 9.2	58.1 ± 8.7	67.9 ± 10.4
sun afront	70.3 ± 8.8	70.0 ± 8.7	70.2 ± 9.0	87.1 ± 4.9	86.7 ± 4.3	86.4 ± 4.6	88.3 ± 6.6	85.6 ± 5.8	83.8 ± 6.2	84.4 ± 10.0	84.5 ± 7.2	84.4 ± 7.5
sun afront	71.5 ± 8.4	71.2 ± 8.4	71.5 ± 8.8	85.0 ± 3.5	85.0 ± 3.2	84.6 ± 3.6	80.7 ± 8.5	79.3 ± 7.5	77.8 ± 8.2	85.3 ± 4.5	85.2 ± 3.0	85.2 ± 3.6
sun on the right	16.0 ± 6.5	17.0 ± 6.4	22.6 ± 8.2	67.0 ± 23.0	79.0 ± 19.8	89.2 ± 16.9	17.0 ± 5.8	15.2 ± 5.3	15.7 ± 5.4	45.9 ± 11.6	53.2 ± 12.0	69.7 ± 16.1
sun on the right	15.1 ± 6.0	13.8 ± 5.5	17.1 ± 6.4	57.3 ± 17.1	67.7 ± 17.4	84.8 ± 17.4	22.3 ± 7.3	21.9 ± 6.8	24.2 ± 7.0	57.0 ± 13.3	63.5 ± 13.5	76.0 ± 15.2
sun behind	20.5 ± 4.3	28.0 ± 4.2	40.7 ± 4.6	87.6 ± 7.2	87.4 ± 4.3	87.4 ± 4.0	27.8 ± 7.0	32.0 ± 4.2	41.0 ± 4.3	86.5 ± 9.5	87.1 ± 6.1	86.9 ± 5.7
sun behind	42.0 ± 5.3	49.9 ± 4.4	61.4 ± 4.1	87.2 ± 5.0	87.0 ± 3.6	87.0 ± 3.5	18.3 ± 4.3	23.4 ± 3.7	32.8 ± 3.6	86.8 ± 8.6	86.9 ± 5.8	87.2 ± 5.4
overcast, direction 1	58.6 ± 9.9	58.3 ± 9.8	58.8 ± 10.0	87.6 ± 7.8	87.5 ± 7.7	87.5 ± 7.7	38.3 ± 5.5	38.3 ± 5.3	39.8 ± 5.5	90.0 ± 7.8	89.8 ± 7.7	89.8 ± 7.7
overcast, direction 1	50.9 ± 9.0	50.1 ± 8.9	50.5 ± 9.0	88.6 ± 7.3	88.5 ± 7.1	88.6 ± 7.1	43.8 ± 7.3	43.7 ± 7.1	44.8 ± 7.3	89.6 ± 7.7	89.9 ± 7.6	89.8 ± 7.6
overcast, direction 2	59.1 ± 11.0	58.1 ± 11.0	58.1 ± 11.0	89.8 ± 7.5	90.0 ± 7.5	90.0 ± 7.5	53.2 ± 7.9	52.3 ± 7.8	52.6 ± 8.0	89.0 ± 6.7	89.0 ± 6.7	89.0 ± 6.7
overcast, direction 2	60.5 ± 12.0	59.9 ± 11.9	60.0 ± 11.9	88.6 ± 8.0	88.6 ± 8.0	88.6 ± 8.0	47.4 ± 6.7	47.0 ± 6.6	47.9 ± 6.9	88.7 ± 6.7	89.0 ± 6.6	89.0 ± 6.8

Table 1.1: Illumination, mean degree of linear polarization *d* ± standard deviation (S.D.) (%), and |α – 90°| ± S.D. (°), where α is the angle of polarization (measured clockwise from the vertical) averaged for the surface area of the two shiny (smooth) and matte (rough) test surfaces used in our field experiments and measured by imaging polarimetry in the red (650 nm), green (550 nm) and blue (450 nm) parts of the spectrum from various directions of view relative to the solar meridian under clear and overcast skies. Under overcast conditions, directions 1 and 2 are perpendicular to each other.

When the direction of measurement was perpendicular to the solar meridian (sunshine coming from left or right), the shiny black test surface reflected light with lower *d* than the

matte one (Figs. 1.2, 1.3, 1.4, Table 1.1). From this direction of view, α of light reflected from the matte black test surface deviated from horizontal so much that the surface could not be polarotactically sensed as water. The shiny black test surface reflected, in turn, nearly horizontally polarized light, independently of the spectral range. Based on these characteristics, a large area of the shiny black test surface was expected to be more attractive to polarotactic insects in all three parts (red, green, blue) of the visible spectrum than the matte one.

When the measurement was positioned so that the sunshine came from behind, the direction of polarization of the light reflected from both test surfaces was approximately horizontal in all three spectral ranges. The difference between the matte and shiny black test surfaces was in the degree of polarization, which was slightly lower for the matte surface than for the shiny one (Figs. 1.2, 1.3, 1.4, Table 1.1). From this direction of view, a larger portion of the area was detected as water in the case of the shiny black test surface and thus, it was expected to be more attractive to polarotactic insects.

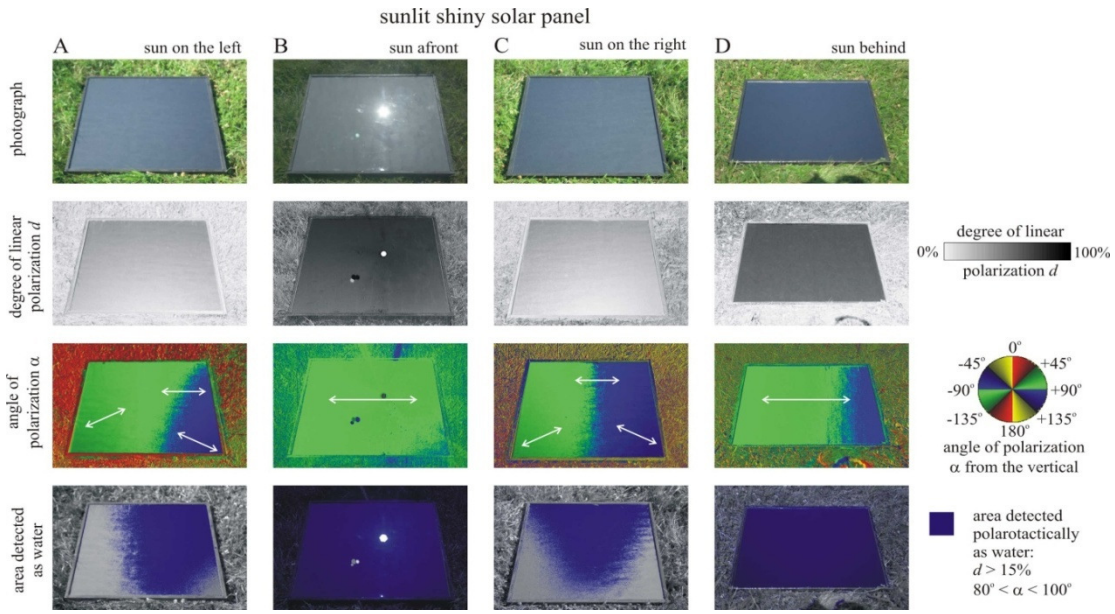

Figure 1.3: Photograph and patterns of the degree of linear polarization d, the angle of polarization α (measured clockwise from the vertical) and the area detected polarotactically as water (for which $d > 15$ % and $80° < \alpha < 100°$) for one of the two shiny black test panels used in our field experiments. d and α were measured by imaging polarimetry in the green (550 nm) spectral range under a clear sky for the following four different directions of view relative to the solar meridian SM: (A) The sun shone from the left, perpendicular to SM. (B)

The sun shone from afront. (C) The sun shone from the right, perpendicular to SM. (D) The sun shone from behind.

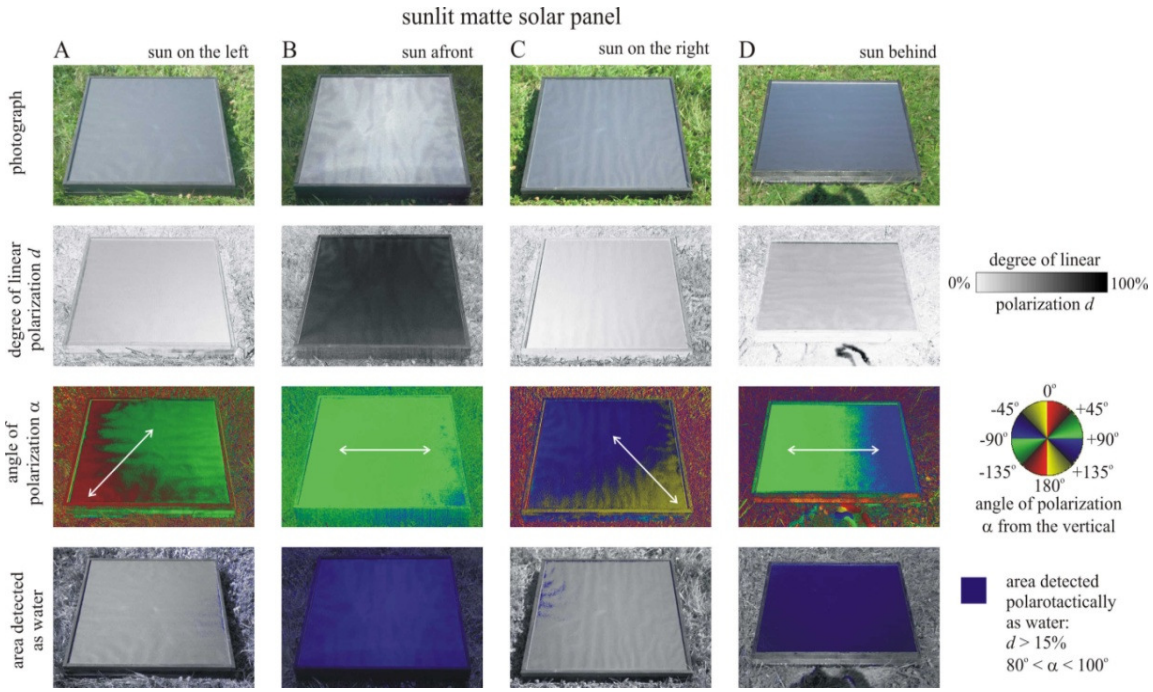

Figure 1.4: As Fig. 1.3 for one of the two matte black test panels used in our field experiments.

Since most of the polarotactic insects have polarization-sensitive photoreceptors with maximal sensitivity in the UV spectral range, we measured the reflection-polarization characteristics of the test surfaces in the UV (350 nm) part of the spectrum. The prediction deducted from the UV polarization patterns of the test surfaces was similar to those predicted for the visible spectral range (Figs. 1.5, 1.6, 1.7, Table 1.2).

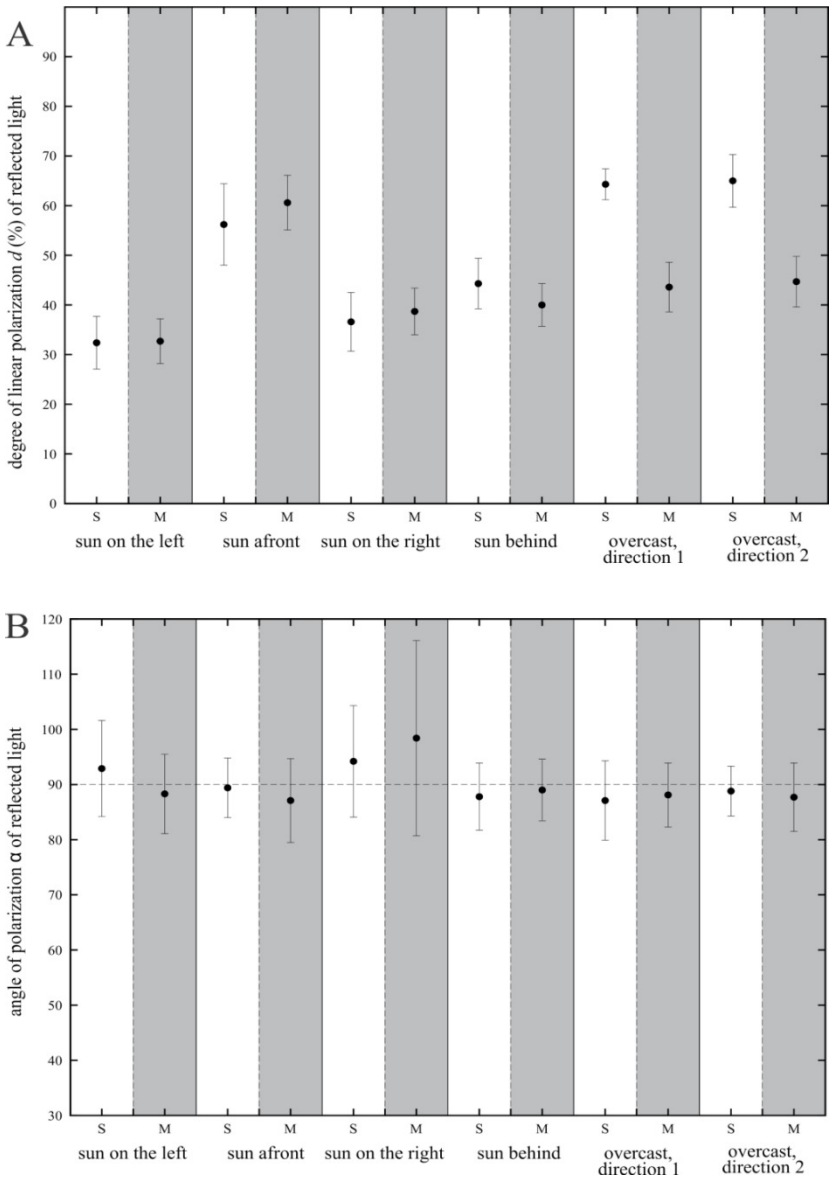

Figure 1.5: As Fig. 1.2 for the ultraviolet (350 nm) spectral range. The numerical values of the data displayed here are in Table 1.2.

illumination	**shiny (smooth) test surface**		**matte (rough) test surface**	
	***d* (%)**	**|α – 90°|**	***d* (%)**	**|α – 90°|**
sun on the left	32.4 ± 5.3	92.9 ± 8.7	32.7 ± 4.5	88.3 ± 7.2
sun afront	56.2 ± 8.2	89.4 ± 5.4	60.6 ± 5.5	87.1 ± 7.6
sun on the right	36.6 ± 5.9	94.2 ± 10.1	38.7 ± 4.7	98.4 ± 17.7
sun behind	44.3 ± 5.1	87.8 ± 6.1	40.0 ± 4.3	89.0 ± 5.6
overcast, direction 1	64.3 ± 3.1	87.1 ± 7.2	43.6 ± 5.0	88.1 ± 5.8
overcast, direction 2	65.0 ± 5.3	88.8 ± 4.5	44.7 ± 5.1	87.7 ± 6.2

Table 1.2: As Table 1.1 for the ultraviolet (350 nm) spectral range.

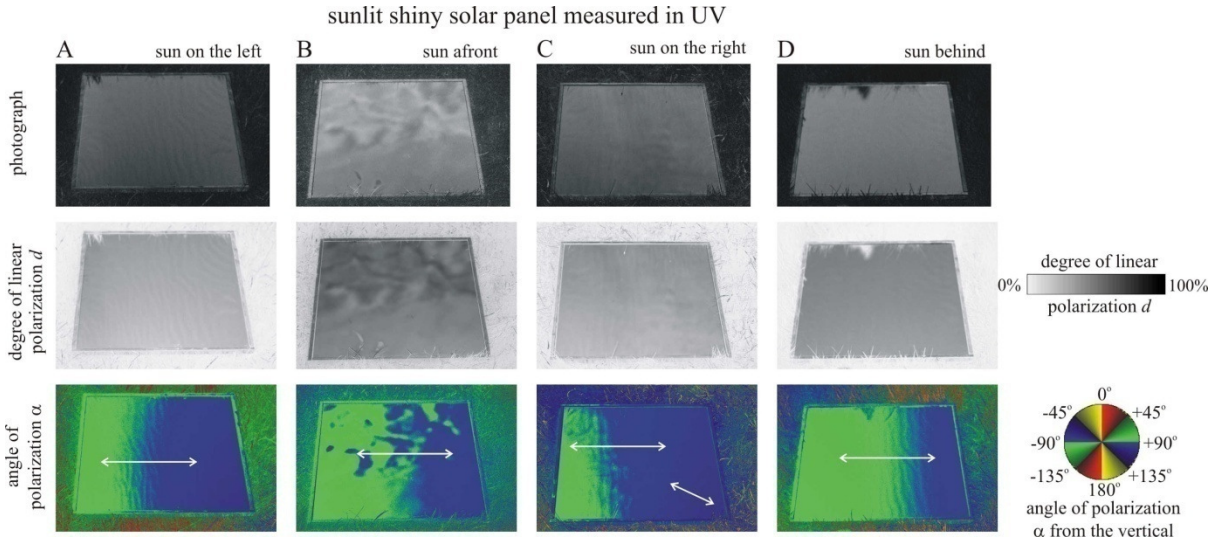

Figure 1.6: As Fig. 1.3 for one of the sunlit shiny test panels measured in the ultraviolet (350 nm) spectral range.

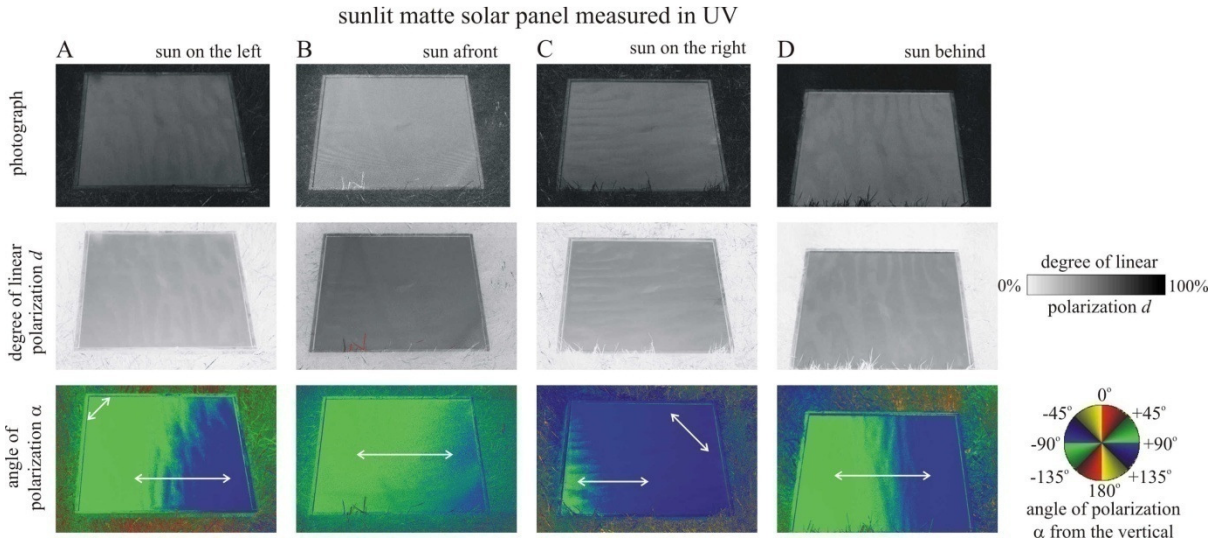

Figure 1.7: As Fig. 1.3 for one of the sunlit matte test panels measured in the ultraviolet (350 nm) spectral range.

When the sky was overcast (no direct sunshine coming to the test surfaces), both the shiny and matte black test surfaces reflected nearly horizontally ($\alpha \approx 90°$) polarized light in the visible spectral range, independently of the measurement direction relative to the invisible Sun (Figs. 1.2, 1.8). The standard deviation of the angle with which the direction of polarization of reflected light deviated from the horizontal was smaller for the matte black test surface (green: $6.6° \leq |\Delta\alpha_{matte}| \leq 7.7°$) than for the shiny one (Green: $7.1° \leq |\Delta\alpha_{shiny}| \leq 8.0°$). The shiny test surface, in turn, reflected light with higher d (green: d_{shiny} = 50.1-59.9 ± 8.9-11.9 %) than the matte (green: d_{matte} = 38.3-52.3 ± 5.9-7.8 %, Figs. 1.2, 1.8). Similar

reflection-polarization characteristics occurred in the UV (350 nm) spectral range when the sky was occluded (Figs. 1.5, 1.9, Table 1.2).

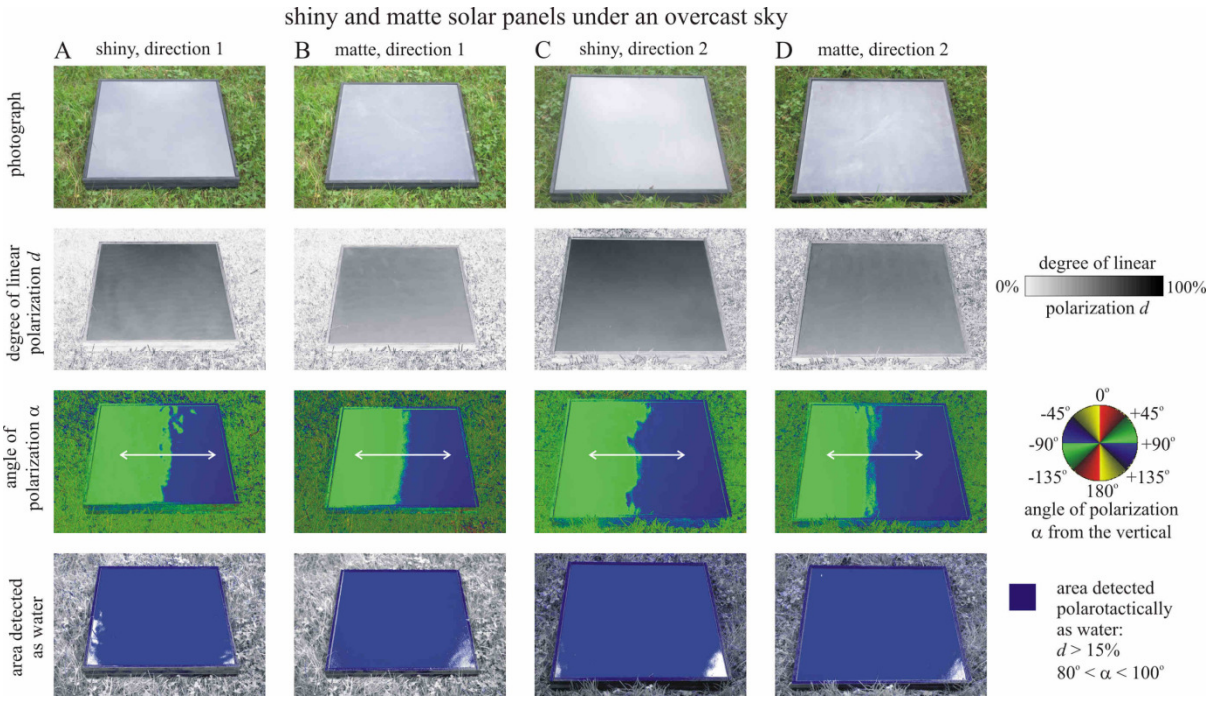

Figure 1.8: As Fig. 1.3 for one of the two shiny (A, C) and matte (B, D) black test panels used in our field experiments under an overcast sky from horizontal directions of view 1 (A, B) and 2 (C, D), which were perpendicular to each other and direction 1 was arbitrary.

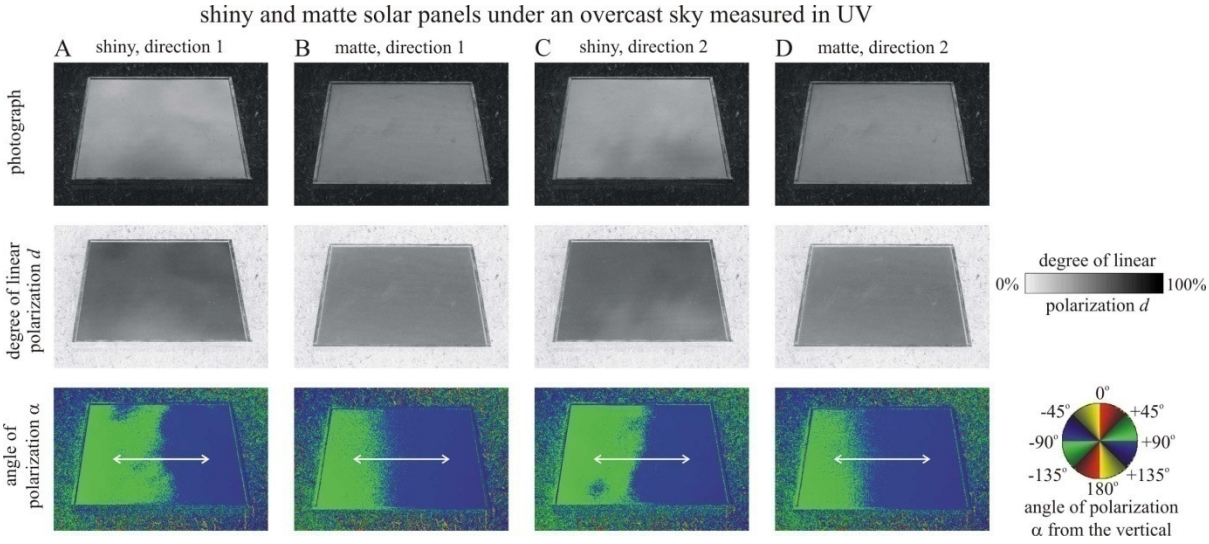

Figure 1.9: As Fig. 1.8 measured in the ultraviolet (350 nm) spectral range under an overcast sky.

1.3.2. Attractiveness of test surfaces to aquatic insects

Experiment 1 lasted for 11 days, during which we observed 2925 loopings and 3579 touch-downs executed by 672 and 717 horseflies, respectively. We counted 812 landings, that added up to more than 7.1 hours spent on the test surfaces in total. In Experiment 2, we recorded the responses of mayflies and non-biting midges to the test surfaces over 8 days, the total number of which was 367 and 1075, respectively. Note, that since the insects were not captured, we could not exclude recounting the returning individuals and thus pseudo-replication. This was, however, appropriately handled by pooling the data for all sampling sessions. In Experiment 1, the horseflies performed more habitat- and oviposition-related behaviour in the vicinity of the shiny black test surface. For reaction groups looping, touching and landing, the shiny test surface was 3.4, 5.6 and 5.2 times more attractive in total than the matte surface, respectively. Regarding the reaction items, the shiny surface was 4.4, 7.5 and 7.2 times more attractive than the matte one for looping, touching and landing, respectively (Fig. 1.10). In Experiment 2, the matte black test surface attracted 4.0 times more mayflies than the shiny one, the non-biting midges, however, found both test surfaces equally attractive (with no statistically significant difference).

Statistical analyses of non-parametric Mann-Whitney U test and Wilcoxon matched pair test gave the same results. Only the difference between the reactions of non-biting midges to matte versus shiny test surfaces was not significant. Detailed data of the latter is shown in Table 1.3.

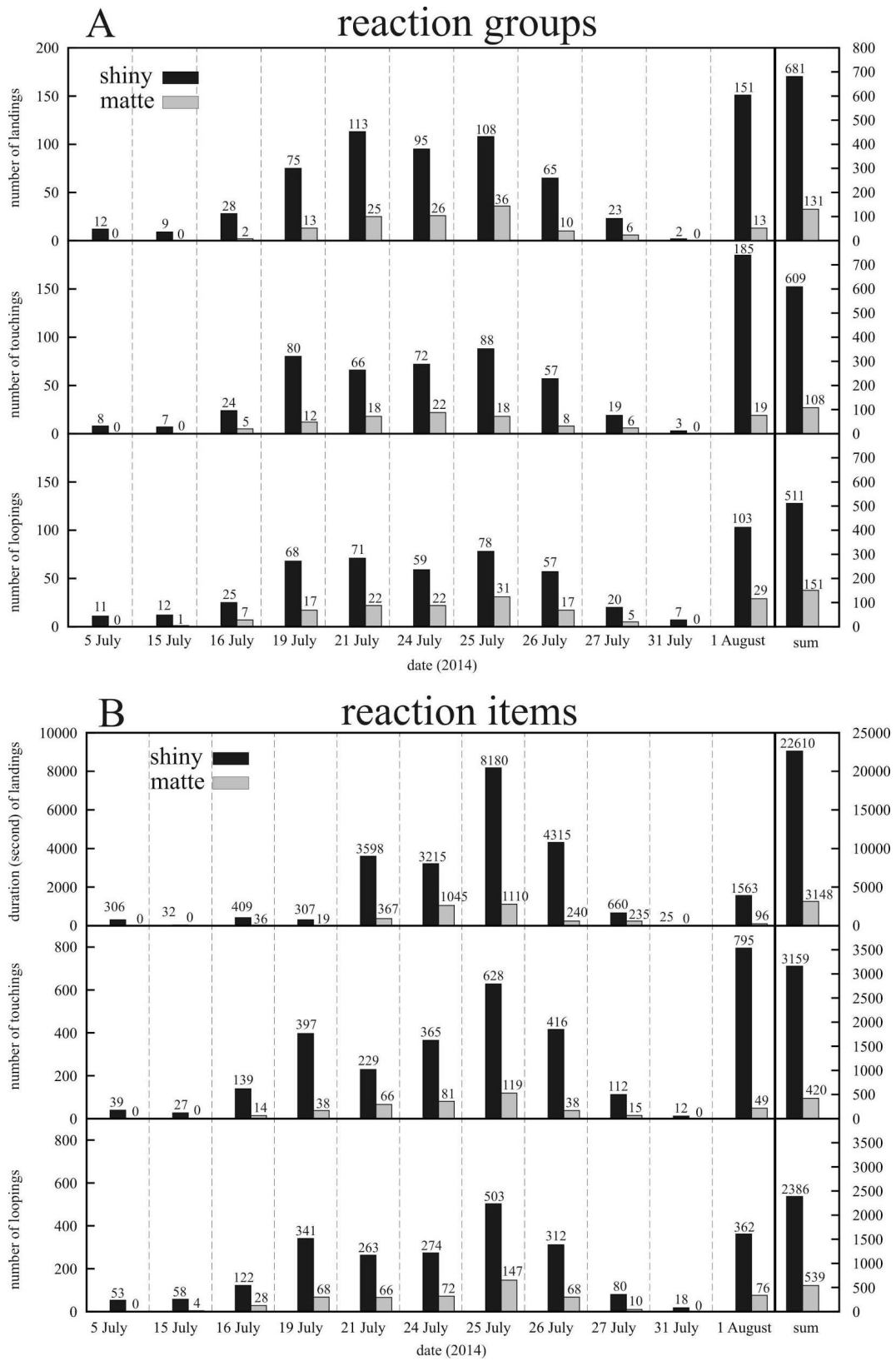

Figure 1.10: Number of reaction groups and number/second of reaction items of horseflies attracted to the shiny and matte black test surfaces used in Experiment 1. In panel B, the duration of landing is measured in seconds (two columns at the right side).

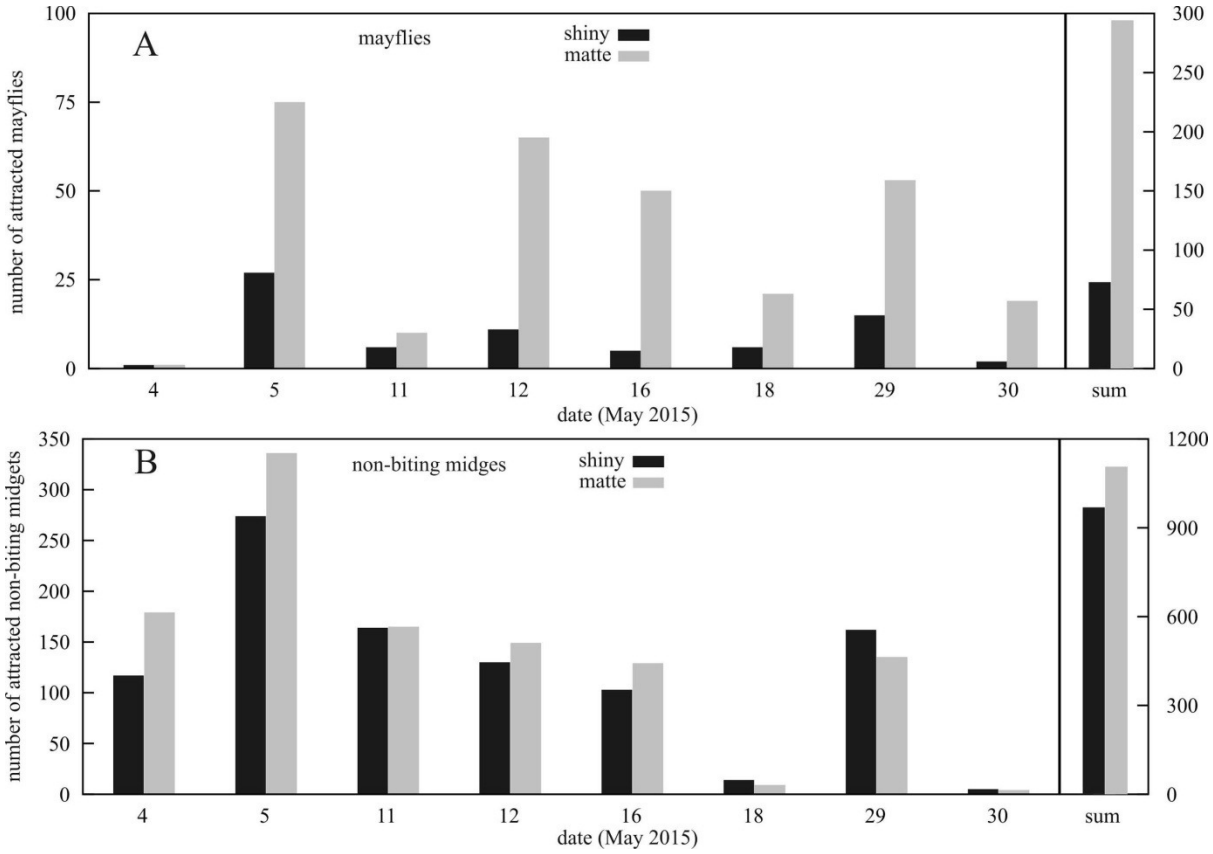

Figure 1.11: Number of mayflies (A) and non-biting midges (B) attracted to the shiny and matte black test surfaces used in Experiment 2.

Horseflies:

reaction groups	**parameters**	**confidence interval (95%)**	**significance**
looping matte vs. shiny	V = 66, p = 0.003346	14.5 – 48.0	p < 0.05, significant
touching matte vs. shiny	V = 66, p = 0.003346	13.0 – 84.5	p < 0.05, significant
landing matte vs. shiny	V = 66, p = 0.003346	17 – 77.5	p < 0.05, significant
reaction items	**parameters**	**confidence interval (95%)**	**significance**
looping matte vs. shiny	V = 66, p = 0.003346	70.0 – 258.5	p < 0.05, significant
touching matte vs. shiny	V = 66, p = 0.003346	76.0 – 421.5	p < 0.05, significant
landing matte vs. shiny	V = 66, p = 0.003346	228.5 – 3653	p < 0.05, significant

Mayflies and non-biting midges:

matte vs. shiny	**parameters**	**confidence interval (95%)**	**significance**
mayflies	V = 28, p = 0.01796	10.5 – 49.5	p < 0.05, significant
non-biting midges	V = 25.5, p = 0.2924	-5.0 – 44.0	p > 0.05, not significant

Table 1.3: Statistical analysis (Wilcoxon matched pair test) of pairwise comparison of the attractiveness of matte versus shiny black test surfaces for reaction groups and items in Experiment 1, and for number of individuals attracted to matte versus shiny test surfaces in Experiment 2.

1.4. Discussion

We have studied the polarized light pollution of matte and shiny solar panels quantified with their attractiveness to positively polarotactic mayflies (Ephemeroptera), horseflies (Tabanidae) and non-biting midges (Chironomidae). The attractiveness was characterized by the number of reactions (looping, touching and landing) of horseflies and the abundance of mayflies and non-biting midges on or in the immediate vicinity above the test surfaces. Depending on the sky condition (clear or cloudy) and the direction of reflection, we experienced categorically different response from each studied aquatic insect groups to the anti-reflective coatings of the solar panels. Horseflies had a reduced attraction to anti-reflective (matte) panels, while mayflies actually preferred them to the shiny ones.

The degree of polarization reflected from natural water bodies at the Brewster's angle can be different in a wide range: 15 % < d < 80 %. We found that there were only two directions of view (when the sun was afront or behind), from where sunlit horizontal matte black solar panels reflected strongly (p > 15 %) and horizontally polarized light that can be attractive to water-seeking polarotactic insects (Figs. 1.2, 1.3, 1.4). From other viewing directions, the direction of polarization was not horizontal, that is unattractive to aquatic insects. In contrast, shiny black solar panels reflected horizontally polarized light with d > 15 % from all directions of view, indicating that panels with no anti-reflective coating could be more important sources of polarized light pollution than the coated ones, maladaptively attracting more aquatic insects. The measured reflection-polarization characteristics were good predictors of horsefly responses to the different test surfaces, knowing that the surfaces were usually sunlit during the experiment. Horseflies did not fly and react to the test surfaces under overcast skies. Our observations are in correspondence with those of Blahó et al. (2014) of matte black car bodies.

The surprisingly strong attraction of mayflies to the matte black test surfaces in Experiment 2 can also be explained by the reflection-polarization characteristics of the surfaces. In this experiment, the test surfaces were placed in the shade of trees and bushes.

These lighting conditions were similar to those measured under overcast skies in Experiment 1 (Figs. 1.2, 1.8). Both the matte and shiny test surfaces reflected horizontally polarized light, nevertheless, d of the matte one was ca. 10 % lower than that of the shiny and the standard deviation $\Delta\alpha_{matte}$ of the angle of polarization α_{matte} of light reflected from the matte solar panels were smaller than that from the shiny ones. Blahó et al. (2014) found similar characteristics and mayfly behaviour when they got the result that cars with matte dark grey car finish and smaller $\Delta\alpha$ were much attractive to the same mayfly species than cars with shiny grey or black car finish and larger $\Delta\alpha$. These optical characteristics are very similar to those of calm waters that is the natural habitat of the investigated mayflies and non-biting midges (Fig. 1.11, Table 1.2, Encalada and Peckarsky 2007). The explanation of this is the following: The angle α of polarization of light reflected from the water body strongly depends on the angle of reflection. If the inclination of the surface changes periodically, the angle of reflection also changes periodically, resulting in the temporal change of the standard deviation $\Delta\alpha$. In the case of water bodies, undulation can cause such temporal alteration of $\Delta\alpha$. The stronger the undulation, the rougher is the water surface and the larger is $\Delta\alpha$. Calm waters have smoother surface, resulting in smaller $\Delta\alpha$. Water-seeking mayflies can detect remotely the roughness of water bodies by sensing the standard deviation $\Delta\alpha$ of the reflected polarized light. Certain mayflies prefer these calm waters, because their larvae can develop only in non-turbulent water. Otherwise their larvae, having weaker musculature, could easily be drifted away by turbulence and undulation (Encalada and Peckarsky 2007).

In Experiment 2, non-biting midges found equally attractive both the matte and shiny solar panels (Fig. 1.11, Table 1.3). Chironomids may be insensitive to the modest reduction of the degree of polarization by applying anti-reflective coating. The thresholds of d necessary to detect polarized light vary in a wide range among taxa (Horváth and Varjú 2004) and the reaction behaviour can also be very different being exposed to various d values (Kriska et al. 2009). In earlier experiments, the attractiveness of a polarized light source to chironomids increased with d over a great range (Horváth et al. 2010a, 2011). This suggests, that the applied anti-reflective coating was not sufficiently effective to reduce chironomid polarotactic attraction.

On the spot of Experiment 2 we observed the polarized-light-polluting effect of the asphalt road running parallel to the creek from where mayflies and non-biting midges emerged. They were swarming above the asphalt road, because the asphalt-reflected horizontally polarized light attracted them. The reflection-polarization characteristics of this asphalt road has been measured earlier (Kriska et al. 1998; Horváth et al. 2010c, 2011). In our

experiment, the horizontally polarizing signal of the asphalt road, which was weaker than that of the test surfaces, functioned as initial attractor of the investigated insects.

To sum up, we have shown, that the studied type of anti-reflective coating of matte solar panels can provide some solution to eliminate the ecological traps created by solar panels. The reduction of polarized light pollution is, however, rather modest and only a partial success in the case of some taxa and under special weather conditions. The preference of certain mayflies for matte solar panels strengthens the effect of the existing ecological trap of solar panels. Our results suggest, that this only occurs under overcast skies and therefore can be problematic in wetter, more temperate areas. In some cases, solar panels are positioned not horizontally but at an angle perpendicular to the sun at noon. This is, unfortunately, not a solution to polarized light pollution, because even vertical polarizers are as effective at triggering maladaptive behaviour as horizontal ones (Kriska et al. 2008). A previous study has shown, that there is a solution that is effective against the insect trapping effect of solar panels: Polycrystalline silicon solar panels consist of several smaller tiles with thin white lines at the fittings. Thus, a dense white grid is formed that makes the whole surface unattractive to polarotactic aquatic insects exposed to the solar panels (Horváth et al. 2010a). Our results suggest that anti-reflective coating may also play a role in reducing the ecological impacts of solar panels on polarotactic species and can work in tandem with gridding. It is not clear that anti-reflectively coated solar panels can play a central role in insect conservation. Even so, our experiments were conducted in a relatively mesic (a habitat with a moderate or well-balanced supply of moisture) ecosystem. Insect species that have evolved in more xeric (a habitat receiving only a small amount of moisture), less-often overcast zones like deserts in which large-scale photovoltaic installations are placed, may have more consistent and positive responses to matte coatings. To test the reactions of a broader array of aquatic taxa to similar surfaces, more research is needed.

Chapter 2.

Dual Light-trap of the Night-swarming Mayfly, *Ephoron virgo* at Lamp-lit Bridges

2.1. Introduction

2.1.1. Polarized light pollution at night

Some examples of polarized light pollution were introduced in Chapter 1. In these cases, the effect was investigated exclusively during the daytime. However, artificial night lighting can also be polarized by reflecting from man-made polarizers (e.g. asphalt roads), creating a strong source of horizontally polarized light that could attract night-active polarotactic aquatic insects, distracting them from natural water bodies. Numerous case studies have shown that polarized and unpolarized light can independently form ecological traps (Robertson et al. 2013) that lure away insects from natural habitats by creating misleading optical cues (Frank 1988; Eisenbeis 2006; Horváth and Kriska 2008; Langevelde et al. 2011). Theoretically, it is possible that the two effects occur at the same time, strengthening one another, yet, such an effect has not been thoroughly quantified. Since ecological traps are capable of causing rapid population declines in the affected species (Kokko and Sutherland 2001; Fletcher et al. 2012), the potential for the two types of ecological traps to reinforce each other is a major conservation concern.

Nocturnal lights with high intensity (e.g. street or security lights, stadium lighting) can emit unpolarized light with wavelengths that attract aquatic insects directly (Eisenbeis 2001; Eisenbeis 2006; Gaston et al. 2013). It is generally believed that the attraction is a maladaptive consequence of the innate tendency of insects to navigate with the help of the moonlight (Frank 1988). Most of the nocturnal artificial light sources are placed above asphalt-paved roadways or parking lots that have relatively smooth surface texture and thus, they are able to polarize reflected light with degree of polarization d higher than 60 % at the Brewster's angle (Kriska et al. 1998; Horváth et al. 2009). Such d-values are typical for dark waters in nature (Gál et al. 2001; Horváth and Kriska 2008). When these optical conditions occur in the vicinity of natural water bodies, insects originally attracted to unpolarized light

could find themselves confronted with horizontally polarized light as a second cue, falsely indicating the presence of a lake or river. A previous study has shown, that some aquatic insects were more attracted to lamp-lit artificial polarizers at night than to unlit polarizing surfaces or unpolarized light sources without polarizers (Boda et al. 2014). In this chapter, I will describe the study of a conservation issue concerning the mayfly species *Ephoron virgo*, caused by the simultaneous effect of polarized and unpolarized attractors that strengthen each other.

2.1.2. Polarization sensitivity of river-dwelling mayflies

A typical swarming behaviour of some river-dwelling mayfly species (e.g. *Palingenia longicauda* or *Ephoron virgo*) is that after a long larval development, male and female mayflies come out of water in a large mass within a short time. The males being not yet in their reproductive form are the so-called subimagos that need to moult once more to reach their final, imago stage. Females, in turn are ready to copulate once they came out of water. After the rapid moulting of males, the two sexes find each other and copulate. Then, the females assemble in a huge swarm and fly a couple of km-s opposite to the river's flow direction before they lay their eggs into the river. This special flying behaviour preceding oviposition is called compensatory flight, with which the females compensate the drifting movement of water while they were coming out of the riverbed, performing moulting and reaching the surface (Kazanci 2013; Kriska et al. 2007).

Kriska et al. (2007) has found that during their compensatory flight, *Palingenia longicauda* mayfly females follow the horizontally polarized optical patterns reflected from the water surface. This signal helps them to orient themselves and to remain in the middle line of the river. This hypothesis was experimentally supported, as well. Málnás et al. (2011) have observed that if during the compensatory flight a bridge intersects the river, the mirror image of the bridge can stop the compensatory-flying insects, making them to turn back forming a swirling congregation near the bridge. The cause of this strange behaviour is the vertically polarized light of the mirror image of the bridge. But why would mayflies be not able to fly under the bridge? In their natural habitat, only the tree barks or the mirror image of the river bank vegetation is vertically polarized. The compensatory-flying mayflies have learned that such a signal means the end of the water surface that they must not leave in order to survive. So, when they come across an unexpected vertically polarized signal like the mirror image of a bridge, they mistakenly consider it as river bank and turn back from it.

2.1.3. The swarming behaviour of *Ephoron virgo*

The development and swarming behaviour of *Ephoron virgo* is in great detail similar to those of *Palingenia longicauda*. *Ephoron virgo* is found throughout most of Europe, Turkey and North Africa. The burrowing larvae inhabit U-shaped tubes in the riverbed where they filter and eat suspended particles from the water current (Kureck and Fontes 1996; Kazanci 2013). The larval habitat consists of sand (Schnoemund 1930) or gravel with sand and fine sediments (Ibanez et al. 1991). The life cycle of *Ephoron virgo* is univoltine (producing one generation in a year) and the eggs laid in late-summer usually hatch in mid-April. The larval growing period lasts until August, when winged adult males and females emerge from the water and swarm for a few hours before they die by the following morning (Cid et al. 2008). The subimagos, the sexually immature form of males, emerge first, move to riparian vegetation where they moult to sexually mature adult males. Mature males return to the river forming aerial swarms (> ~300 individuals) above the water surface at around 19:30 h. As the swarming progresses, the number of copulating mayflies increases. Swarm densities increase between 19:40 h and 20:45 h. After copulation, female mayflies start their compensatory flight, then they lay egg batches on the water surface *en masse* (Kazanci 2013) and perish soon after.

In this chapter, I describe a series of observations and experiments that explain this phenomenon as a maladaptive behavioural response of mayflies to both unpolarized and polarized light pollution. We used imaging polarimetry to characterize the reflection-polarization patterns of various surfaces of the bridge and the river-section below. We conducted experiments to verify that *Ephoron virgo* are independently attracted to polarized and unpolarized light, and documented the spatial distribution and behaviour of mayflies in relation to both types of light sources.

Our research was motivated by various anecdotal reports on mayfly mass congregation and maladaptive behaviour near nocturnal lightings. Kureck (1992) and Tobias (1996) reported about large mayfly swarms (including *Ephoron virgo*) around nocturnal illumination along riversides and bridges, describing the phenomenon as ‘summer snow drifts’. This incredibly dense aggregation of mayflies (1.5 million individuals on an illuminated road surface) formed later a 1.5 cm thick layer of ovipositing females under the lamps on the asphalt road. In the summers of 2012 and 2013, the years of our experiments,

we also observed a similarly dense mass swarming of *Ephoron virgo* at a lamp-lit bridge over the Danube near the village Tahitótfalu.

2.2. Materials and Methods

2.2.1. Preliminary observation of the mass swarming and sex ratio determination

The mass swarming of *Ephoron virgo* (depending on the location and the river-section) usually takes place within a 2-week-long time interval between 15 July and 15 September. We observed the swarming every evening between 15 August and 2 September 2012 and 2013 at the Zoltán Tildy road bridge (47° 75' N, 19° 08' E) overarching the Danube near Tahitótfalu. During the mass swarming on 1 September 2012, we collected fallen mayfly specimens from the asphalt road of the bridge between 19:30 and 20:30 (local summer time = GMT + 2 hours) when the congregation around the bridge-lamps was abundant. We collected, altogether, 10 samples from under four consecutive lamps containing approximately 100 individuals, each. Later, in the laboratory, we determined the sex ratio of the collected samples. The method for this was the following: Male *Ephoron virgo* is easy to recognise by its much longer tails (called caudal filaments) having two of them, while those of the females are shorter and they have three of them. Males also possess a fork-like proleg that helps them to grab and hold onto females during copulation. With an optical microscope, these morphological differences are well observable, so the sex of the mayflies could be easily determined.

In 2012, during the peak abundance of the *Ephoron virgo* swarming period, we used hand-held flashlights to test the effect of a concentrated, collimated unpolarized light beam on the movement and distribution of mayflies. We predicted that the mayflies interact with the light beam that attracts them to these portable light sources concentrating them into the beam. This experiment was repeated on the river bank at a height of 1 m above the water surface and 1 km far from the bridge in a non-illuminated area. Standing on the bank, we pointed the lightbeam towards the arriving compensatory-flying mayflies and observed the behaviour of the swarm.

2.2.2. Estimating the swarming intensity of mayflies at bridge-lamps

The swarming intensity of mayflies at the bridge-lamps was qualitatively characterized by a dual nomenclature: (i) Mass swarming occurred when the mayflies formed a 2-5 m-long, continuously moving and bending plume around each bridge-lamp that contained at least 50 individuals. (ii) At low swarmings, these plumes contained less than 50 mayflies. We took photographs about the swarms at each lamp and using our self-developed computer program (see 2.2.5.), the number of mayflies were counted.

Figure 2.1: Spatial variation in the distribution of mayfly swarms at bridge-lamps. Near the river's edge, lamps closer to the Danube (left side in the picture) attract several thousands of mayflies, whereas at the neighbouring lamp farther from the river (more inland, right side in the picture) only a few tens of *Ephoron virgos* were swarming.

2.2.3. Imaging polarimetry of the bridge and the underlying river-section

The applied method of imaging polarimetry was similar to that described in Chapter 1.2.2., developed by Horváth and Varjú (1997, 2004). We measured the reflection-polarization characteristics of the river surface in the area below the bridge in the red (650 nm), green

(550 nm) and blue (450 nm) spectral ranges on 23 September 2013. We choose a daytime for our measurements, when the solar elevation corresponded to that of the full moon in the preceding swarming period. Thus, the illumination circumstances were similar and the intensity of the reflected light was high enough to make the polarimeter usable. Otherwise, under poor illumination at night, we could not have been able to perform polarimetric measurements. We also measured the reflection-polarization patterns of the asphalt road of the bridge before sunset (when direct light from the clear sky illuminated the road) and at night (when only the bridge-lamps illuminated the road). In this case, the light intensity of the bridge-lamps was high enough for adequate imaging polarimetry. Although we measured the polarization patterns in three spectral ranges, we chose the blue range for later comparisons. Mayflies have ultraviolet-, blue- and green-sensitive photoreceptors (Menzel 1979; Horridge et al. 1982), thus blue represents the middle of their wavelength sensitivity range. It is still unknown, however, in which spectral range *Ephoron virgo* and other mayfly species perceive the polarization of reflected light.

2.2.4. Torchlight experiments with linear polarizers

After the preliminary torchlight experiment described in subsection 2.2.1., we performed field experiments to examine the effect of light sources with different polarization characteristics on *Ephoron virgo*. We also wanted to prove the assumption about the linear polarization sensitivity of this mayfly species. The field experiments took place on 23, 24, 27 and 28 August 2013, near Tahitótfalu, 110 m far from the Zoltán Tildy public bridge at the bank of the river Danube. A torch of high-intensity LED light sources (UltraFire C8 Cree XM-L T6 LED) was fixed to a tripod on the bank of the river, only a couple of cm far from the water. The beam of the torchlight was pointed towards the compensatory-flying swarm of mayflies, that were arriving from upstream the river's flow direction. Although, the actual bridge-lamps were normal incandescent lamps, in this experiment, we used a LED torch because this kind of lamps produced a collimated beam of light with an intensity high enough to reach the mayflies in the river mid-line.

First, a horizontally polarizing filter was placed directly in front of the torch, that functioned as a horizontally polarized light source. The filter had a multi-layered composition having the following elements: a depolarizing common tracing paper and a linear polarizer (diameter = 15 cm, thickness = 1 mm, type: XP42-18 from ITOS, Mainz, Germany). The latter was placed outside, that is farther from the torch. In a second experiment, we applied

the filter with the elements in the reversed order, thus, the emitted light was practically unpolarized. We verified the polarization characteristics of the applied filters with imaging polarimetry: the composition used in the first experiment had degrees of linear polarization $d > 95$ % being practically totally linearly polarized, while d in the second experiment was < 5 % (Fig. 2.2) that cannot be perceived by the polarization-sensitive mayfly species studied until now (Horváth and Varjú 2004; Horváth 2014). Although, the threshold d^* of polarization sensitivity is unknown for *Ephoron virgo*, it is probably similar to that of other mayfly species, the d^* of which is the following in the blue spectral part: 32 % $< d^* <$ 55 % for *Baetis rhodani*, 55 % $< d^* <$ 92 % for *Ephemera danica*, *Epeorus silvicola* and *Rhithrogena semicolorata*.

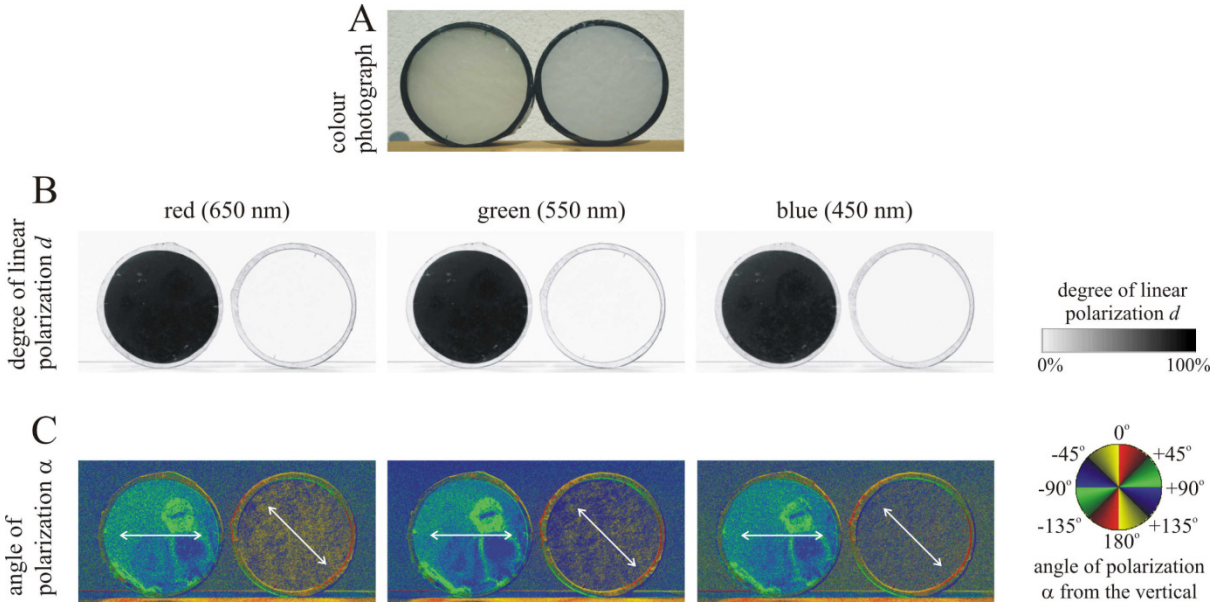

Figure 2.2: Polarizing (left) and depolarizing (right) filters used for field experiments with *Ephoron virgo* mayflies. The light transmitted through the filter on the left in each picture/pattern is totally linearly polarized ($d > 95$ %), that of on the right is practically unpolarized ($d < 5$ % which is not perceived by any known polarization-sensitive animal). In the α-pattern double-headed arrows show the direction of polarization of filter-transmitted light, which is horizontal and tilted at 45° from the horizontal for the left and right filter, respectively. The polarization patterns were measured by imaging polarimetry in the red (650 nm), green (550 nm) and blue (450 nm) parts of the spectrum.

We started the experiments when the compensatory-flying swarm arrived and continued until the cessation of the swarming. The longest time interval lasted from 20:15 to 21:20 (GMT +

2 h) and over the course of our study the starting and ending times were shifted earlier by about 5 minutes each day.

One measurement session was the following for both experiments: We took 10 photographs of the area under the light beam with digital cameras (Nikon D90 and D3200) to quantitatively assess the mayfly responses. After a photograph was taken, we switched off the torch for 10 seconds, so that the attracted mayflies could rejoin to the main swarm. After switching it on again, we waited another 5 seconds before we started taking another photograph. Thus, we could expectedly photograph new individuals and minimize pseudo-replication. We repeated this altogether 100-second-long process four times at the same place, then we changed the polarization filter. We continued this process until the end of swarming. We used only one type of filters at the same time, because we wanted to study the mayfly attracting ability of polarized and unpolarized light sources and not the choice response of mayflies to different light sources.

2.2.5. Image processing

During the torchlight experiment, we took above 1500 photographs with a resolution of 3430 × 2278 pixels. These images were scaled to 80 % of their original size for evaluation with a computer software (AlgoNet: http://www.estrato.hu/algonet), that is a framework for designing and executing image processing algorithms. In this task, the software semi-automatically counted the mayfly individuals on the photographs, for which we created the following algorithm: (1) Since the photographs were taken at night, the illuminated mayflies were clearly visible in front of a homogeneous dark background. Filed objects with similar colours may be recognized falsely by colour-based algorithms, thus, we converted the pattern of intensity I in the green (550 nm) channel of photographs to a binary black ($I < I^*$) and white ($I > I^*$), applying an appropriate threshold $I^* = 50$, where the intensity maximum in the green channel was $I_{max} = 255$. (2) The mayflies were characterized as a bunch of white pixels (blobs) the contours of which were recognised by scanning the binary image line-by-line and then the lines pixel-by-pixel until the border is detected, according to the method of Suzuki and Abe (1985). The algorithm determined whether the found border is of outer or inner manner, that is, if there is a hole or void in the blob. The software stored the transition information (black-white or white-black transition) about the border and continued the scan until a new border was found. After scanning the whole image, the areas within the outermost borders were considered as blobs. (3) From the recognised blobs only those were kept for

further analysis which had an area between 4 and 10000 pixels. (4) The overlapping blobs or those being close to each other (with a distance less than 20 pixels) were merged into a single blob. The distance between two blobs was defined by the Euclidean distance of their centers which was obtained using its image moments (Teague 1980). The final number of blobs gave as a result the number of identified mayflies in the light beam.

We calibrated the efficacy of this software on 20 photographs containing known numbers (100-1000) of mayflies. The mayflies were counted visually in advance, then these photos were evaluated by the software. The difference between the visually- and computer-determined numbers of recognised mayflies was lower than 5 %.

2.2.6. Statistical analysis

We used non-parametric Mann-Whitney U test to compare the numbers of mayflies attracted to horizontally polarized light and unpolarized light. This test was chosen for statistical evaluation, because the distribution of the measured data (the numbers of attracted mayflies) differed so much from normal distribution, that conventional parametric tests could not have been applied without a data transformation, which could have falsified the result of the test.

2.3. Results

2.3.1. Mass congregation of mayflies

We observed 23 mass swarmings of *Ephoron virgo* between 15 August and 2 September 2012 and 2013 in Tahitótfalu, Hungary at the bridge named after Zoltán Tildy overarching the river Danube (Table 2.1). A congregation was considered swarming, if the number of mayflies in the swarm was at least 300. Swarming did not occur in rainy, cool nights. During the swarming interval at night, the mayflies often changed their flight direction but remained constantly above the water surface at a height about 10-50 cm. The mayflies occupied the space within this height above the whole river surface except for a couple-of-meter-long lane next to the bank. The typical upstream-flying compensatory swarm appeared several meters above the water surface in the river mid-line and continued its flight towards the bridge every warm night after 20:30 h (GMT + 2 h). The compensatory-flying female mayflies jammed in front of the bridge and, after a while, they moved directly towards the high-intensity bridge-lamps or landed immediately on the asphalt road of the bridge. Since the direction of the

compensatory flight always faced the river's flow direction, the flying females always approached the bridge from the southern side. The swarming above the river finished around 21:30 h.

date	**swarming intensity of *Ephoron virgo***	
	mass swarming	**low swarming**
15 August 2012		+
16 August 2012		+
17 August 2012		+
18 August 2012	+	
19 August 2012	+	
20 August 2012	+	
21 August 2012	+	
22 August 2012	+	
23 August 2012	+	
24 August 2012	+	
25 August 2012	+	
26 August 2012		+
27 August 2012		+
28 August 2012	+	
29 August 2012	+	
30 August 2012	+	
31 August 2012		+
1 September 2012	+	
2 September 2012	+	
15 August 2013		+
16 August 2013		+

17 August 2013		+
18 August 2013		+
19 August 2013	+	
20 August 2013		+
21 August 2013	+	
22 August 2013	+	
23 August 2013	+	
24 August 2013	+	
25 August 2013	+	
26 August 2013	+	
27 August 2013	+	
28 August 2013	+	
29 August 2013		+
30 August 2013		+
31 August 2013	+	
1 September 2013		+
2 September 2013		+
sum	**23 mass swarmings**	**15 low swarmings**

Table 2.1: Swarming intensity of *Ephoron virgo* mayflies between 15 August and 2 September 2012 and 2013 estimated on the basis of photographs taken at four bridge-lamps. Mass swarming: At each lamp mayflies formed a 2-5 m long, continuously moving and bending tail containing more than 50 individuals. Low swarming: Fewer than 50 mayflies were swarming at each lamp.

Large mayfly swarms which were formed around the turned-on lamps appeared only at the bridge section that was directly above the water. The lamp at the edge of the river still attracted thousands of individuals, while the adjacent lamp above the bank had a swarm of fewer than 50 mayflies. The lamps located farther from the river attracted no mayflies. The

congregated mayflies formed continuously swirling and bending 'tails' starting at each bridge-lamp and elongated southward in the direction of the blowing wind. Sometimes, these tails touched the asphalt road, where several hundreds of *Ephoron virgo* landed and oviposited on the asphalt surface. The females died within a short time afterwards.

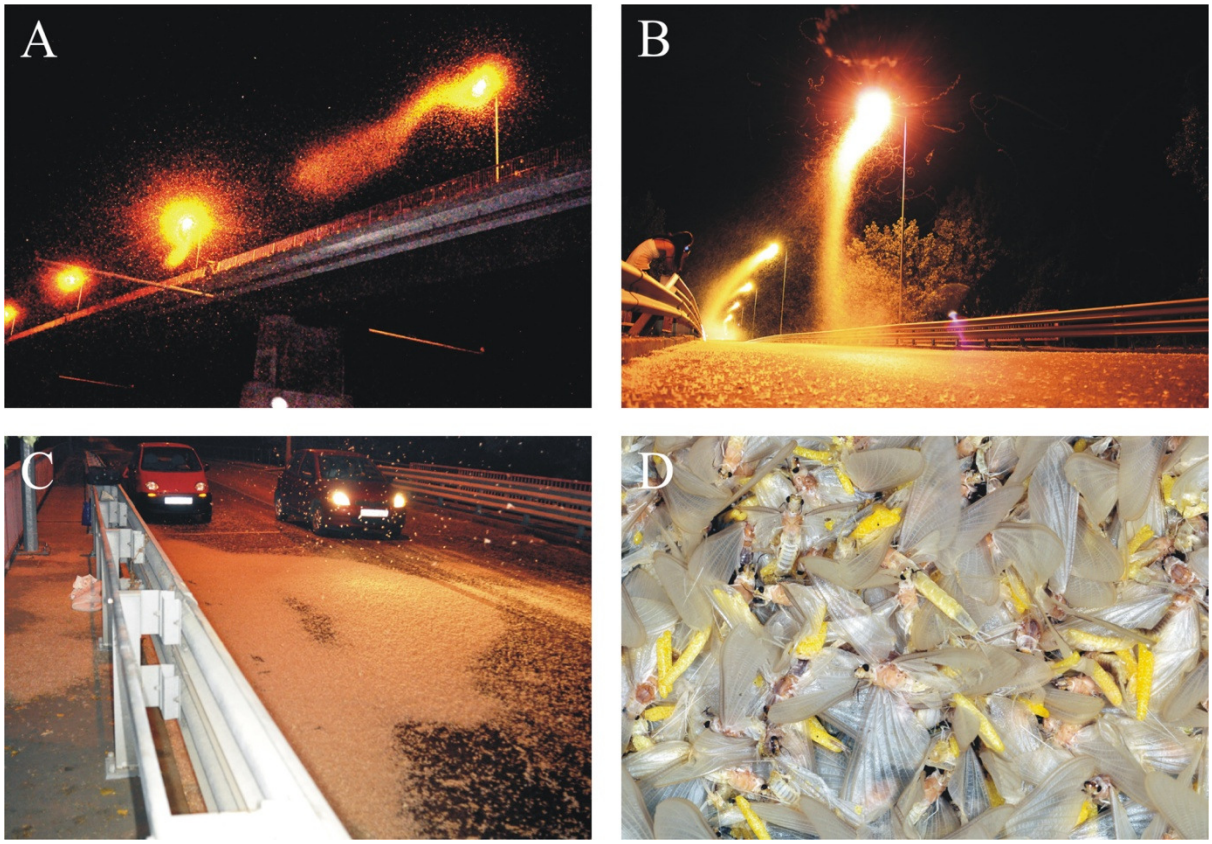

Figure 2.3: (A) Mass swarming of *Ephoron virgo* mayflies at night in Tahitótfalu (Hungary) at a bridge overarching the river Danube. (B) During the swarming we could observe that female mayflies performing their compensatory flight, flew up to the bridge-lamps. One part of females reaching the bridge landed on the asphalt road to oviposit, whereas the others joined to the swarm of several thousands individuals around the bridge-lamps. (C) With the progress of mass congregation the ovipositing females covered an increasing area of the asphalt road of the bridge. The mass of mayflies containing already perished and still ovipositing individuals formed large, extended, white stains. (D) The yellow egg batches are easy to recognise in the white crowd of mayflies, that consisted of several thousand eggs each.

2.3.2. Sex-dependent behaviour

Based on the sex ratio determination of the collected mayfly carcass samples on the bridge, the vast majority of the fallen mayflies were females (99.0 ± 0.03% = mean ± standard deviation, Fig. 2.3D). This shifted ratio compared to the natural 50-50 % male-female occurrence can be explained by the compensatory flight of females. The majority of upstream-moving *Ephoron virgo* females flew directly to the bridge-lamps where they formed continuously growing swarms. A smaller proportion of the compensatory-flying females landed on the asphalt road where they oviposited and perished within 15 minutes.

The compensatory flight in the vicinity of the bridge ceased every night at 21:30 h, thus after this time, the swarm around the bridge-lamps did not grow further. However, the swarming at the lamps did not stop at this time, it continued until 23:30 h. As the swarming progressed, more and more females landed on the asphalt surface and laid their yellow egg batches. After a while, the road was covered by several-cm-thick layer of white mayflies and yellow egg batches in increasing areas (Fig. 2.3C,D). The abundance of the landed mayflies was so high that the newly arriving females could only land on the top of the already oviposited and/or perished individuals. The layer formed by the vast amount of mayfly carcasses and eggs depolarized the asphalt-reflected light as seen in the patterns of the degree of polarization in Fig. 2.4. The non-polarizing or only weakly polarizing parts of the road are marked in white or light-grey shades. This depolarizing phenomenon practically eliminated the polarization signal of the asphalt surface. The layer of the fallen mayflies was the densest right below the bridge-lamps, which suggests that beyond the polarization signal, the light intensity was also an important cue that governed the behaviour of the swarming females.

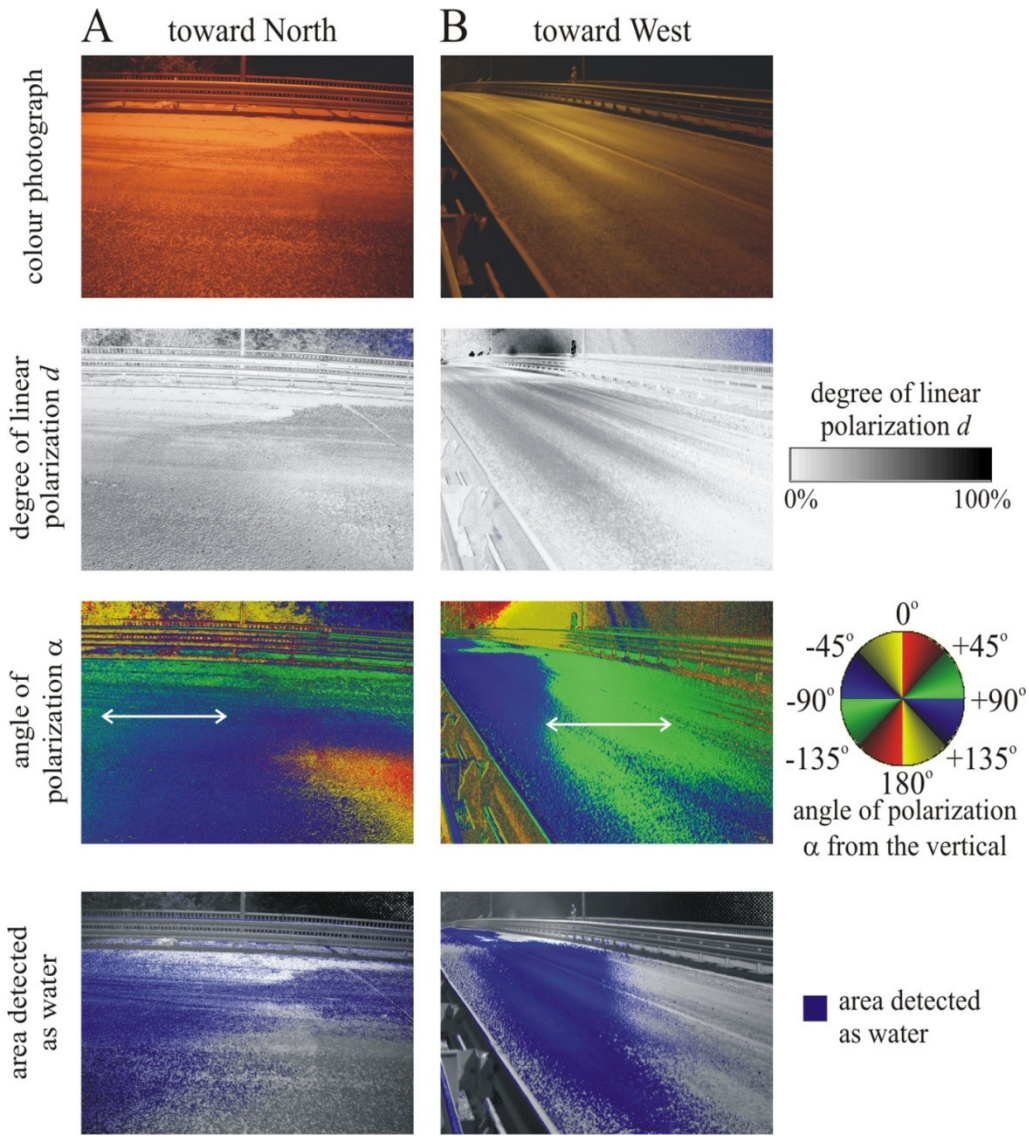

Figure 2.4: (A, B) Colour photograph, patterns of the degree *d* and angle α (clockwise from the vertical) of linear polarization, and areas detected polarotactically as water (for which $d > 15$ % and $80° < \alpha < 100°$) of the dry asphalt road on the bridge (above the river Danube at Tahitótfalu) illuminated by bridge-lamps at night during the mass congregation of *Ephoron virgo* mayflies. The patterns were measured by imaging polarimetry in the blue (450 nm) part of the spectrum from two different directions of view, when the optical axis of the polarimeter pointed toward North (A) and West (B). The angle of elevation of the optical axis of the polarimeter was 20° from the horizontal. In the α-pattern the local direction of polarization of asphalt-reflected light is shown by a double-headed arrow. The white spot composed of millions of *Ephoron virgo* carcasses on the asphalt road below the bridge-lamp is well visible on the photographs as well as in the patterns of the degree of polarization *d* and the area detected as water.

Male subimagos started to emerge every day about an hour before the arrival of the female compensatory swarm. After emergence they sought and landed on non-polarizing (d < 5 %) surfaces, such as the grey, matte concrete pavement running on the southern edge of the bridge where they moulted to imagos (Fig. 2.5). After moulting, male imagos flew to the lamps and joined the main mayfly swarms.

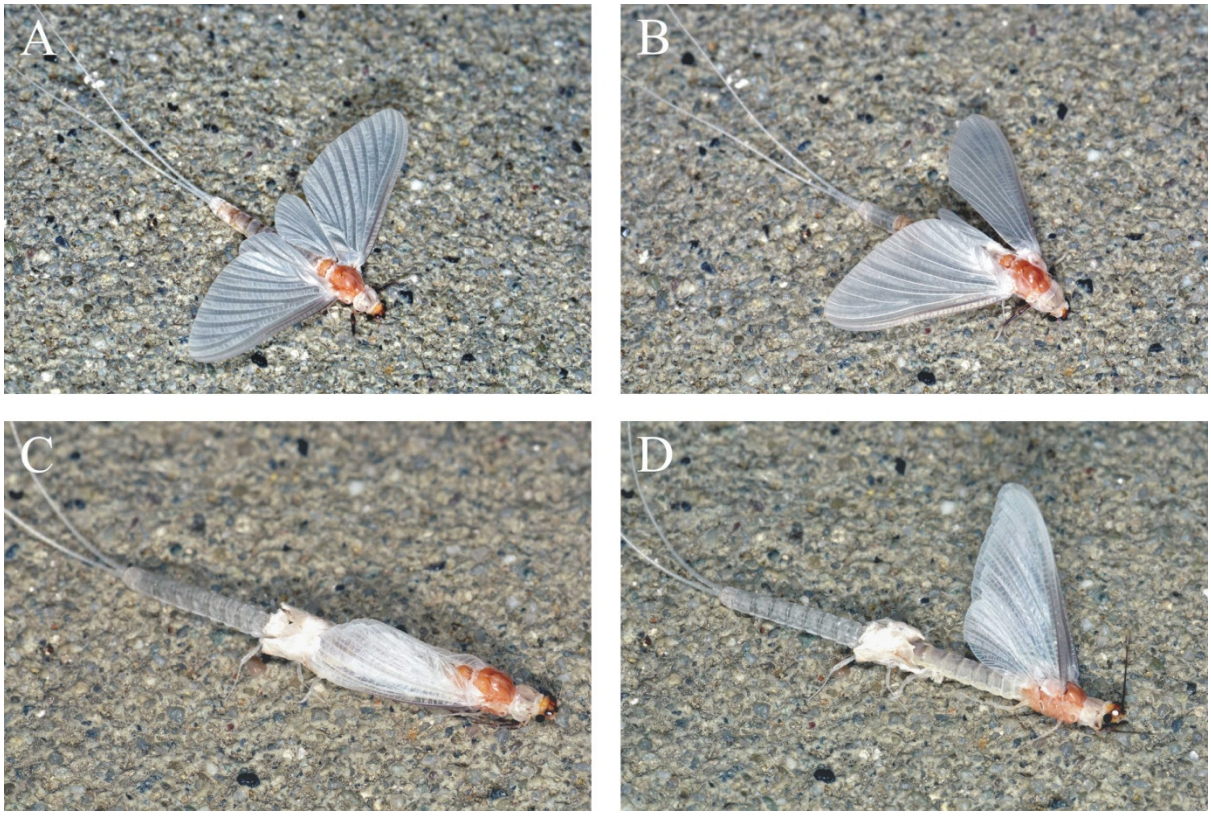

Figure 2.5: Photographs of a male subimago of *Ephoron virgo* mayfly moulting to imago (A: start, D: end) on the light grey, matt, non-polarizing (d < 5 %) concrete pavement of a Danube bridge. The subimago is a metamorphic phenotype of the sexually immature male.

2.3.3. Experiments with hand-held flashlights

When the compensatory-flight of females reached its peak intensity, we pointed a beam of flashlight towards the arriving mayflies in the direction of the river mid-line. The flashlight attracted mayflies away from their original flight direction. After repeating the experiment with the swirling swarms around the bridge-lamps, the concentrated intensity of flashlight beam could attract again several hundreds of individuals (counted on photographs) from the main swarm towards the center of the beam. The distracted mayflies continuously followed

the beam after being redirected. Once the flashlights were turned off, the swarms associated with the beam immediately broke up and the mayflies rejoined the main swarm from where they had been distracted before.

2.3.4. Distribution of mayflies at bridge-lamps

After the compensatory ceased and the size of swarms around the bridge-lamps reached its maximum and stopped growing (21:30-23:30 h), the elongated tail of the mayfly swarm often reached the asphalt road. Individuals nearest to the surface were more likely to settle and oviposit on the asphalt than those close to the lamp. The concentration of living ovipositing individuals and already dead mayflies was the highest directly around the bridge-lamps (Fig. 2.3C-D). However, we also could find both living and dead mayflies on parts of the bridge which were not directly illuminated, but had a higher degree of polarization *d* of reflected light due to the less carcasses that could have depolarized the surface.

2.3.5. Behavioural responses of mayflies to polarized light sources

We took above 1500 photographs during four swarming days, on which we identified approximately 150000 individuals using our image processing software. The number of co-occurring mayflies peaked between 19:50 and 20:20 h. Depending on the swarming day and thus the general intensity of the daily swarming, the horizontally polarized light attracted on average 5-10 times more mayflies than the unpolarized one (Fig. 2.6). These differences were statistically significant according to the non-parametric Mann-Whitney U-test with the following parameters: 23 August, $N = 11582$, $U = 181$, $Z = 10.302$, $p < 0.00001$ significant (Fig. 2.6A); 24 August, $N = 22786$, $U = 674.5$, $Z = 11.388$, $p < 0.00001$ significant (Fig. 2.6B); 27 August, $N = 5425$, $U = 303.5$, $Z = 8.945$, $p < 0.00001$ significant (Fig. 2.6C); 28 August, $N = 93935$, $U = 8682$, $Z = 10.465$, $p < 0.00001$ significant (Fig. 2.6D), where N is the number of total mayfly detections, U is the parameter giving the sum of ranks used in the non-parametric method, Z is the standard deviation of data for a given p, and p is the level of significance ($p < 0.05$ means significant).

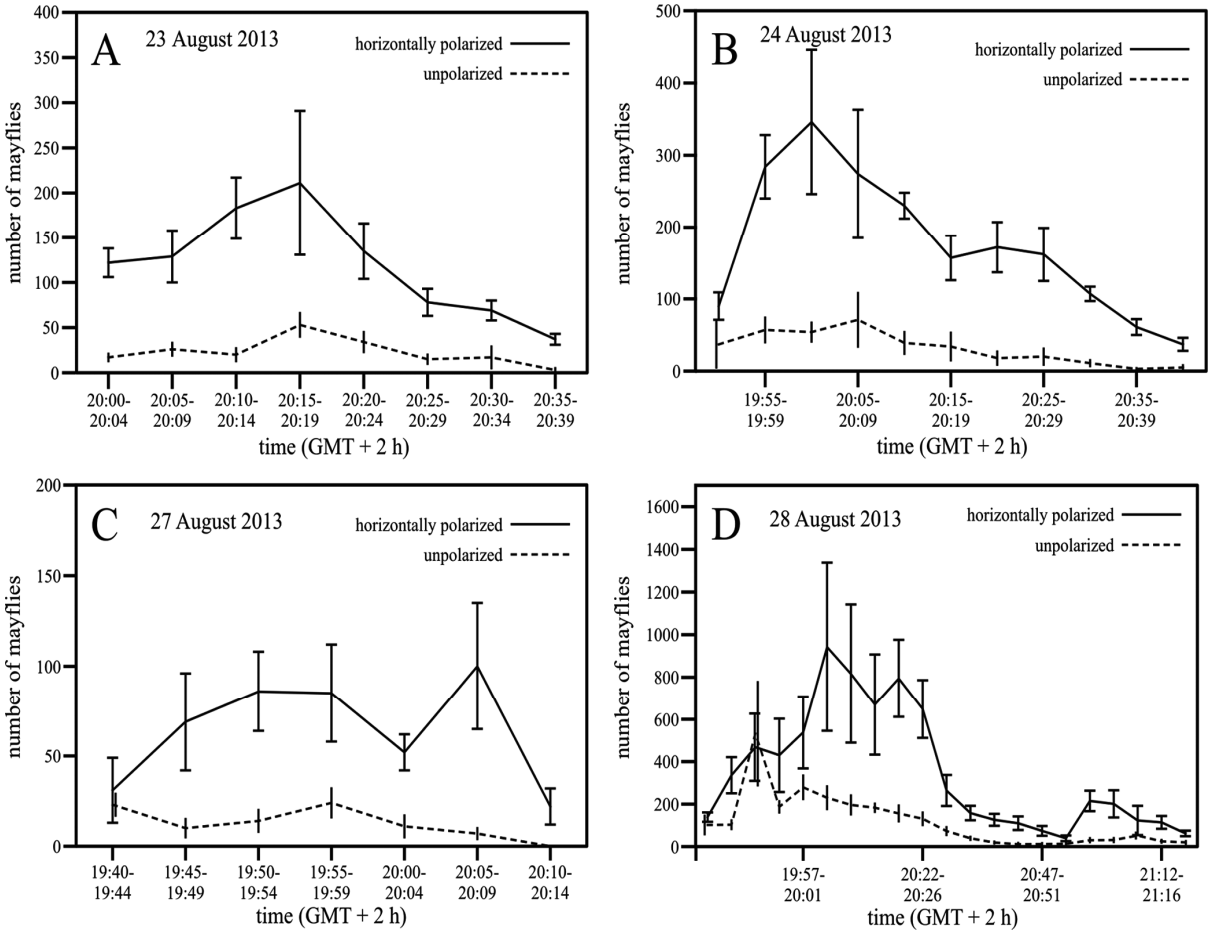

Figure 2.6: Estimated numbers of *Ephoron virgo* mayflies attracted to polarized and unpolarized light sources placed above the Danube river on four dates in 2012. Number (mean ± standard deviation) of mayflies attracted to horizontally polarized (continuous line) and unpolarized (dashed line) light as a function of time (GMT + 2 hours, where GMT = Greenwich Mean Time). Each estimate is based on 10 photographs (see Chapter 2.2.4).

2.3.6. Polarization characteristics of the bridge and the river surface

After evaluating the measured polarization patterns, we found that the river surface reflected predominantly horizontally polarized light, except for the parts where the mirror image of the bridge was reflected from the water surface. These areas were weakly (d < 15 %) and vertically polarized. The measurement was taken from downstream, the arrival direction of mayflies. From this point of view, the otherwise homogeneous horizontally polarized signature of the river was interrupted only one side of the bridge (Fig. 2.7).

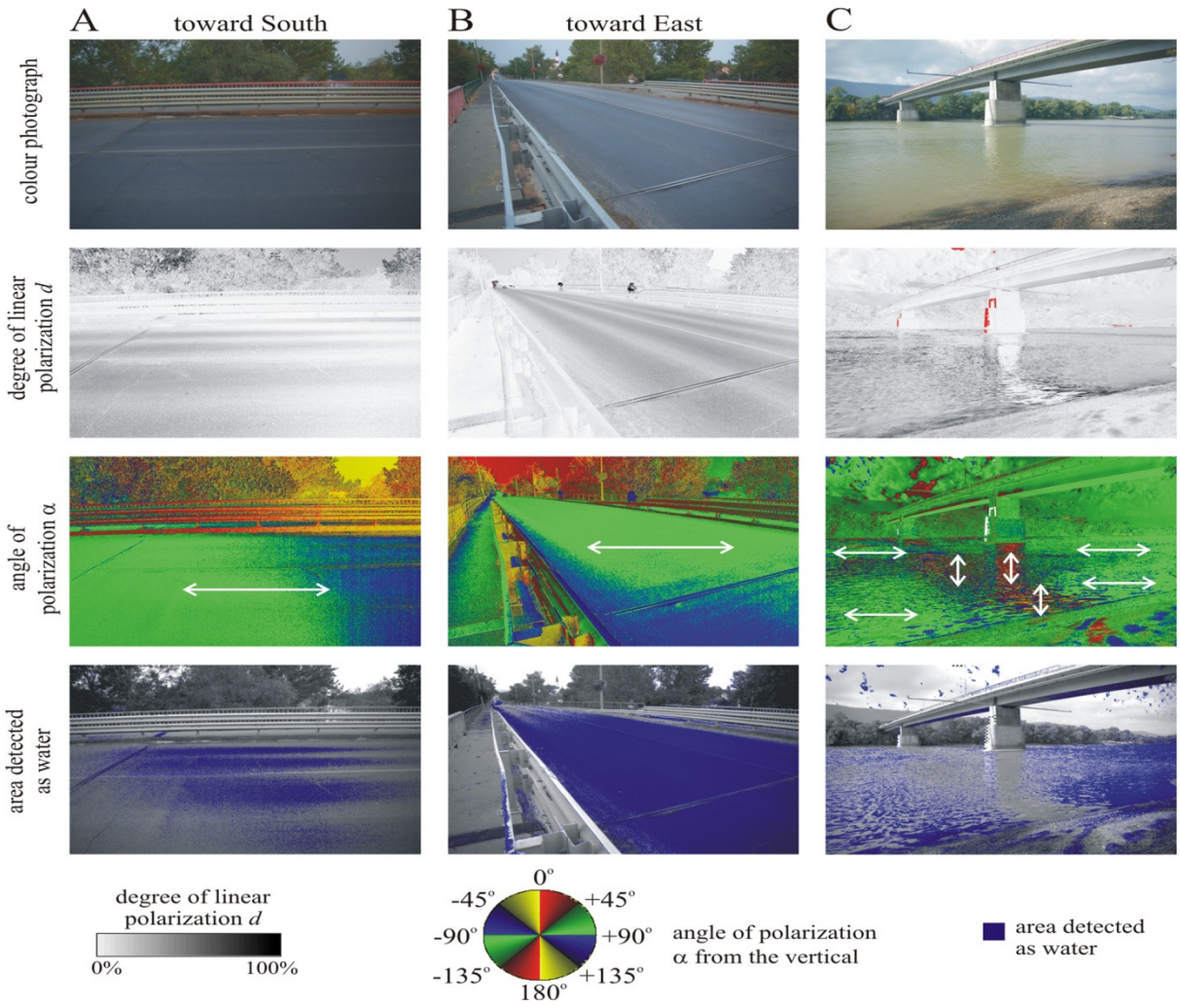

Figure 2.7: As Fig. 2.4 for the same asphalt road illuminated by light from the clear sky after sunset and measured from two different directions of view, when the optical axis of the polarimeter pointed toward South (A) and East (B). (C) As A and B for the downstream side of the bridge and the Danube river.

The asphalt road on the bridge reflected linearly (d > 20 %) and almost horizontally (80° < α < 100°, measured from vertical) polarized light from any direction. The patterns were similar before sunset, when the bridge was illuminated by skylight, and at night, when it was illuminated by bridge-lamps, in all the three (red, green, blue) spectral ranges (Figs. 2.4 and 2.7A,B). When the fallen mayflies formed a thick, white, circle-shaped layer under the lamps, parts of the asphalt covered by mayflies and their carcasses reflected entirely unpolarized (d = 0 %) light (Fig. 2.4A).

2.4. Discussion

Through our thorough observations and field experiments with torchlights of different polarization properties in the vicinity and at a bridge overarching the Danube, we have shown that *Ephoron virgo* mayflies were independently attracted both to unpolarized and polarized light sources. The performed maladaptive swarming and oviposition behaviour can be explained by their positive phototaxis and polarotaxis. The experimental work of Boda et al. (2014) and previous anecdotal observations of mass swarmings near illuminated bridges and other man-made structures along or above rivers have suggested that polarized and unpolarized light pollution should interact to attract insects to unsuitable oviposition sites in the wild. Our results represent a case study providing evidence for the occurrence of such a phenomenon.

Previous field experiments have demonstrated that the water detection of mayflies is based on the horizontal polarization of water-reflected light (Kriska et al. 1998; Kriska et al. 2007; Kriska et al. 2009), and this behaviour is a general evolutionary adaptation associated with nearly every aquatic and water-associated insect species (Schwind 1991; Horváth and Varjú 2004; Csabai et al. 2006; Kriska et al. 2006a,b; Egri et al. 2012a; Horváth 2014). During their fully developed adult life, horizontally polarized light drives both mayfly sexes to swarm and mate. It is also what drives females to oviposit on the surface of the water or the asphalt road of a bridge in our study (Kriska et al. 1998; Horváth and Kriska 2008; Málnás et al. 2011). In the case of *Ephoron virgo* mayflies, the oviposition activity was the highest where horizontally polarized light sources were generally the strongest: most directly under the high-intensity bridge-lamps, the light of which was horizontally polarized after reflection from the asphalt. Females tended to avoid unpolarized parts of the bridge (e.g. concrete pavements, pylons and sides), less illuminated areas (asphalt regions between bridge-lamps), and those parts that reflected vertically or obliquely polarized light (railings and walls). Nevertheless, male subimagos emerging from the river, that were attracted to the bridge to moult, avoided strongly polarizing asphalt and preferred the grey, matt, non-polarizing ($d < 5\%$) concrete pavement (Fig. 2.5). In the wild, they usually moult on riverbanks (Ibanez et al. 1991) that have low degrees of polarization, thus, their preference of choice is explained by their natural behaviour. These observations suggest that positively polarotactic *Ephoron virgo* mayflies might have mistakenly perceived the asphalt road as a strongly and horizontally polarizing water surface.

Málnás et al. (2011) have found that the upstream-directed compensatory flight, that females of *Palingenia longicauda* mayflies perform after moulting to imagos and emergence from the water, is guided by the long, unbroken, horizontally polarized light signature of the river. In that study, the observed mayfly species swarmed in daylight, before sunset, thus the bridge over the river was not illuminated by artificial night lights, but interrupted the continuous horizontally polarized light trail of the river by its weakly and vertically polarized mirror image on the water surface, forcing the compensatory flying females to halt and turn back. *Palingenia longicauda* females responded by forming a swarm above the water and downstream of the bridge and then they oviposited into the river. The bridge in our study created an identical break in the horizontally polarized light signature of the river, but *Ephoron virgo* females responded differently. They moved vertically upward to swarm around the bridge-lamps and above the bridge, then oviposited on the asphalt road. The explanation for this different behaviour is the following: Although *Ephoron virgo* very likely guides its compensatory flight using the same mechanism, attraction to the bridge-lamps is the consequence of the positive phototaxis elicited by the high-intensity unpolarized lights, that overwhelmed the stopping and back-turning effect of the loss of horizontally polarized signal of the river surface. This phenomenon in this species is an evidence that unpolarized light pollution near bridges is causitive in luring females away from the river surface.

Our results also suggest that unpolarized light of high intensity can be a more attractive cue than polarized light in guiding the compensatory flight of mayflies. However, the bridge-lights in our study were at a great height (about 20 m) above the water, thus there were less light falling on the water surface and becoming horizontally polarized than if unpolarized light sources were closer to the river. Consequently, the bridge height and the intensity of night lighting can alter the relative intensity of unpolarized versus polarized light cues that female mayflies perceive while approaching the bridge. In fact, we found during our experiments that close to the water surface, more females were consistently attracted to horizontally polarized light sources than to equal intensity unpolarized lights, suggesting that females weight one cue more than another in guiding behaviour. The relative importance of these two cues in triggering the evolutionary trap we documented, remained unclear and might have been dependent on the compensatory flight and oviposition behaviours separately. Nevertheless, attraction to unpolarized bridge-lamps in our study did not completely suppress the attraction of mayflies to asphalt-polarized light, since females having previously attracted to the lamps, eventually oviposited on the road. Regardless of the relative importance of different light cues, evidence based on our observations and documentations is most

consistent with a model of sequential attraction, in which *Ephoron virgo* mayflies are initially lured away from the water surface by high-intensity unpolarized light (Figs. 2.3A,B, 2.8), and subsequently attracted to illuminated asphalt surfaces eliciting polarotaxis as polarized light traps (Figs. 2.3B,C, 2.4).

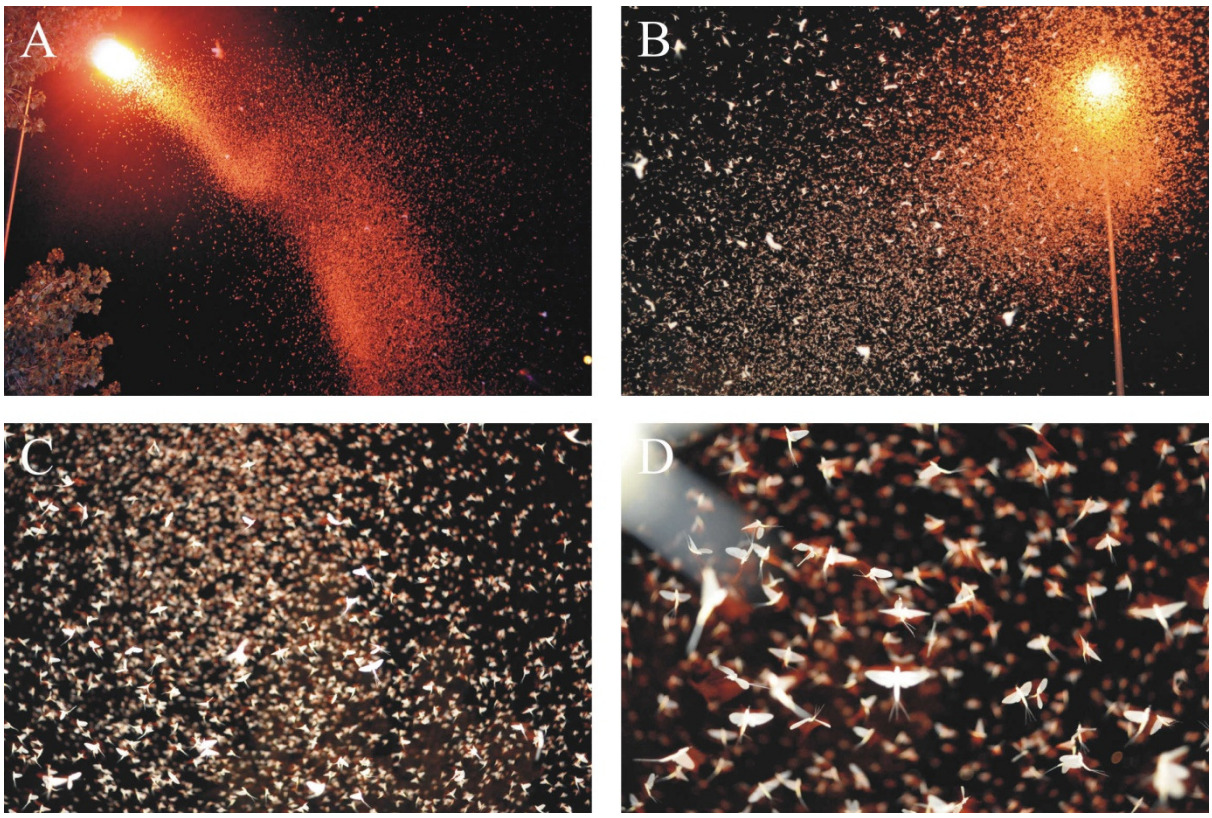

Figure 2.8: Photographs of swarming *Ephoron virgo* mayflies at one of the lamps of a Danube bridge with increasing magnification from A to D. The mass of mayflies starting at the lamp and elongating in the blow direction of the dominant slight wind continuously changed its shape. The swarm consisted of several thousands of individuals estimated by our computer program.

We measured the reflection-polarization characteristics of the river surface only in daylight, because the detector of our polarimeter was not sensitive enough under the dim illumination conditions at night. Since both the degree and the angle of polarization of river-reflected light are independent of the intensity of incident light (Gál et al. 2001; Horváth and Varjú 2004; Horváth et al. 2010c; Horváth 2014), polarization patterns of our daytime measurements were otherwise similar to those that could have observed the nocturnal mayfly, *Ephoron virgo*. Consequently, the daytime reflection-polarization patterns of the river surface (Fig. 2.7C) are

comparable with the daytime (Fig. 2.7A,B) and night-time (Fig. 2.4) polarization patterns of the studied bridge.

The intensity and spectrum of torch-light used in our experiments were different from those of the bridge-lights. Thus, the insects' reactions to torch- and bridge-light are not directly comparable. Nevertheless, the torch-light experiment demonstrated that a light beam of relatively low intensity can attract a bunch of mayflies even from bridge-lamps with the highest swarming intensity. This is an important practical result, which demonstrates that the mayflies attracted to the unpolarized bridge-lamps and polarized asphalt road can be protected by a barrier of lights composed of a series of smaller lamps with appropriate intensity, spectrum and polarization positioned at an appropriate height above the river surface, being lower than the bridge illumination. The flying mayflies are expected to detect this cue first and gather in the beams of this protecting light barrier, rather than of the bridge-lamps.

Polarized light pollution can occur in the absence of unpolarized artificial nocturnal lighting, as well, when moonlight is reflected from artificial polarizers (e.g. asphalt, solar panels, etc.), yet this kind of photopollution can only be as intense as the unpolarized light source, so, artificial polarizers illuminated by high-intensity street-lights will often be more attractive than those illuminated by the Moon (Boda et al 2014). The emergence and activity of aquatic insects often decline when the moon is full (Bowden 1981; Bowden 1982; Eisenbeis 2001) and so the attractiveness of the evolutionary trap we documented might have actually be mitigated during bright moonlit nights. Despite this, we experienced larger numbers of mayflies in the swarms at or around full moon, which suggests that illumination coming from above could be a driving force for mayfly larvae to moult into imagos or subimagos. High- and low-pressure sodium, metalhalide and LED lights are all common forms of unpolarized nocturnal lighting that vary in the wavelengths of light they produce (Gaston et al. 2013) and based on this, they vary in the attractiveness to different aquatic insect species (Schwind 1995).

Light pollution has a broad range of negative impacts on animal populations and biodiversity. Its most general effect is to restructure freshwater food chains by removing elements and to alter the function of freshwater ecosystems (Longcore and rich 2004; Moore et al. 2006; Perkin et al. 2011). In our case, this is compounded by the existence of an evolutionary trap. Evolutionary traps are rapid environmental changes, that reduce the fitness of animals by forcing them to alter their formerly reliable behavioural cues (Schlaepfer et al. 2002; Robertson and Hutto 2006). Since traps are highly attractive to the concerned

individuals, they can act to crash populations of affected species more rapidly than other causes of habitat degradation, mortality or reproductive failure (Fletcher et al. 2012), making them a quickly emerging conservation issue (Schlaepfer et al. 2002; Robertson et al. 2013).

The general solution of this problem is to eliminate the concerned evolutionary trap that can be accomplished by a) eliminating the attractive behavioural cues, b) increasing the fitness consequences of responding to cues or c) both (Robertson 2012; Robertson et al. 2013). In our case, the asphalt road of the bridge cannot be made suitable for mayfly reproduction, thus only the elimination of the trap is the only solution of the problem. This can be executed through the reduction and control of unpolarized and polarized light cues. Complete removal of lights from this bridge would be a simple and reasonable way to solve the issue. However, if bridge-lighting is necessary for safe driving on a bridge with traffic, switching off the lights is out of option. Bridge-lamps would likely attract fewer insects from the river surface if they were located closer to the road surface and shaded or otherwise directed downward towards the road and away from the river. An extra row of lights at the base of the support pylons with a beam pointing towards the river could preferentially prevent mayflies from flying up to the elevated road surface lighting and would ensure that they properly oviposit on the water. The drawback of this method is that it could attract predators which consume ovipositing females and thus another evolutionary trap via a different mechanism could be formed (Young and Watt 1996; Metcalf et al. 1997). Concrete roads and asphalt roads with a high gravel content are poor polarizers (Horváth et al. 2010c) and so resurfacing bridges with these materials would likely reduce or eliminate nocturnal polarized light pollution, but mayflies would still be attracted to unpolarized bridge-lights where they may experience enhanced predation and/or exhaustion (Eisenbeis 2006; Moore et al. 2006), potentially distracting them from mating or ovipositing (Kriska et al. 2008).

Regarding the high number of eggs laid by ovipositing *Ephoron virgo* mayflies, the studied bridge (alone) is unlikely to represent a threat to the population or the offspring generation in the Danube (Bij et al. 1992; Kureck and Fontes 1996). However, on river sections with a higher proportion of similar illuminated riparian structures (especially in larger cities), reproductive success can be decreased so dramatically (Perkin et al. 2011) that populations could decline. More importantly, the generality of aquatic insect attraction to horizontally polarized light suggests that evolutionary traps formed by this dual driving cue have similar impacts on other aquatic insect species and can cause declines in the populations which are smaller, or the survival strategy of which makes them more susceptible to increased mortality or reproductive failure (Horváth and Varjú 2004; Horváth 2014). Since

attraction to linearly polarized light has also evolved in many non-aquatic arthropod species for the purpose of orientation or navigation (Horváth and Varjú 2004; Horváth 2014), nocturnal polarized light pollution may be a significant conservation problem even for entirely terrestrial arthropod species. It is still unclear, whether the negative demographic impacts of evolutionary traps are sufficiently severe to reduce mayfly abundance in a river. Demographic models that illustrate the potentials of traps to reduce population growth in wildlife have been developed only for vertebrates with longer lifespan. Empirical studies are entirely lacking.

2.5. Further Studies

In this chapter, I have shown the results of our observations and field experiments concerning the swarming behaviour and polarization sensitivity of the night-swarming mayfly, *Ephoron virgo* performed in the years 2012 and 2013. Our results have provided evidence of an ecological and evolutionary trap driven by dual optical cues, polarotaxis and phototaxis, the simultaneous attraction of which is stronger to mayflies than that of each optical signal alone. I have described the ecological importance of this issue and suggested some methods for protecting mayflies from approaching the bridge-lamps. In the later years, we continued the field experiments, where I was involved in studying the attraction of *Ephoron virgo* to vertically polarized light sources (Farkas et al. 2016) and based on our results, we started to develop the method and prototype of a light barrier that could protect any night-swarming mayfly species from being perished by the ecological trap of illuminated bridges (Egri et al. 2017). The detailed description of these studies were out of the scope of my thesis.

Chapter 3.

Accuracy of Sky-polarimetric Viking Navigation

3.1. Introduction

Between the 9th and 13th century, the northern area of the Atlantic Ocean was ruled by Viking seafarers. They discovered Iceland and Greenland, where they established colonies and reached the coasts of North America, as well. Due to the harsh environment, the colonies depended on trading with the motherland, thus a continuous trading route had to be maintained. To cover such a long distance, the Vikings needed to keep the sailing route accurately. However, it is a mystery, how they could orient themselves during the several-week-long journey before the magnetic compass and other modern navigational equipments appeared in Europe. In this chapter, I introduce the famous hypothesis of sky-polarimetric Viking navigation, a method that has been accepted for decades by the scientific community without knowing its accuracy. During my PhD work, I measured the error function of the different steps of this navigational method and determined the resulting error propagation through the four steps of sky-polarimetric Viking navigation under different weather circumstances and for three different sunstone crystals.

3.1.1. The Viking age

The Vikings, the ancestors of the Danish, Swedish and Norwegian people, originally inhabited the Scandinavian Peninsula and Jylland Peninsula, where they established their settlements within the upper areas of the well-navigable fjords. Even Tacitus and Plinius characterized these people of their bravery and lust for adventure in the 1st century. Although, they lived on agriculture and livestock breeding, they also traded with the surrounding coastal folks. Besides, they were excellent ship-builders and were good at weapon crafting. Travelling on water became a determinant factor for them, which was necessary because of their feudal system, in which the land was undivided and had to be inherited by the oldest son (Brøndsted 1983; Pörtner 1983). The excellence of their ships is proved by famous shipwrecks, such as the Oseberg or the Skuldelev ships (Olsen and Crumlin-Pedersen 1978).

As an easy and profitable way of getting by, they raided coastal settlements in the area of the British Islands, when the sea was calm enough for sailing. The most well-known case of invading was the raid on the closter of Lindisfarne in 793. After that point, the Vikings became dreaded and the Viking era is registered. Despite their notorious fame, not every Viking was fond of robbery and murder, some of them set sail just to discover new regions or get a job as mercenaries. They reached the coasts of the Black Sea in the East, arrived at Shetland and Orkney Islands around 820, discovered the Feroer Islands then Iceland in 861 and Greenland in 982 (Brøndsted 1983; Pörtner 1983; McGovern et al. 2007).

Iceland provided green pastures for sheep breeding, rivers full of fishes and forests to gain wood for building settlements. The Southern coast was heated by the Gulf Stream which benefited the agriculture (Diamond 2007). The other regions of the island, however, was uninhabitable due to the thick ice coverage and volcano activity (Dugmore et al. 2007; Behringer 2010). On Greenland, the South-Western side was free of ice, where the Vikings could establish the Eastern and Western Settlement (Pörtner 1983; McGhee 1984; Vésteinsson et al. 2002). The climate was too harsh for wheat growing, they bred goat, sheep and horse instead. Hunting played a vital role in the colonies' life, they earned seal skin, polar bear pelt and walrus fang, that could be traded in the European markets (Brøndsted 1983; Diamond 2007; Ogilvie et al. 2009). Since, the summer in Greenland was restricted to a couple of weeks, trading became essential to survive in the colonies. Thus, they had to maintain a continuous trading route between the colonies and the Scandinavian motherland along the 61° latitude.

Nowadays, the North Atlantic region is covered in ice most of the year, thus, maintaining such a trading route would be possible only in the summer months. However, the Viking age fell into the period of the Medieval Climatic Optimum, which was a warm period between the 9th and 13th century, when the average temperature was 1-2 °C warmer than today (Lamb 1965; Hughes and Diaz 1994; McGovern 1997; Ogilvie et al. 2000; Behringer 2010). The temperature of the ocean could be 2-4 °C warmer in the region, making the area navigable between the spring and autumn equinox. The start of the climatic optimum dates back to between 650 and 880, while the end was around 1030-1220 (Grove 2001). Pollen analyses have shown, that in the Scandinavian region wheat was grown up to 63° latitude and wheat was grown up to 70° latitude during the climatic optimum (Lamb 1965; Hughes and Diaz 1994; Behringer 2010).

The Vikings disappeared from Greenland in the middle of the 15th century. In this process, among others, the decline of climatic circumstances played an important role. From

1270, the weather changed for the worse, summers were always colder and agriculture collapsed (McGovern 1991, 1997; Grove 2001; Broecker 2001; Bradley et al. 2003; Orlove 2005). In the beginning of the Little Ice Age, the Vikings left their colonies in Greenland, since they could not care for themselves and the former trading routes could not be maintained anymore (Behringer 2010; Ribeiro et al. 2012). The final abandonment of Iceland is regarded to the elevated volcanic activity between the 13th and 16th century (Hammer et al. 1981; Crowley et al. 2008).

3.1.2. Viking navigation

In the Viking age, travelling on the open ocean was extremely dangerous. Without detailed navigation maps, magnetic compasses and light towers, they risked their life during every journey. According to written sources, their sailing routes, however, ended with success in most of of the times. This means that they found a way to keep direction and navigate accurately, in spite of the fierce circumstances. The average speed of a 20 m long Viking ship is estimated to 11.5 km/h, with which it could cover a distance of 275 km per day (Ingstad 1972; Pörtner 1983).

For short-time navigation along the coastline, the Vikings might have aligned themselves to natural objects e.g. mountains, bays, islands, specific trees and stones, they could follow the routes of certain animals, such as whales and birds, as well (Pörtner 1983; Thirslund 1997; Horváth et al. 2014a). Their open-sea navigation method is, however, barely known. They surely used cardinal direction but not in the same way as we do today. They might have selected reference points (a well-known mountain or island) and gave the directions with respect to that (Thirslund 1997). In the Viking age, the position of the star, Polaris differed from the geographical North Pole by 6°, thus it could not have been used for accurate navigation at night (Horváth et al. 2014a). They gained knowledge gradually about sailing duration between known places, about tides, ice and climate and this knowledge spread by saying.

Vikings might have been familiar with typical atmospheric optical phenomena in the Northern Atlantic Ocean. Mirages could help the seafarers to glance the mountains of an island from large distances (Sawatzky and Lehn 1976, Horváth et al. 2014a). In the northern region, superior mirages are typical, which form when the air temperature is low close to the surface and rapidly increases with height, causing a temperature inversion. The low surface temperature is caused by the cooling effect of ice, snow or cold sea water. The refractive

index of light is different in the air layers with different temperatures and this multiple refraction results in the appearance of the mirage image of a distant island or mountain in an elevated upside down position. In rare cases, a second image of the object is observable above the former in a straight and more elevated position. These elongated images of the real object could help the Vikings to notice objects that are originally below the horizon due to the curvature of the Earth's surface (Lehn and Schroeder 1979). Since superior mirages are frequent today, they were supposed to occur in the Viking era, as well. Nevertheless, there is no scientific evidence that the Vikings used this phenomenon for navigation.

The only archaeological evidence related to open-sea Viking navigation is a fragment of a wooden dial, which was found in the vicinity of the one-time Eastern Settlement in Greenland in 1948. The artifact was prepared around 1000 and turned out to be part of a navigation equipment, a sun-compass (Sølver 1953; Thirslund 1991, 1993). The Viking legends, the so-called sagas mention another mysterious navigation tool, called sunstones, which help the sailors to find the Sun in the sky even under overcast circumstances, as also mentioned in the legend of King Olaf, the Holy. Although, no archaeological findings have come to light, the existence of sunstones is scientifically imaginable. Combining these two instruments, the Danish archaelogist, Ramskou (1967) came up with the hypothesis of sky-polarization Viking navigation, that has became popular and accepted in the last decades, without knowing how accurately this method could work.

3.1.3. The Viking sun-compass

The sun-compass fragment found in Greenland at the fjord Uunartoq was originally a wooden dial made of spruce or larch with a diameter of 70 mm with a hole in the middle of 17 mm diameter. The outer rim of the dial was covered with triangular carvings at nearly equal distances. First, the finding was believed to be a part of a contemporary ornament but after forensic trace analysis, superficial lines were discovered that were carved deliberately and not the results of random damages. The significance of these lines has been proven and were connected to navigation (Sølver 1953). According to Sølver, a shadow caster, so-called gnomon was placed into the hole in the middle of the dial and the tip of this gnomon shadow followed the lines on the surface. One straight line referred to a specific date, the spring equinox, and a hyperbolic line symbolized the summer solstice being pre-carved into the surface. The other carvings were supposed to be guidelines for compass-preparation. To use this equipment, the Viking navigator had to know the date of the departure and the length of

the journey and had to carve the corresponding gnomonic line into the dial surface. When the tip of the gnomon shadow reached the line, a well visible marking (coinciding with the mirror symmetry axis of the hyperbolic gnomonic line) showed the reference direction. Then, on the open ocean, the navigator had to rotate the sun-compass until the shadow tip reached the appropriate gnomonic line and the reference marking showed the direction to their destination. The same line could be used only for a couple of days, thus for longer journeys several shadow lines were necessary (Sølver 1953, 1954). This hypothesis is corroborated by the fact, that other primitive sun-dials were found in the one-time Viking habitat.

Figure 3.1: Photograph of the wooden dial fragment found at the fjord Uunatroq in 1948.

3.1.4. An alleged instrument: the shadow-stick

Every application of the Uunartoq artifact requires sunshine for the formation of shadow of the central gnomon. However, according the theory of Ramskou (1967), the sun-compass could also be used when the sky was occluded by clouds or fog and the gnomon shadow could not be seen. Under these circumstances, the Vikings not only had to determine the Sun's position but they also had to replace the shadow to make the sun-compass functional

again. One solution for replacing the shadow is to hold a torch at the solar elevation of the occluded Sun, however the measurement with a gnomon shadow cast by the continuously moving torch flame would be rather inaccurate (Horváth et al. 2008b). Another logical solution would be the application of a shadow-stick being an elongated arrow-shaped bar made of stone, wood or ivory with pre-carved holes on its surface. The holes would denote different solar elevations and by fitting the stick with the corresponding hole to the gnomon, its length could refer to the unseen shadow length, making the sun-compass fully functional (Bernáth et al. 2013). We do not know of such an archaelogical finding, however there are medals and jewelries with holes on their surface in museums from the Viking age that resemble the hypothetical shadow-stick.

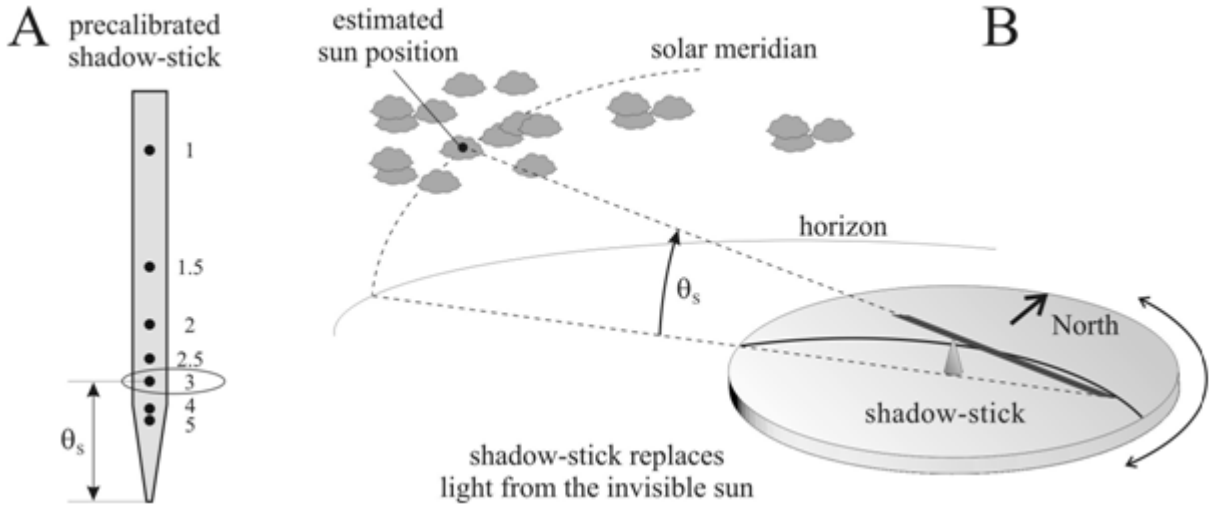

Figure 3.2: Model of the hypothesized shadow-stick with which the gnomonic shadow could be replaced in cloudy weather.

3.1.5. Estimation of the Sun's location based on the intensity patterns of clouds

In cloudy or foggy weather, the key element of sky-polarimetric Viking navigation is to find the occluded Sun. Some scientists agree that the Vikings could determine its position with several simple methods, without the need of complicated instruments (Roslund and Beckman 1994). One of this method was to estimate the Sun's position by the intensity patterns of the clouds seen with the naked eye. After knowing this position, they could use the sun-compass for navigation again. Another guide to find the Sun was the Tyndall effect, an atmospheric optical phenomenon, where light beams diverging from the Sun could refer to its position. In this phenomenon, scattered light does not reach the eye from sky areas covered with clouds,

while from clear parts the scattered light can reach the eye unhindered (Minnaert 1993). Since these beams point towards the Sun, it is easy to find behind the clouds (Horváth et al. 2014a).

Barta et al. (2005) measured in two psychophysical experiments, how accurately the Sun can be determined by naked eye. They used colour photos of 35 different sky situations with 180° viewing angle, which were taken in Oulu, the island of Hailuoto in the Scandinavian region. In all photos, the Sun was covered by clouds and the task of 18 test persons was to estimate the Sun's position on a computer screen only by the light intensity patterns of the clouds. The maximal errors of the angular distance between the real and estimated Sun position in the experiments ranged between 8° and 163° depending on the sky situation. In situations having only thin clouds, the estimations had an average standard deviation of 1°, while the standard deviation of situations with thick clouds was 20-25°. The explanation for this large difference is that through thin clouds a bright patch of light is well visible in the immediate vicinity around the Sun. The thicker the clouds are, the less intense this light patch is around the Sun. At low solar elevations (around twilight or dawn) the maximal error of the angular distance between the real and the estimated Sun position ranged between 2.1° and 99°, while their standard deviations ranged between 0.6° and 42°. In situations with the Sun below the horizon, position determination became more inaccurate (Barta et al. 2005).

These results suggest, that determining the Sun position behind the clouds is not as simple and accurate as Roslund and Beckman (1994) has previously imagined. Navigation in the open ocean solely with this method would be problematic and very erroneous.

3.1.6. Viking navigation based on Haidinger's brushes

A different way to locate the Sun is to use the pattern of the angle of polarization of skylight being almost identical under any meteorological circumstances (Horváth et al. 2008b, 2011a; see subchapter 3.1.9.). Many animals use this characteristics and orient themselves by means of skylight-polarization (Hotváth and Varjú 2004; Horváth 2014). Mammals and thus humans, usually are not able to perceive light polarization. The only exception is the optical illusion of Haidinger's brushes. This two blue and yellow 8-shaped figures are formed due to of the radial orientation of photoreceptor axons in the fovea of the human retina and are mediated by dichroic carotenoids in the macula lutea (Foster 1954; Sloan and Naquin 1955; Lester 1970; Zhevandrov 1995; Fairbairn 2001; Horváth and Varjú 2004; McGregor et al.

2014). When someone moves their head sideways, they will detect blue brushes parallel to the direction of polarization of the stimulus and yellow brushes perpendicular to the direction of polarization, with an angular extension of 5°. If someone looks at the clear blue sky from which light with high enough degree of polarization d originates (for example, at 90° from the Sun, where d is maximal), the yellow Haidinger's brushes can be perceived, while the blue brushes are practically invisible, because the intensity of the blue sky fades them. The blue brushes can only be perceived if the sky is not blue, that is around sunset or sunrise when large portions of the sky are red and orange, or when the sky is covered by clouds or fog. However, in the latter cases the d of skylight can be so low that it falls below the perception threshold d^* of Haidinger's brushes (Hegedüs et al. 2007a,b; Horváth et al. 2011a, 2014a). The brushes are visible with the best contrast when d approaches 100 %, for instance looking at a white LCD computer screen which employs a linear polarizer as part of the image-forming technology (Ovcharenko and Yegorenkov 2002; McGregor et al. 2014).

Using Haidinger's brushes to locate the Sun is a sound idea and has the advantage that Viking navigators did not need any additional optical instrument (e.g. calcite, cordierite or tourmaline sunstones, see subchapter 3.1.8.) to analyse sky polarization, because they had their own analyzer embedded in their eyes. The weakness of this hypothesis is that the Haidinger's brushes are very faint and fade quickly within a few seconds due to visual adaptation. But they can be perceived again for some seconds if the fovea of the eye is restimulated by polarized skylight after changing the position or orientation of gaze in the sky by moving or rotating the head.

Temple et al. (2015) measured the degree of polarization threshold d^* at which humans could just detect Haidinger's brushes. They found that participants were, on average, able to perceive the brushes at a threshold of $d^*_{ave} = 56 \pm 3$ %, and there was a normal continuous distribution of threshold values extending down to as low as $d^*_{min} = 23$ % and up to as high as $d^*_{max} = 87$ %. Applying these finding, Horváth et al. (2017) studied the atmospheric optical prerequisites of this Viking navigation hypothesis. They analysed 1296 different meteorological conditions measured by full-sky imaging polarimetry with different solar elevation angles θ and cloud coverage ρ in Hungary. From the measured d-patterns of a given sky, they determined the proportion of the sky for which $d > d^*$, that is for which the Haidinger's brushes can be perceived. Providing that the navigators could perceive Haidinger's brushes the best among Vikings (with $d^* = 23$ %), the proportion of the sky suitable for perceiving them was high under numerous meteorological conditions, particularly when the Sun was low on the horizon ($\theta \approx 0°$) and when the sky was clear of clouds ($\rho \approx 0$

%). When the Sun was below the horizon ($-5° \leq \theta < 0°$), and therefore not possible to be seen or accurately located, the mean proportion of the sky suitable for sky-polarimetric navigation with Haidinger's brushes was between 26.4 % and 76.2 %, depending on the cloud coverage (Horváth et al. 2017).

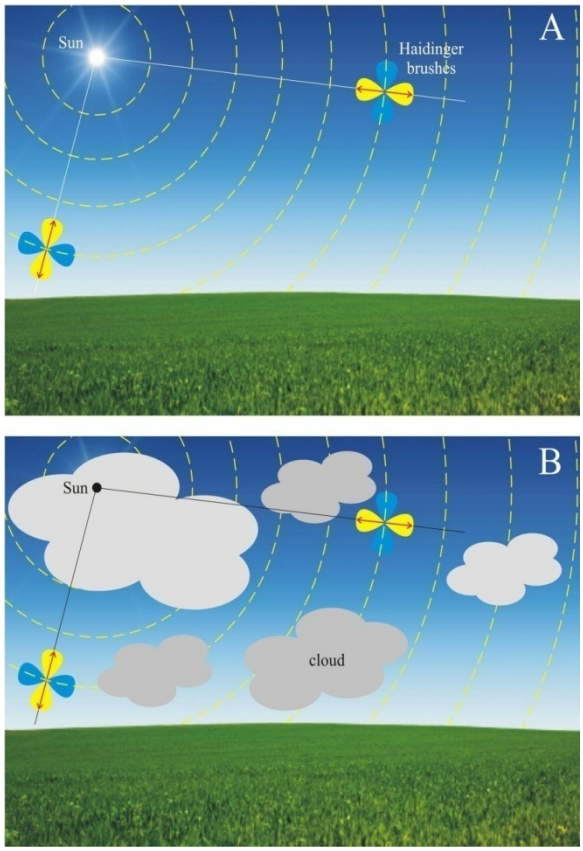

Figure 3.3: Principle of sky-polarimetric Viking navigation based on Haidinger's brushes. (A) Clear sky. (B) Cloudy sky. Yellow bars: local direction of polarization of skylight. Red double-headed arrow: axis of mirror symmetry of the yellow Haidinger's brush being perpendicular to the direction of polarization. The symmetry axis of the blue Haidinger's brush is parallel to the direction of polarization (Figure reused from Horváth et al. 2017).

To decide whether this method could have actually been used for reliable navigation, further factors needs to be determined. For example, it is questionable whether the few seconds before Haidinger's brushes fade when looking at the polarized sky with a fixed head are enough to determine the position of the occluded Sun in the sky. It would be worth studying the accuracy and reliability of Viking navigation based on Haidinger's brushes under real open-air conditions that can be the task of a future study.

3.1.7. The hypothesis of sky-polarimetric Viking navigation

If the Vikings wanted to survive several-week-long voyages, they had to find a way to orient themselves accurately. One tool to do this was the Uunartoq artifact, the sun-compass, which was effective in sunny weather. Under thick clouds or fog, this compass did not work alone. However, with the supplement of a hypothetical shadow-stick, the unseen gnomon shadow could be replaced, if the navigator found the occluded Sun. Previous studies have shown, that estimating the Sun position with the naked eye using the intensity pattern of the sky is not accurate enough (Bernáth et al. 2015). Another way of detecting the Sun is based on the polarization pattern of skylight, that would be accurate enough. However, the naked human eye can perceive polarization only through the optical illusion of Haidinger's brushes and the meteorological prerequisites for their perception occur too rarely for accurate navigation (Horváth et al. 2017).

In the Viking legends, there was a frequently mentioned mysterious tool, the sunstone, with which the Sun could be detected behind the clouds (Foote 1956). This tool might have perfectly completed the sun-compass to make it usable under overcast weather circumstances. Ramskou (1967) hypothesized that these stones might have been dichroic or birefringent minerals with which the polarization of skylight could be analyzed. Based on these crystals that were available in the onetime Viking habitats, sunstones could have been made most possibly of dichroic cordierite, tourmaline, andalusite or birefringent calcite (Walker 1978; Schaefer 1997; Wild and Fromme 2007; Ball 2011; Hawthorne and Dirlam 2011; Karman et al. 2012; Ropars et al. 2012). Looking through these crystals, the Vikings might have seen the periodic change of the intensity of transmitted skylight that refer to the angle of polarization α. This phenomenon is more intense when the degree of polarization d is higher. Combining the sun-compass with the application of sunstones and the shadow-stick, we get the hypothesis of sky-polarimetric Viking navigation. This theory has been cited and accepted for decades (e.g. Kreithen and Keeton 1974; Wehner 1976; Können 1985; Schaefer 1997; Vilhjálmsson 1997, 1999; Thirslund 2001; Wild and Fromme 2007), but nobody measured its accuracy until very recently. The sky-polarimetric Viking navigation method consisted of the following steps:

- **Calibration step**: The Viking navigator rotated the sunstone in front of his eyes, until he found a well-recognizable alignment (e.g. where the intensity of transmitted skylight was minimal or maximal) and put a well-visible marking on the crystal surface pointing towards the Sun. Due to Rayleigh scattering, the great circle, which

is perpendicularly to the direction of skylight polarization in any celestial point, crosses the Sun. Thus, the marking on the calibrated sunstone always points towards the Sun, even in cloudy weather.

- **First step**: Under overcast weather conditions, the Viking navigator adjusted the sunstone to the well-visible alignment used during the calibration by rotating it in front of his eyes. He repeated this action at two different celestial points, through which he could determine the directions perpendicular to the local direction of skylight polarization.
- **Second step**: At these two sunstone alignments, the previously carved markings gave the directions of two celestial great circles, in the intersection of which the occluded Sun could be found. The navigator had to determine this intersection by the naked eye.
- **Third step**: Once the position of the Sun was found, the navigator had to measure its elevation angle with his fists and fingers, in order to reproduce the Sun shadow for using the sun-compass.
- **Fourth step**: Finally, the shadow-stick of the sun-compass should be aligned parallel to the meridian (vertical azimuth plane) of the invisible Sun.

Although the Vikings surely were not aware of the meaning of sky polarization, they could easily learn the usage of such simple tools. Similarly, a lot of animals can navigate using the sky-polarization without knowing about its physics. The difference is that the instrument for perceiving polarization is located in their eyes instead of sunstones (Wehner 1976; Horváth et al. 1999; Kriska 2000; Horváth and Varjú 2004).

Before the GPS navigation became widespread, the Scandinavian Airlines used a navigation system for North determination around the North Pole, that worked similarly to the Viking sunstones. The so-called Kollsman's Sky-Compass measured the polarization of the zenith using lenses and an adequately calibrated calcite crystal. The crystal had to be rotated around its vertical axis until the transmitted intensity of the partially linearly polarized light was the brightest or the darkest. With this method, the navigator could reach higher accuracy than navigating with a magnetic compass that became inaccurate around the poles (Ramskou 1967; Horváth et al. 2011a).

Recently, a calcite crystal has been found besides navigation instruments in a shipwreck that sunk in the 16th century (Le Floch et al. 2013). Although Vikings had lived centuries before, the discovery of this crystal raised the possibility of using birefringent or dichroic crystals for navigation before the appearance of the magnetic compass in Europe.

The method of sky-polarimetric Viking navigation works with the highest accuracy when the degree of polarization *d* of the sky is the highest. Clouds, fog or mist can drastically decrease *d* and thus the accuracy of the method. In addition, all steps of the navigation can be erroneous. In my PhD thesis, I describe psychophysical experiments and their results through which we determined the error function of the first, third and fourth steps, and knowing them, we computed the accuracy of the method for 1080 sky situations with different solar elevations and cloud coverages. Although, I also took part in measuring the error of the second step, its detailed description was out of the scope of my thesis (see subchapter 3.5.1.).

3.1.8. Meteorological prerequisites of sky-polarimetric Viking navigation

The Viking navigators could only use their sunstones if the following prerequisites were fulfilled: (i) *d* of skylight was high enough and (ii) α of skylight was perpendicular to the light-scattering plane (determined by the observer, the observed celestial point and the Sun). The latter has to be equal to the direction predicted by Rayleigh's model (Horváth et al 2008b, 2011a). According to Rayleigh's model, the incoming photons scatter only once in the atmosphere before reaching the observer. Thus, *d* is minimal (zero) at the Sun, then increases with increasing angular distance from the Sun and reaches its maximum at 90°, from where it decreases, and in the anti-solar point its value is zero again. In reality, photons can scatter multiple times before reaching the observer, thus the polarization pattern of the sky can differ from that predicted by Rayleigh's model (Gál et al. 1998). These differences result that certain parts of the sky are not suitable for Viking navigation.

Between 1999 and 2005 different real sky situations were measured by imaging polarimetry to determine the area of the sky suitable for sky-polarimetric Viking navigation under various sky conditions based on the above prerequisites (Pomozi et al. 2001; Hegedüs et al. 2007a,b). Clear and partially cloudy skies were measured in the Tunisian desert, where 13-67 % of the sky was suitable for sky-polarimetric navigation. Under clear sky, however, the Vikings would not have had to use the polarization of skylight for navigation. When the sky was cloudy, the possibility of multiple light scattering increased, thus only 4-69 % of the sky was applicable for navigation and the degree of polarization decreased drastically (d_{cloudy} = 14-16 %), as well. Horváth et al. (2008b, 2011a) found, that this ratio also depends on the solar elevation. At low solar elevations, similar polarization patterns can be formed even in cloudy weather as under clear sky, meaning that the presence of clouds does not exclude the applicability of the method.

In 2005, totally overcast skies were measured in Hungary and around the Arctic (Hegedüs et al. 2007a; Horváth et al. 2008b, 2011a). Although, the polarization patterns of these skies were similar to those of the clear sky, the degree of polarization decreased so much (d_{overcast} = 3-8 %) that the intensity change of skylight transmitted through sunstones could have been barely seen. It is quite uncertain that the Vikings could have determined the Sun position under these circumstances. The same result was obtained in the case of foggy skies.

The above results suggest that the method of sky-polarimetric Viking navigation fails to work in situations when it is the most needed. However, on northern voyages, there is frequently fog or mist around the horizon only that covers the Sun but the sky around the zenith remains clear that favours for detecting the sun with sunstones (Hegedüs et al. 2015). To test the applicability of this method under real-life circumstances, further studies were needed.

3.1.9. Psychophysical field experiment of sky-polarimetric Viking navigation

Involving numerous test persons, Bernáth et al. (2013) performed field experiments, during which the accuracy of sky-polarimetric Viking navigation was tested under real-life situations. They compiled three different tasks, during which the test persons had to estimate the geographic North. Since the field experiments were performed in Hungary, the error of the estimation could be given relative to the magnetic North measured by a magnetic compass. The three tasks were the the followings: (1) Under clear skies, the test persons had to use the sun-compass to determine the geographic North. (2) In partly cloudy weather, the test persons had to estimate the Sun position by the light intensity patterns of the sky, then they could use the sun-compass with a shadow-stick to detect the geographic North. (3) Under totally overcast skies, the test persons had to use two calcite sunstone crystals to locate the Sun and then they determined the geographic North with the sun-compass and shadow-stick.

The results of tasks (1) and (2) were documented by photographing the adjusted sun-compass compared to a magnetic compass, the former and latter was regarded as the geographic and magnetic North direction, respectively. For task (3), the test persons were taken to the outskirts of Budapest by car, with their eyes covered, and unaware of their current position, they had to determine the geographic North by adjusting the sun-compass accordingly. This alignment of the compass was photographed and compared to the magnetic

North showed by the magnetic compass. After each measurement, a new location was selected, so that they were not influenced by the previous measurement.

Experiment (1) and (2) had an average error and standard deviation of –0.9° ± 5.9° and –8° ± 12.3°, respectively. In experiment (3), the test persons performed their task with an error of +12.5° ± 16.1°, when the sky was bright enough to determine which half of the skydome should be used. When the sky was so overcast that this could not have been done, the error was 4.3° ± 89.9° on everage. That is, the test persons managed to locate the anti-solar point in some cases (Bernáth et al. 2013).

In this field experiment, we had no information about the accuracy of the different navigation steps, thus we did not know, at which point the test persons committed the highest error. To be aware of how the individual errors influenced each other, we measured the error functions of each step in different psychophysical experiments and computed the error propagation, determining the net navigation error for 1080 different sky situations. In this chapter, I describe the results of these studies in detail.

3.2. Materials and methods

To determine the accuracy of sky-polarimetric Viking navigation, we measured in separate experiments the error functions of the first, third and fourth steps and numerically determined the occurring error for the possible situations in the second step, based on the results of Farkas et al. (2014). Knowing these individual errors, we could compute the propagation of these errors through the four steps and determined the North error, the degree with which the adjusted direction differed from the true reference direction being the geographical North in our studies.

3.2.1. Determination of the error functions of the first step

The error functions of the first step was measured in two psychophysical experiments performed in the Environmental Optics Laboratory of Eötvös University (Budapest, Hungary) in 2014 and 2015. In experiment 1, 10 test persons participated, aged between 24 and 63 years, while in experiment 2, the number of participants was 11, aged between 22 and 65 years.

3.2.1.1. Experimental setup and procedure to measure the error functions of the first tep

The experimental setup consisted of a 500 W incandescent lamp producing high-intensity white light (representing the sunlight), a linear polarizer (diameter = 40 cm, thickness = 1 mm, type: XP42–18 from ITOS, Mainz, Germany) placed on a large (diameter = 0.5 m) rotatable dial (representing the variable direction of polarization of skylight), 12 sand-blasted, colourless glass panes (500 mm × 500 mm × 4 mm) as diffusing depolarizers (with which we simulated the different degrees d of skylight polarization of the same intensity under various weather conditions), and rotatable metal sockets (Fig. 3.4b,c; diameter = 50 mm) with a cordierite and a tourmaline crystal in experiment 1 (modelling dichroic sunstones) and four calcites of different quality in experiment 2 (modelling birefringent sunstones) placed on a metal panel on the wall of a darkened cabin (1.5 m × 1.5 m × 2 m) covered with a depolarizing matt white cloth from inside. The optical device and the cabin were in a darkened laboratory room with matt white walls. The current test person sat in the cabin, where no outer light sources disturbed him, and the weak light reflected from the cabin wall was unpolarized. The adjusted orientations of the dichroic sunstone crystals were registered with digital goniometers, the accuracy of which was ±0.5°. The angle of polarization α of the practically totally linearly polarized light with d = 99.98 % produced by the polarizing dial could be adjusted with an accuracy of ±0.5° between 0° and 180° with respect to the horizontal. This totally polarized light was more or less depolarized after it passed through some diffusing depolarizers (wooden-framed glass panes, both sides of which were sand-blasted and one glass pane with only one sand-blasted side). In the light path, there were always 12 depolarizers. When all 12 depolarizers were placed between the lamp and the polarizing dial, the analyzers were illuminated by totally polarized light ($d \approx 100$ %). Placing increasing numbers (N = 0, 1, 2, ... , 12) of depolarizers from the side of the polarizing dial facing the lamp to its other side facing the analyzers (Fig. 3.4a), the d of light illuminating the analyzers decreased stepwise (if N = 0, 1, 2, 3, 4, 5, 7, 9, 11, 12, then d = 99.26, 88.08, 76.88, 63.48, 50.02, 36.88, 20.61, 11.36, 7.14, 5.45 %, Fig. 3.4d). When all 12 depolarizers were between the polarizing dial and the analyzers, the latter were illuminated by practically unpolarized light (d = 5.5 %). Since always 12 depolarizers were placed in the light path, the intensity and spectrum of light arriving to the analyzers was constant, independently of d. With this depolarization method, we could simulate the various degrees of skylight polarization occurring under different meteorological conditions.

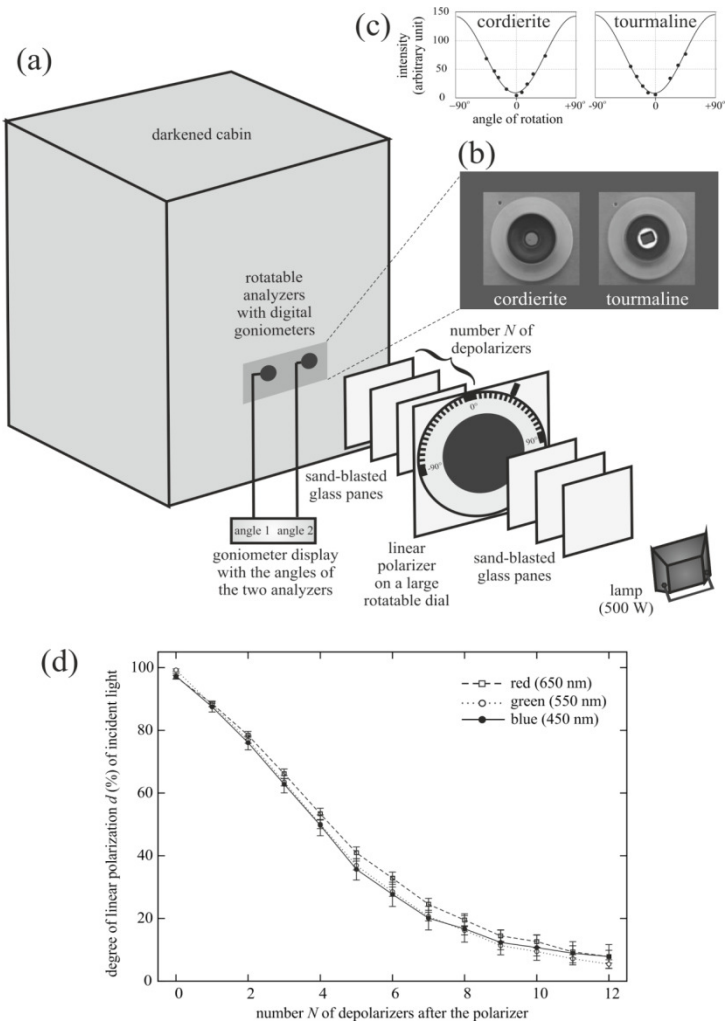

Figure 3.4: (a) Schematics of the experimental setup with which we measured the error of the first step of sky-polarimetric Viking navigation. The number N of depolarizers between the polarizing dial and the analyzers ranged between 0 and 12. (b) The rotatable minerals as seen by the test persons from the darkened cabin. (c) Change of the intensity of light transmitted through the analyzers as a function of the angle of rotation. Dots: measured intensity values of green light transmitted by a fixed linear polarizer. Continuous curve: sinusoid function fitted to the measured data with the method of least squares. (d) Average (dots) and standard deviation (vertical I-shaped bars) of the degree of linear polarization d of light illuminating the analyzers (cordierite and tourmaline) in the experiment as a function of the number N of sand-blasted glass depolarizers between the polarizing dial and the analyzers measured by imaging polarimetry in the red (650 nm), green (550 nm) and blue (450 nm) parts of the spectrum.

Using sand-blasted glass panes as depolarizers had the advantage that glass is optically inactive, so it does not change the state of polarization of transmitted light. Using imaging polarimetry (Horváth and Varjú 1997, 2004), we measured the degree d and angle α of polarization of light incident on the rotatable analyzers in the red (650 nm), green (550 nm) and blue (450 nm) spectral ranges as a function of the number N of depolarizers between the polarizing dial and the analyzers. The average of α was practically constant, but its standard deviation slightly increased with decreasing d.

The rectangular cordierite and tourmaline fragments (12 mm × 8 mm × 1 mm) were split from larger crystals (obtained from the Department of Mineralogy of Eötvös University, Budapest) so that they functioned as ideal linear polarizers (Fig 3.4c). Obviously, Viking navigators could not use such ideal crystals, but could apply similar crystals of poorer quality.

In experiment 2, two test persons were different from the ones in experiment 1. The experimental setup and procedure were the same as in experiment 1. The calcite crystals had different opacities (calcites 1 and 4 had more surface scratches than calcites 2 and 3) and colour (calcites 1 and 4 were white, while calcites 2 and 3 were yellowish). Their thickness was 22 mm with the same length of optical path of transmitted light. Calcites 2 and 3 were split from the same major crystal with the difference that the surface of the latter was polished. One side of the calcite crystals was covered with a black cardboard, from which a small hole with a diameter of 3 mm was cut out. After placing the crystals in the analyzer sockets, a double-image of the holes was formed due to the birefringence of calcite. The direction of polarization of these two light spots was perpendicular to each other. The calcite crystals were intentionally different, because we wanted to simulate that the Vikings might have used sunstones of different optical qualities.

3.2.1.2. Task of the test persons in the laboratory experiments

In both experiments, each test persons had to do the same measurement series 10 times, on different days. In experiment 1, the task of the test person was to adjust the analyzers (the cordierite and tourmaline crystals) sequentially into the orientation when the intensity of light transmitted through the crystal was the lowest. The search for the minimal (rather than the maximal) transmitted intensity was motivated by the fact that Viking navigators used the sunstones under a bright sky: in front of a bright background (sky), it is easier to find the darkest state of a light spot (rotating dichroic sunstones) than the brightest one. After each session, the experiment leader changed both the degree d and angle α of polarization of the

incident white light of constant intensity. One measurement session consisted of 10 different (d, α) pairs modelling 10 different states of skylight polarization. We also asked the test persons to signal whether they could or could not see intensity change through the analyzers while rotating them, in order to determine the lowest d*-value at which the test persons could still detect the maxima and minima of the sinusoidally changing intensity of light transmitted through the dichroic sunstone crystals. The experiment leader read the orientations (angles from the horizontal) of the adjusted analyzers and the polarizing dial on the digital goniometers.

In experiment 2, the test persons had to execute two tasks in two different sessions, because due to birefringence, the calcites had two optical paths: (1) the crystals had to be rotated until the same intensity of the two light spots was seen; (2) the crystals had to be rotated until the maximal difference between the intensities of the two spots was found. Since, it is unknown, which method the Vikings might have used to locate the Sun and it is not trivial, whether the accuracies of the two methods are the same, we expected that the angle of polarization of incident light could be determined with different accuracies using these two adjustment tasks. After the test person adjusted one calcite analyzer, the experiment leader changed randomly the angle α of polarization of the incident white light of constant intensity and spectrum. After all four calcite crystals were measured, the experiment leader changed the degree d of polarization of incident light randomly. One measurement session consisted of the measurement of all four calcites with 10 different d-values of the incident light. During one task (1 or 2), the same measurement session was repeated 10 times. In experiment 2, we asked the test persons again to signal whether they could see any intensity change of the two light spots while rotating the calcite crystals. We compared the thresholds d*, at which intensity change could still be perceived, obtained in the two tasks to decide which method results in a higher accuracy. We determined the number of measurements for each d-value being above the uncertainty level of d* = 10 % and 50 % for all the measurement in each task.

3.2.1.3. Data evaluation of the laboratory experiments

In both experiments, the measured data were evaluated with a self-written computer software, computing the degree with which the sunstone adjustment differed from the known correct direction. After the process, we obtained the following parameters: (i) mean μ with standard deviation σ and median ε of the adjustment angle errors of the analyzers averaged for the 10

measurements of each test person, and (ii) μ, σ and ε averaged over the 100 and 110 measurements performed with the 10 and 11 male test persons in experiment 1 and 2, respectively. After getting the mean errors μ for the different analyzers, we plotted the value of $\mu+\sigma$ against d giving the maximal possible navigation error a navigator could commit under a specific weather condition with a given degree of skylight polarization d. Since we measured errors only for discrete d_i-values (i = 1, 2, . . . , 10), we fitted a hyperbolic function to the obtained data points, getting the error function $e_{1st}(d)$ for each analyzer (Fig. 3.11). The degree of polarization d can never be negative ($d \geq 0$), thus we used only the hyperbola part above the horizontal asymptote. The part below the asymptote could be ignored, since $d < 0$ did not exist in our case. Although the error function $e_{1st}(d)$ is bounded (where the maximal possible error is 90° for both the cordierite and tourmaline), the d-values at which the fitted functions reach these boundary values are d = 0.04 % for cordietite and 0.39 % for tourmaline. These values are far below the threshold above which the test persons could perceive intensity changes in the sunstone crystals. Consequently, in all studied cases, the fitted hyperbolic function was an adequate choice to represent the error function $e_{1st}(d)$ for 5 % < d < 90 %, that is the degree of polarization range used for North error determination (see subchapter 3.2.5.).

During the evaluation of the data of experiment 2, we had to solve the following problem: because of surface scratches and impurities/defects (called contaminations further on) in the calcite crystals, the absorption, scattering and internal reflections in the two optical paths, formed due to birefringence, can be different, which influence the accuracy of sunstone adjustment in tasks 1 and 2.

In task 1, the calcite had to be rotated until the intensities of the two light spots were equal. During a full, 360° rotation, there are four such orientations. If the calcite contaminations between the two optical paths are the same, these four angles of equal intensities are independent of the degree of polarization d of incident light and are 90° apart from each other. However, if the contaminations between the two optical paths differ, the equal intensity angles depend on d. Furthermore, there is a threshold p^+ below which the light spot belonging to the less contaminated optical path is always brighter than the other (Fig. 3.5). In this case, the navigator could not have scratched a single mark pointing towards the Sun onto the sunstone, since the direction of this mark would have depended on d making this method practically unusable for a Viking navigator. To temporarily overcome this issue in order to still be able to determine the accuracy of the equal intensity adjustment of the crystals, we have previously measured the intensity of light seen through the spots for each

calcite crystal. We determined the intensity difference $\Delta I = I_{spot1} - I_{spot2}$ of the two light spots for every degree of polarization d set in our experiment, in every 10° rotation of the calcite. Where this difference was zero, that angle was considered as the exact equal-intensity angle. To the measured intensity differences, we fitted the function $y(x) = a\ sin(2x+b) + c$, where y is the intensity difference, x is the angle rotated from the reference direction, a, b and c are fitting parameters. Using $y(x)$, we determined the equal-intensity angles, that were regarded as the correct adjustment direction during the evaluation. When the degree of polarization d of incident light was so low ($d < d^+$) that no equal-intensity angle occurred, we assumed that the test person rotated an ideal calcite (without contaminations) randomly with no systematic error, which could result in an error between 0° and 45° according to uniform distribution, the expected error value of which is 22.5°. Thus, $e(d < d^+) = 22.5°$, while for $d > d^+$ the error function $e_{1st}(d)$ was calculated according to the hyperbolic fit.

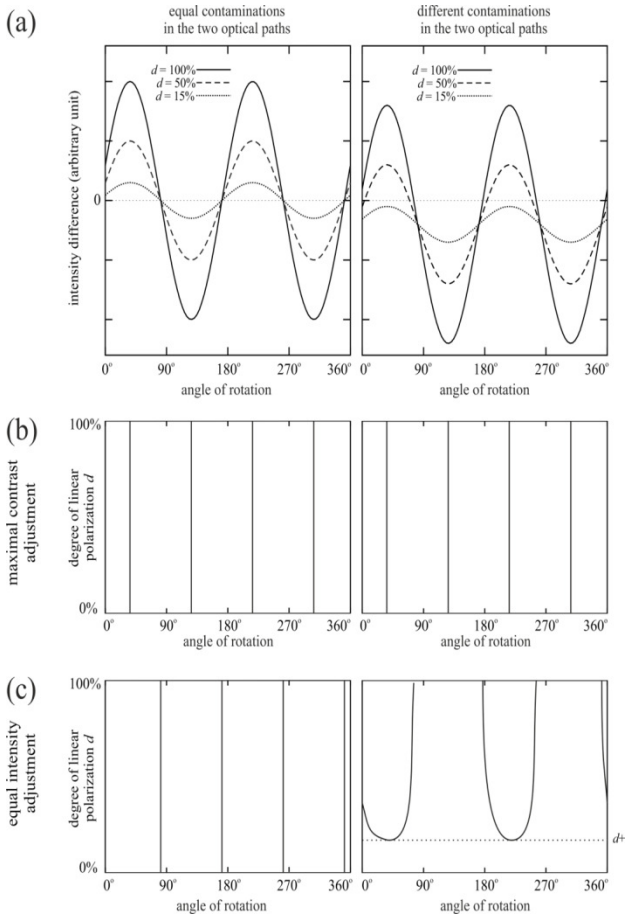

Figure 3.5: Demonstration of the effect occurring due to the different contaminations in the two optical paths of a calcite crystal. (a) Intensity difference between the two light spots seen in the rotating calcite illuminated by white light with different degrees of linear polarization d if the contaminations are equal (left) and different (right) in the two optical paths. (b)

Maximal intensity difference orientation of the calcite if the contaminations are equal (left) and different (right) in the two optical paths. (c) Equal-intensity difference orientation of the calcite if the contaminations are equal (left) and different (right) in the two optical paths. Calcite crystals with different contaminations have a threshold d^+ of the degree of polarization, under which ($d < d^+$) no equal intensity of the two light spots can be detected.

In task 2, such corrections were not necessary, since angles where the intensity difference is maximal between the two light spots are independent of the degree of polarization of incident light and of the disturbing differences in calcite contamination between the two optical paths. Such orientations occur four times with 90° periodicity during a full, 360° rotation of the crystal.

3.2.2. Errors of the second step

Farkas et al. (2014) measured the accuracy of the second step of sky-polarimetric Viking navigation in a psychophysical experiment performed in the planetarium of Eötvös University in Hungary. They determined the elevation and azimuth error of finding the intersection of two celestial great circles mentally based on two predefined directions that represented the errorless adjusted directions in the first step. To determine the errors of the second step, we used up their results and characterized the occurring situations with the same four free parameters: (i) the elevation angle θ_S of the estimated Sun, (ii) γ_1 and (iii) γ_2 meaning the angular distance of the two observed celestial points from the estimated Sun and (iv) angle δ enclosed by the planes of the two celestial great circles. We created 72 parameter groups (θ_S, γ_1, γ_2, δ) based on the following intervals: θ_S: 5°–25°, 35°–55°; γ_1, γ_2: 35°–55°, 65°–85°, 95°–115°; δ: 35°–55°, 65°–85°, 95°–115°, 125°–145°. Each group was characterized with the average elevation error $\Delta\theta$ and the average azimuth error $\Delta\varphi$ that defined a vector $\boldsymbol{e}_{\mathbf{2nd}}(\Delta\theta, \Delta\varphi)$ in spherical coordinate system that gave the error vector with which the estimated Sun position differed from the real one on the surface of the hypothetical sky dome (Table 3.1).

parameters δ, θ_S, γ_1, γ_2 (°)	**Δθ (°)**	**σ_θ (°)**	**Δφ (°)**	**σ_φ (°)**
125–145, 35–55, 35–55, 35–55	14	53	–36	118
125–145, 35–55, 35–55, 65–85	02	107	130	275
125–145, 35–55, 65–85, 35–55	–16	93	–46	223
125–145, 35–55, 65–85, 65–85	19	80	–62	309
125–145, 35–55, 65–85, 95–115	38	81	104	374
125–145, 35–55, 95–115, 35–55	–35	84	–60	329
125–145, 35–55, 95–115, 65–85	33	73	–133	364
125–145, 35–55, 95–115, 95–115	27	106	28	318
125–145, 5–25, 35–55, 35–55	31	26	12	65
125–145, 5–25, 35–55, 65–85	57	26	–140	181
125–145, 5–25, 35–55, 95–115	62	59	–277	315
125–145, 5–25, 65–85, 35–55	–19	64	263	237
125–145, 5–25, 65–85, 65–85	100	54	17	266
125–145, 5–25, 65–85, 95–115	84	74	–148	323
125–145, 5–25, 95–115, 35–55	74	35	212	297
125–145, 5–25, 95–115, 65–85	31	87	212	278
125–145, 5–25, 95–115, 95–115	110	73	–183	374
35–55, 35–55, 35–55, 35–55	22	45	07	79
35–55, 35–55, 35–55, 65–85	62	65	–24	140
35–55, 35–55, 35–55, 95–115	33	127	–80	230
35–55, 35–55, 65–85, 35–55	–05	84	–22	117
35–55, 35–55, 65–85, 65–85	05	108	50	159
35–55, 35–55, 65–85, 95–115	28	123	–20	177
35–55, 35–55, 95–115, 35–55	–31	114	–24	240
35–55, 35–55, 95–115, 65–85	–30	175	–09	184
35–55, 35–55, 95–115, 95–115	–03	143	12	220
35–55, 5–25, 35–55, 35–55	30	47	07	30
35–55, 5–25, 35–55, 65–85	144	100	32	52
35–55, 5–25, 35–55, 95–115	30	44	164	225
35–55, 5–25, 65–85, 35–55	137	60	33	26
35–55, 5–25, 65–85, 65–85	110	92	–04	110
35–55, 5–25, 65–85, 95–115	78	132	138	259

35–55, 5–25, 95–115, 35–55	112	127	72	70
35–55, 5–25, 95–115, 65–85	149	116	105	73
35–55, 5–25, 95–115, 95–115	112	122	–22	203
65–85, 35–55, 35–55, 35–55	45	32	–08	54
65–85, 35–55, 35–55, 65–85	27	65	52	166
65–85, 35–55, 35–55, 95–115	34	93	–75	189
65–85, 35–55, 65–85, 35–55	14	62	–10	174
65–85, 35–55, 65–85, 65–85	16	102	–37	194
65–85, 35–55, 65–85, 95–115	10	124	26	190
65–85, 35–55, 95–115, 35–55	–23	53	50	265
65–85, 35–55, 95–115, 65–85	39	89	–18	235
65–85, 35–55, 95–115, 95–115	13	141	–004	215
65–85, 5–25, 35–55, 35–55	41	52	06	38
65–85, 5–25, 35–55, 65–85	56	58	22	108
65–85, 5–25, 65–85, 35–55	114	51	–05	20
65–85, 5–25, 65–85, 65–85	125	72	30	109
65–85, 5–25, 65–85, 95–115	109	113	–33	189
65–85, 5–25, 95–115, 35–55	138	104	74	117
65–85, 5–25, 95–115, 95–115	159	92	58	208
95–115, 35–55, 35–55, 35–55	24	43	–03	73
95–115, 35–55, 35–55, 65–85	07	75	56	163
95–115, 35–55, 35–55, 95–115	–30	65	28	240
95–115, 35–55, 65–85, 65–85	18	107	20	253
95–115, 35–55, 65–85, 95–115	30	73	34	315
95–115, 35–55, 95–115, 35–55	04	58	–70	241
95–115, 35–55, 95–115, 65–85	13	119	–27	358
95–115, 35–55, 95–115, 95–115	40	130	–01	315
95–115, 5–25, 35–55, 35–55	47	51	06	85
95–115, 5–25, 35–55, 65–85	76	43	–85	125
95–115, 5–25, 35–55, 95–115	98	76	–147	180
95–115, 5–25, 65–85, 35–55	69	59	52	112
95–115, 5–25, 65–85, 65–85	89	72	–10	179
95–115, 5–25, 65–85, 95–115	204	57	–20	141

95–115, 5–25, 95–115, 35–55	50	66	22	113
95–115, 5–25, 95–115, 65–85	119	75	55	212
95–115, 5–25, 95–115, 95–115	158	112	–40	253

Table 3.1: Elevation errors $\Delta\theta$, azimuth errors $\Delta\varphi$ and their standard deviations σ_θ and σ_φ for the different parameter intervals in the second step of sky-polarimetric Viking navigation.

3.2.3. Determination of the error function of the third step

In the third step of sky-polarimetric Viking navigation, the navigator had to determine the elevation of the estimated Sun, in order to determine the length of the gnomonic shadow to be replaced for the sun-compass. Since there was no archaelogical clue how the Vikings might have performed this measurement, we assumed that they used the most obvious measuring tools, their own fists and fingers. We studied the accuracy of measuring the solar elevation using only fists and fingers in the digital planetarium of Eötvös University in Hungary, where any Sun position could be simulated. The error measurement of these virtual solar elevations was performed with 10 male test persons, aged between 24 and 52 years, in autumn 2015. The diameter of the dome of the planetarium was 8 m and a fixed central single-lens Digitarium ε projector (Digitalis Education Solutions Inc., Bremerton, WA, USA) with a circumferential resolution of 2400 pixels was used for projecting pictures onto the dome canvas. The test persons sat in the geometric middle point of the dome, in the immediate vicinity (30 cm) of the planetarium projector with their eye level about 5 cm below the projector lens in order not to be dazzled by the projector light and to minimize the parallax error. The measurements of one test person consisted of five 20-minute sessions. To minimize exhaustion and learning of test persons, each session was performed on a different day, so that the test persons could not memorize their previous estimations.

Every session started with a calibration, during which the fists and fingers of the test person was measured to numeric elevation values in degrees. A scale of the elevation angles was projected onto the dome (Fig. 3.6a,b), that started at $\theta = 8°$ elevation above the horizon, because the horizontal circular bottom edge of the planetarium dome, representing the horizon, was 8° above the eye level of the test persons (Fig. 3.6c). The test person had to stretch out his arm and close his fist with his four fingers (the thumb did not play a role in this measurement) together. Then, he had to determine the apparent elevation of his fists and fingers with 1° accuracy up to $\theta = 60°$. According to the method described by Bernáth et al.

(2013a), one fist was equal to four fingers and each finger was considered to be of equal width. We had to apply this process to each test person, because the arm length to fist size ratio was slightly different for everyone. At the end of each session, the calibration was repeated, thus one test person had 10 calibration data points altogether. We determined the average and standard deviation of angles for each fist–finger unit that were used as reference values for the evaluation of the measurement data.

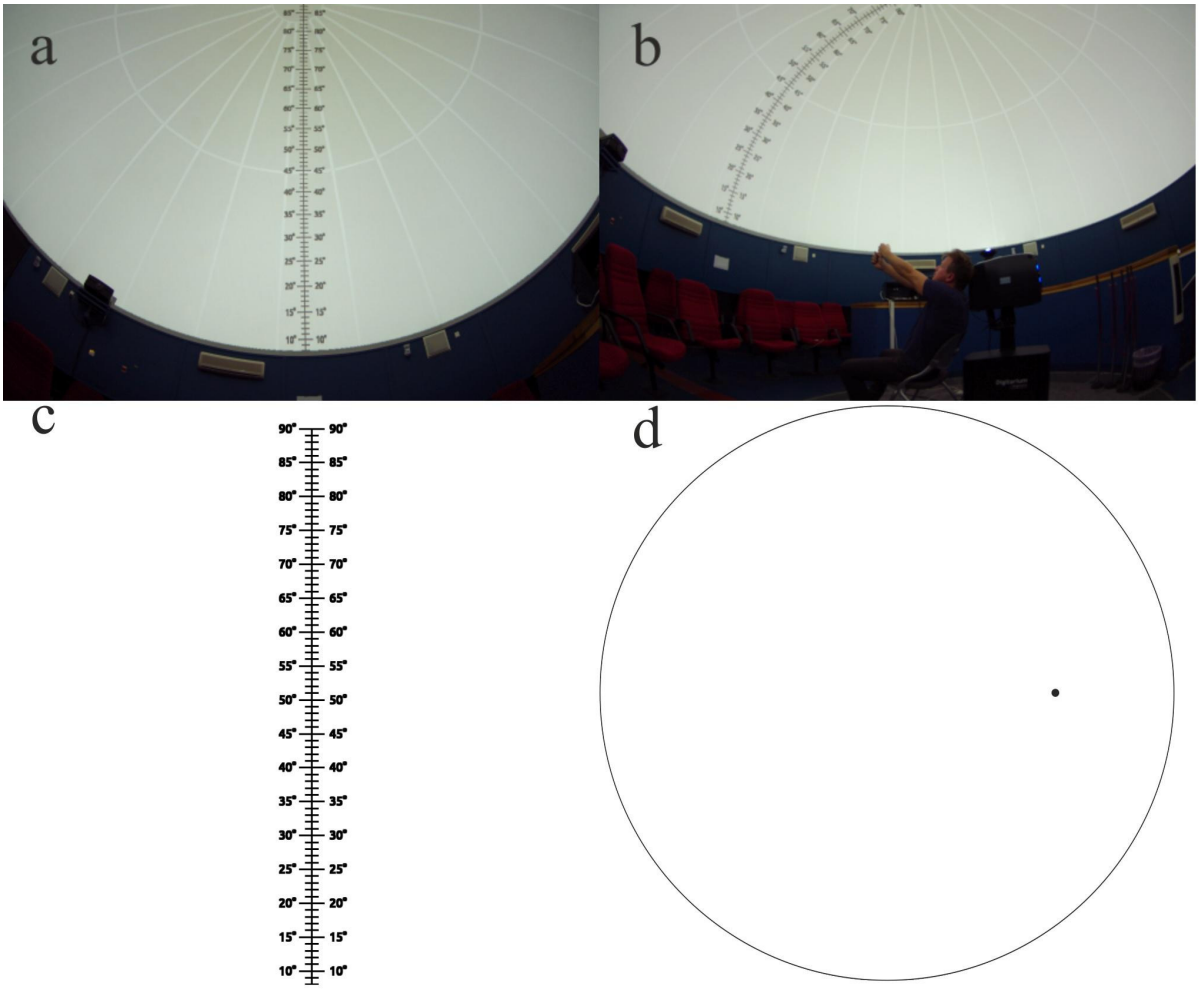

Figure 3.6: (a) Wide-angle photograph of the calibration image that the test persons saw projected onto the planetarium canvas. (b) Photo of the calibration process. The test person sat in the middle point of the planetarium under the dome and tried to perform the calibration using his fists and fingers. (c) Image of the calibration scale which began at an elevation θ = 8°, because the horizontal circular bottom edge of the planetarium dome was 8° above the eye level of the test persons. (d) An example of the projected measurement situation.

For the estimation of virtual solar elevations, the experiment leader projected clearly visible black dots (representing the virtual invisible Sun) in front of a white background (Fig. 3.6d) onto the planetarium dome. The elevation angle of these dots varied randomly between $\theta = 8°$ and 55°, thus altogether 48 dots were projected randomly during one session. The azimuth angle of the dots remained the same during the measurement, so that the test person did not have to rotate itself while sitting in a chair. The lower boundary of elevation was aligned to the bottom edge of the dome, since dots below this level could not have been projected. The upper elevation boundary of 55° was set, because at the 61° latitude, along which the Vikings sailed the most frequently, the maximal elevation could not be higher than 52.5° (Thirslund 2001; Száz et al. 2016a). The test persons' task was to estimate the elevation of the projected black dot by using their fists and fingers without knowing the true elevation angle. At the end of the five sessions, each test person had five estimated values for each elevation in fist–finger units. Thus, altogether $5 \times 48 \times 10 = 2400$ elevation estimations were performed by the 10 test persons.

The results were evaluated with a self-written computer software according to the following method. (i) First, we evaluated the calibration results for the test persons separately by calculating the average angle and standard deviation for each fist-finger combination. (ii) Based on the calibration of a test person, we determined the estimated elevation in degrees of a given fist-finger value. Thus, we got a list of the true elevations and the estimated values belonging to them in degrees, according to the test person's measurements. (iii) Knowing these values, we calculated the errors with sign (+, −) to mark whether the test person over- or underestimated the true elevation. Since we had five estimations for each true elevation, we calculated the average μ and standard deviation σ of these errors for each test person. However, these results were very different and the average elevations of the 10 test persons would be far from a real-life situation, where the navigator obviously had the best navigational skills. Thus, to characterize the performance of the test persons, we introduced the cumulated elevation error $\sum = \sum_{i=1}^{48} |\mu(\theta_i)| + \sigma(\theta_i)|$, meaning the sum of the absolute values of the average $\mu(\theta_i)$ plus standard deviation $\sigma(\theta_i)$ for every θ_i elevation. The sense of the intorduction of this cumulated elevation error was to compare the performance of the test persons. The index i runs from 1 to 48, because the elevation θ_i was measured from 8° to 55° by 1° steps. The person with the highest and lowest Σ-value was, by definition, the worst and best navigator, respectively.

We also determined the distribution of the elevation errors for each measured data. We created a histogram by dividing the elevation errors into 0.5° intervals and counted the occurrences of the cases within the 2400 estimations. Then, we fitted a Gaussian function to the symmetric part of the distribution around the peak to quantify the position of the distribution peak.

To derive the error function $e_{3rd}(\theta)$ of the third step, we selected three test persons: the one with the lowest Σ-value, the one with the largest Σ-value, and one whose Σ-value fell inbetween. Then, we calculated $|\mu(\theta_i)| + \sigma(\theta_i)$ (average + standard deviation) for each elevation angle θ_i, which characterized the maximum possible error of a given test person at elevation θ_i, then we fitted a power function $e_{3rd}(\theta) = a\theta^b$ with the method of least squares, where a and b are the fitting parameters seen in Table 3.2. The error function was determined for these three test persons, that give the possible maximum absolute elevation error for any θ_i-value. Since the Viking navigator was supposed to possess exceptional navigation skills, we only used the error function of the best test person for North error determination (see subchapter 3.2.5.)

test person	**parameters**			
	a	**±Δ*a***	***b***	**±Δ*b***
1	0.1125	0.0656	0.7840	0.1594
7	1.2273	0.4294	0.3534	0.0991
10	0.0256	0.0065	1.5853	0.0672

Table 3.2: Numerical values of the parameters and asymptotic errors of the error function $e_{3rd}(\theta) = a\theta^b$ of the third step of sky-polarimetric Viking naigation obtained for the elevation error of the three selected test persons.

3.2.4. Determination of the error function of the fourth step

Once the navigator located the invisible Sun, he had to use the shadow-stick to replace the gnomonic shadow on the surface of the sun-compass. To do this, the shadow-stick had to be aligned parallel to the azimuth direction of the located Sun. This alignment, however could be erroneous, resulting in the error function of the fourth step of sky-polarimetric Viking navigation that we measured in the planetarium of Eötvös University in Hungary, in the autumn of 2016.

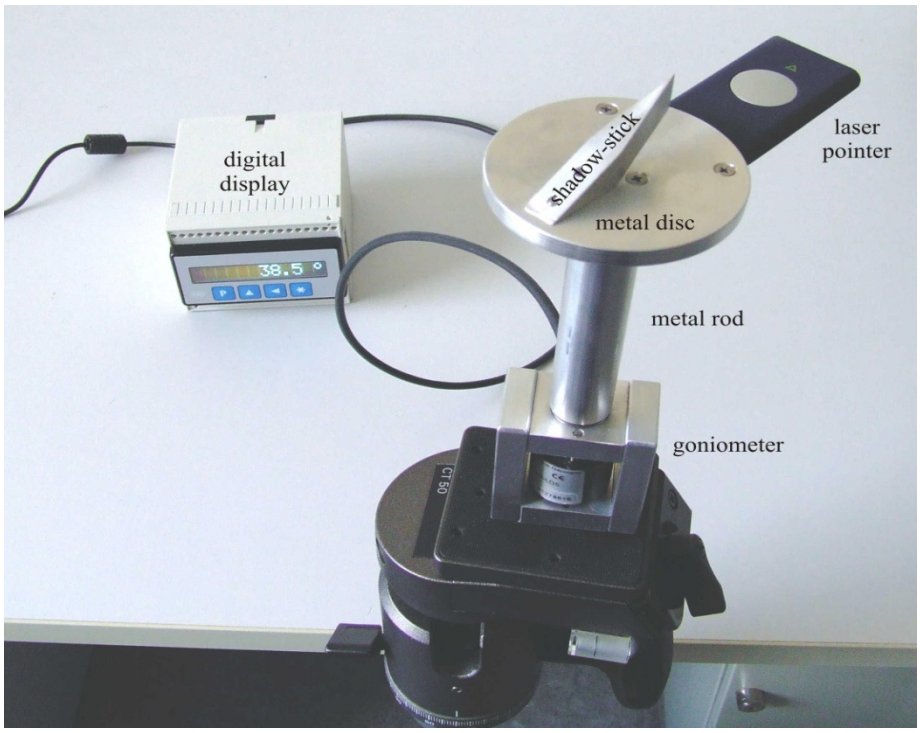

Figure 3.7: The digital goniometer and its display used in the psychophysical planetarium experiment measuring the error function of the fourth step of sky-polarimetric Viking navigation.

A black dot with an angular extension of 0.25° was projected on the white planetarium dome with an azimuth angle φ (ranging between −45° and +45° from an arbitrary horizontal reference direction) and an elevation angle θ (ranging from 0° to 55°). The test person sitting in the geometric centre of the planetarium had to estimate the azimuth angle of this dot with the help of a digital goniometer modelling the Viking sun-compass (Fig. 3.7). The person had to rotate an elongated metal plate (70 mm long, tilted with 45° from the horizontal, forming the shape of a shadow-stick) along its vertical axis until its long axis became parallel to the estimated azimuth direction of the projected dot. The difference $\Delta = \varphi_e - \varphi_r$ between the estimated (φ_e) and real (φ_r) azimuth angles of the dot was registered. The test person had to perform this estimation for 48 dots with φ- and θ-values in randomized order. We performed this measurement 10 times with 10 male test persons, whose ages ranged between 23 and 54 years. Thus, altogether we got 10 × 10 × 48 = 4800 different Δ-values, from which 100 belonged to a given θ. These data were averaged, thus we obtained the average $\langle\Delta\rangle \pm$ standard deviation σ_φ for 48 different θ-values. Since the average $\langle\Delta\rangle$-values approximated zero (as expected), the error function of the fourth step of sky-polarimetric navigation was

defined as $e_{4th}(\theta) = \sigma_\varphi(\theta)$ that we obtained by fitting a parabola to the measured $\sigma_\varphi(\theta)$-values. Further on, this error function was used for North error determination (see subchapter 3.2.5.)

3.2.5. Determination of the net North error

Knowing the occurring error in each step, we determined how these errors propagated through the navigation process while the navigator followed the steps of sky-polarimetric Viking navigation. To do that, we created a software that could calculate this error propagation for any two possible point pairs in the sky that the navigator could choose to start the navigation process. Since the accuracy of the first step is dependent on the degree of skylight polarization in the two chosen points which are dependent on the current weather situation at the moment of the measurement, we selected 1080 different meteorological situations to simulate many possible weather circumstances.

3.2.5.1. Selection of 1080 different meteorological situations

For North error determination, we selected images of patterns of the degree of polarization d of skylight of 1080 different meteorological situations. These sky polarization data have been collected for 3 years with an automatic full-sky imaging polarimeter that was set up in the Gothard Astronomical Observatory of the Eötvös University in Szombathely, Hungary. The method of the measurement is described in detail by Barta et al. (2015). During these 3 years, the polarimeter measured several thousands of sky polarization patterns, from which we selected 1080 different skies that were grouped by the following two parameters: (i) elevation angle θ of the Sun above the horizon ranging from 0° to 50° (higher solar elevations did not occur at the 61° northern latitude, the main Viking sailing route) and (ii) cloud coverage ρ (percentage of the full sky covered by clouds). The selected θ-range was divided into 10 equal intervals with an increment of 5° as follows: $0° \leq \theta_1 < 5°$; $5° \leq \theta_2 < 10°$; $10° \leq \theta_3 < 15°$; $15° \leq \theta_4 < 20°$; $20° \leq \theta_5 < 25°$; $25° \leq \theta_6 < 30°$; $30° \leq \theta_7 < 35°$; $35° \leq \theta_8 < 40°$; $40° \leq \theta_9 < 45°$; $45° \leq \theta_{10} \leq 50°$. The cloud coverage was determined by a cloud detection method using kNN (k Nearest Neighbour) pattern recognition algorithm described in detail by Barta et al. (2015). The full interval $0\ \% \leq \rho \leq 100\ \%$ was divided into 9 categories called oktas, the common units used in meteorology for estimating the cloud coverage of the sky by the naked eye (Pasini 2005). Oktas from 0 to 8 refer to more and more intense cloud coverage (Cazorla et al. 2008): okta 0 = totally clear sky, oktas 1–2 = few clouds, oktas 3–4 = scattered clouds,

oktas 5–7 = broken clouds, okta 8 = totally overcast. Based on this generally accepted method, okta 0 corresponds to $\rho_0 = 0$ %, and the further categories are composed of eight equal intervals with an increment $\Delta\rho = 12.5$ % as follows: 0 % $\leq \rho_1 <$ 12.5 %, 12.5 % $\leq \rho_2 <$ 25 %, 25 % $\leq \rho_3 <$ 37.5 %, 37.5 % $\leq \rho_4 <$ 50 %, 50 % $\leq \rho_5 <$ 62.5 %, 62.5 % $\leq \rho_6 <$ 75 %, 75 % $\leq \rho_7 <$ 87.5 % and 87.5 % $\leq \rho_8 \leq$ 100 %. The cloudless case ($\rho_0 = 0$ %) is easy to recognize, therefore its separation is logical in our measurements. These selected situations were also used by Horváth et al. (2017).

We created 10 × 9 = 90 (θ, ρ) groups. In each group, we selected 12 different skies from our polarimetric sky archives and finally obtained 90 × 12 = 1080 different sky situations, where in a given group θ- and ρ-values were similar. Further on, we used the polarization patterns of these skies measured by imaging polarimetry in the green (550 nm) spectral range, in which the human eye is the most sensitive (Sharpe et al. 2005).

3.2.5.2. Error propagation and North error determination

The navigation uncertainty (North error) was determined for the above 1080 sky situations, supposing that the Viking navigators used one of the three sunstone crystals. To quantify the North error, we calculated the error propagation through the four steps of sky-polarimetric Viking navigation with a self-developed software, the applied algorithm of which was the following:

(1) In a given sky, we excluded areas with $d < 5$ % and $d > 90$ %. The former d-values are below the sensitivity threshold of the human eye, the latter do not occur under normal circumstances, only when the clouds cause motion artefact (Hovárth and Varjú 2004; Horváth 2014). Besides, we used a mask to filter out pixels of field objects.

(2) We chose point pairs (m_1, m_2) from the non-excluded sky areas. The first point m_1 was chosen from a celestial quadratic grid with a side length of 30 pixels (Fig. 3.8a). The used sky image was taken with a digital camera applying a 180° field-of-view fisheye lens. Thus, the 2D representation of a chosen point m_1 in the circular fisheye image had to be transformed to 3D Cartesian representation. We performed this in two steps: (i) First, the 2D fisheye representation was transformed to 3D polar coordinates, then (ii) the 3D polar representation was transformed to 3D Cartesian coordinates: $f(x^*, y^*) \rightarrow g(r, \theta, \varphi) \rightarrow h(x, y, z)$, where x^*, y^* are the planar coordinates of the fisheye representation, r is the radius of the sky dome, θ is

the elevation angle measured from the horizon, φ is the azimuth angle measured clockwise in the horizontal plane and x, y, z are Cartesian coordinates. In step (i), the chosen sky point was positioned on the surface of the imaginary sky dome, the radius of which was chosen to be 1 in the representation. Thus, the 3D polar coordinates were the followings: $r = 1$, $\theta = (x^{*2} + y^{*2})^{1/2}$, $\varphi = \arctan(y^*/x^*)$. In step (ii), the coordinates of 3D Cartesian representation obtained from the 3D polar representation were the followings: $x = r \cdot \sin\theta \cdot \cos\varphi$, $y = r \cdot \sin\theta \cdot \sin\varphi$, $z = r \cdot \cos\theta$. The second point m_2 was chosen from a celestial polar grid with 20° resolution between angular distances $45° \leq \tau \leq 90°$ from m_1 (Fig. 3.8b). According to our earlier field experience with sunstones (Bernáth et al. 2013), point m_2 could not be too close to ($0° < \tau < 45°$) or too far ($90° < \tau \leq 180°$) from m_1, otherwise, the accuracy of the second step of sky-polarimetric navigation would have decreased considerably. For determining τ, we used the fisheye representation and obtained the following form expressed with planar coordinates:

$$\tau = \left| \sqrt{x_{m_1}^{*2} + x_{m_1}^{*2}} - \sqrt{x_{m_1}^{*2} - x_{m_1}^{*2}} \right| .$$

(3) Using the measured degrees of polarization d_1 and d_2 in sky points m_1 and m_2, we calculated the errors $e_1 = e_{1st}(d_1)$ and $e_2 = e_{1st}(d_2)$ of sunstone adjustment, where $e_{1st}(d)$ is the error function of the first step measured earlier for cordierite, tourmaline and (best-performing) calcite crystals.

(4) After knowing the adjusted direction, we determined the intersection of the two celestial great circles in the following way: Let C_{1E} and C_{2E} be the great circles passing through the sunstone centres m_1 and m_2 parallel to the straight markings engraved into the sunstone surface during calibration. The estimated Sun position E is the intersection of circles C_{1E} and C_{2E} (Fig. 3.8c). Let C_{1S} and C_{2S} be the celestial great circles connecting the Sun S with points m_1 and m_2 (Fig. 3.8d). For each member m_i of the point pair m_1 and m_2, we considered the two great circles C_{i+} and C_{i-} enclosing an angle $2e_i(d_i)$ with each other around the great circle C_{iS} connecting points m_i and S, where $i = 1, 2$. C_{i+} and C_{i-} enclose an angle $+e_i(d_i)$ and $-e_i(d_i)$ with C_{iS} , respectively (Fig. 3.8d). The intersections of circles C_{1+}, C_{1-} and C_{2+}, C_{2-} appoint a spherical tetragon (marked with grey in Fig. 3.8d) involving the real Sun position S. Owing to the maximum errors $\pm e_i(d_i)$ of sunstone adjustments, all possible estimated Sun positions E are within this grey tetragon for the given point pair m_1 and m_2. The area of this tetragon was divided into 100 points along a grid with tenth of the tetragon's side length. Thus, we got 100

estimated Sun positions E with which we computed further on. Such trimming of data points was necessary to reduce the computation time of the algorithm.

The general mathematical description of finding the intersection point was the following: Let P_1 and P_1' be two known points of the first great circle, P_2 and P_2' two known points of the second great circle. Similarly, let $\underline{p}_1$ and $\underline{p}_1$' the vectors pointing towards P_1 and P_1', respectively, $\underline{p}_2$ and $\underline{p}_2$' the vectors pointing towards P_2 and P_2'. By taking the cross product ($\times$) of $\underline{p}_1$' and $\underline{p}_1$, we get a vector being perpendicular to the plane of the first great circle. Similarly, we took the cross product of $\underline{p}_2$' and $\underline{p}_2$ and get a vector perpendicular to the second great circle. By normalizing the two vectors, we got the followings:

$$\underline{a}_1 = \frac{\underline{p}_1' \times \underline{p}_1}{\left|\underline{p}_1' \times \underline{p}_1\right|} = \frac{\underline{p}_1' \times \underline{p}_1}{\left|\underline{p}_1'\right| \cdot \left|\underline{p}_1\right| \cdot \sin\alpha}$$, where α is the angle inclined by vectors $\underline{p}_1$ and $\underline{p}_1$';

$$\underline{a}_2 = \frac{\underline{p}_2' \times \underline{p}_2}{\left|\underline{p}_2' \times \underline{p}_2\right|} = \frac{\underline{p}_2' \times \underline{p}_2}{\left|\underline{p}_2'\right| \cdot \left|\underline{p}_2\right| \cdot \sin\beta}$$, where β is the angle inclined by vectors $\underline{p}_2$ and $\underline{p}_2$'.

The normalized cross product of $\underline{a}_1$' and $\underline{a}_2$' is a vector, the length of which is 1 (meaning that it is on the surface of the unit sky dome), and it gives one of the two possible intersections of the two great circles: $\underline{I} = \frac{\underline{a}_1 \times \underline{a}_2}{\left|\underline{a}_1 \times \underline{a}_2\right|}$. If the vertical z component of $\underline{I}$ is not smaller than 0, we found the wanted intersection. If it is negative, we need to take $-\underline{I}$ instead of $\underline{I}$. When the sunstone adjustment is correct (with no error), the vectors pointing towards the real Sun S can be chosen as $\underline{p}_1$' and $\underline{p}_2$'. Then, we can define the followings:

$$\underline{a}_{S1} = \frac{\underline{s} \times \underline{p}_1}{\left|\underline{s} \times \underline{p}_1\right|} = \frac{\underline{s} \times \underline{p}_1}{\left|\underline{s}\right| \cdot \left|\underline{p}_1\right| \cdot \sin\alpha} \quad \text{and} \quad \underline{a}_{S2} = \frac{\underline{s} \times \underline{p}_2}{\left|\underline{s} \times \underline{p}_2\right|} = \frac{\underline{s} \times \underline{p}_2}{\left|\underline{s}\right| \cdot \left|\underline{p}_2\right| \cdot \sin\alpha}.$$

If $e_{1st}(d) > 0$, we defined a spherical tetragon given by the intersections of 4 great circles. These great circles are obtained by rotating the plane of the great circles with adjustment uncertainty $\pm e(d)$ around the studied sky point. Thus, the four intersections determining the rectangular area are the followings:

$$\underline{I}_1 = \frac{\underline{a}_{S1+\varepsilon} \times \underline{a}_{S2+\varepsilon}}{\left|\underline{a}_{S1+\varepsilon} \times \underline{a}_{S2+\varepsilon}\right|}, \quad \underline{I}_2 = \frac{\underline{a}_{S1+\varepsilon} \times \underline{a}_{S2-\varepsilon}}{\left|\underline{a}_{S1+\varepsilon} \times \underline{a}_{S2-\varepsilon}\right|}, \quad \underline{I}_3 = \frac{\underline{a}_{S1-\varepsilon} \times \underline{a}_{S2+\varepsilon}}{\left|\underline{a}_{S1-\varepsilon} \times \underline{a}_{S2+\varepsilon}\right|}, \quad \underline{I}_4 = \frac{\underline{a}_{S1-\varepsilon} \times \underline{a}_{S2-\varepsilon}}{\left|\underline{a}_{S1-\varepsilon} \times \underline{a}_{S2-\varepsilon}\right|}.$$

We checked the sign of the vertical component of the intersections, and if it was negative, we took $-\underline{I}_i$ instead. Here the $\pm\varepsilon$ in the lower index means that the vector is rotated by $\pm\varepsilon = \pm e(d)$ angle. The general mathematics of the rotation of a 3D vector around an axis by a given degree is the following: If we rotate vector $\underline{v}(x,y,z)$ around axis $\underline{a}(a_x,a_y,a_z)$ with angle α, then we get vector $\underline{v}'(x',y',z')$, the coordinates of which are:

$$x' = x\left[\cos\alpha + (1-\cos\alpha)a_x^2\right] + y\left[(1-\cos\alpha)a_x a_y - a_z\sin\alpha\right] + z\left[(1-\cos\alpha)a_x a_z + a_y\sin\alpha\right],$$
$$y' = x\left[(1-\cos\alpha)a_x a_y + a_z\sin\alpha\right] + y\left[\cos\alpha + (1-\cos\alpha)a_y^2\right] + z\left[(1-\cos\alpha)a_y a_z - a_x\sin\alpha\right],$$
$$z' = x\left[(1-\cos\alpha)a_x a_z - a_y\sin\alpha\right] + y\left[(1-\cos\alpha)a_y a_z + a_x\sin\alpha\right] + z\left[\cos\alpha + (1-\cos\alpha)a_z^2\right].$$

(5) From the estimated Sun positions E, we selected only those that fell into the 72 parameter intervals obtained from numerical error determination of the second step (see subchapter 3.2.2.). We used the error vector $\boldsymbol{e}_{2nd}(\Delta\theta, \Delta\varphi)$ to shift these E-values on the surface of the sky dome and obtained the shifted estimated Sun positions E_{sh}. To do these shifts, first we converted the Cartesian representation of the estimated Suns to 3D polar representation: $f(x', y', z') \rightarrow g(r, \theta, \varphi)$. Then, the converted coordinates were the followings:

$$r = \sqrt{x'^2 + y'^2 + z'^2}, \quad \theta = \arccos(z'), \quad \phi = \arctan(y'/x'),$$

where r is the vector length, θ is the elevation angle measured from the horizon, and φ is the azimuth angle measured clockwise in the horizontal plane. After shifting, we obtained the new coordinates:

$r' = r$, $\theta' = \theta + \Delta\theta$, $\varphi' = \varphi + \Delta\varphi$.

(6) For each position E_{sh}, we calculated the elevation error $\Delta\theta_E$ based on the error function $e_{3rd}(\theta)$ of the third step. For each E_{sh}, we got an interval between $E_{sh} - \Delta\theta_E$ and $E_{sh} + \Delta\theta_E$ that was divided into equal vertical angular distances by 0.2°. Thus, instead of one E_{sh} point, we

got several points marked with $P_\theta(r, \theta'', \varphi')$ based on the elevation error of the third step. These points differed from E_{sh} only in the elevation coordinate being $\theta' - \Delta\theta_E \leq \theta'' \leq \theta' + \Delta\theta_E$.

(7) In the fourth step, the navigator had to align the shadow-stick parallel to the solar meridian, thus for each P_θ, we determined the alignment error $e_{4th}(\theta)$. Then, the new azimuth direction of a given point fell in the following interval: $\varphi' - e_{4th} \leq \varphi'' \leq \varphi' + e_{4th}$. The new estimated position of the Sun can be characterized as $P_E(r, \theta'', \varphi'')$. Thus, instead of each P_θ, we got several points possessing the errors of all the four steps performed in the navigation process (Fig. 3.8g).

(8) The direction ω_N of the geographical North was derived in the following way: The final estimated Sun P_E had to be projected to the 2D surface of the sun-compass using the shadow-stick, the tip of which represented the tip of the invisible gnomonic shadow $S_E(x_S, y_S)$. Its coordinates can be described as $x_S = \tan(\theta'')\cdot\cos(-\varphi'')$ and $y_S = \tan(\theta'')\cdot\sin(-\varphi'')$. Then, the sun-compass had to be rotated until the shadow tip of the vertical gnomon falls on the appropriate gnomonic line engraved in the compass' surface. After the rotation, we get the new coordinates of the projected point: $x_S' = x_S\cdot\cos(\alpha) - y_S\cdot\sin(\alpha)$, $y_S' = x_S\cdot\sin(\alpha) + y_S\cdot\cos(\alpha)$, where α is the angle of rotation. The symmetry axis of the gnomonic line would exactly point towards the geographical North, if there were no errors. Since in reality the four navigation steps have more or less errors, the symmetry axis of the gnomonic line points towards a direction that differs from the geographical North with an angle ω_N when the shadow tip falls on the gnomonic line. Since the gnomonic line is well visible, we considered the minimal error of this rotation (which did not affect the navigation) as negligible. This angle ω_N is the navigation error belonging to (i) a specific pair of sky points m_1 and m_2 with uncertainties e_1 and e_2 of sunstone adjustment in the first step, (ii) a parameter group (θ_S, γ_1, γ_2, δ) with elevation and azimuth uncertainties ($\Delta\theta$, $\Delta\varphi$) of intersection finding in the second step, (iii) an estimated solar elevation θ_E with elevation error $\Delta\theta_E$ in the third step and (iv) an estimated azimuth error of the shadow-stick alignment $e_{4th}(\theta)$ of sky-polarimetric Viking navigation in the fourth step for a given date (e.g. spring equinox or summer solstice).

(9) For a given sky situation, we obtained the navigation error $\Delta\omega_N$ in the following way: Angles ω_N for each estimated Sun position P_E were collected into a histogram, that was smoothed (convoluted) by a normalized Gaussian function with 5° half-kernel size and 5°

standard deviation. This smoothed curve represented the distribution of the North error $\Delta\omega_N$ with a maximum at angle ω_{max} and a half bandwidth $\Delta\omega$ meaning the full width at half maximum (Fig. 3.8h). The smaller $|\omega_{max}|$ and $\Delta\omega$ were, the more accurate the sky-polarimetric navigation was.

(10) There were always two possibilities to project the gnomonic shadow cast by the estimated Sun position P_E onto the gnomonic line (Fig. 3.8i): either in the forenoon (when the sun-compass had to be rotated until the shadow tip fell on the forenoon half of the gnomonic line) or in the afternoon (when the sun-compass had to be rotated until the shadow tip fell on the afternoon half of the gnomonic line). Thus, we determined the navigation errors ω_N for both forenoon and afternoon.

We performed these steps applying three different sunstone crystals (calcite, cordierite, tourmaline) for two astronomically momentous dates (spring equinox and summer solstice, Fig. 3.8j) and for forenoon and afternoon. Thus, for one sky situation we obtained $3 \times 2 \times 2 = 12$ different $\Delta\omega_N$ data. In all the 1080 investigated sky situations, we used only such solar elevations that could have occurred during the onetime Viking main sailing route along the 61° northern latitude. Thus, the maximal solar elevations were 29° and 52° for spring equinox and summer solstice, respectively. Sky situations above these elevation limits were removed from data evaluation. The gnomonic lines were calculated with the program developed by Bernáth et al. (2013a).

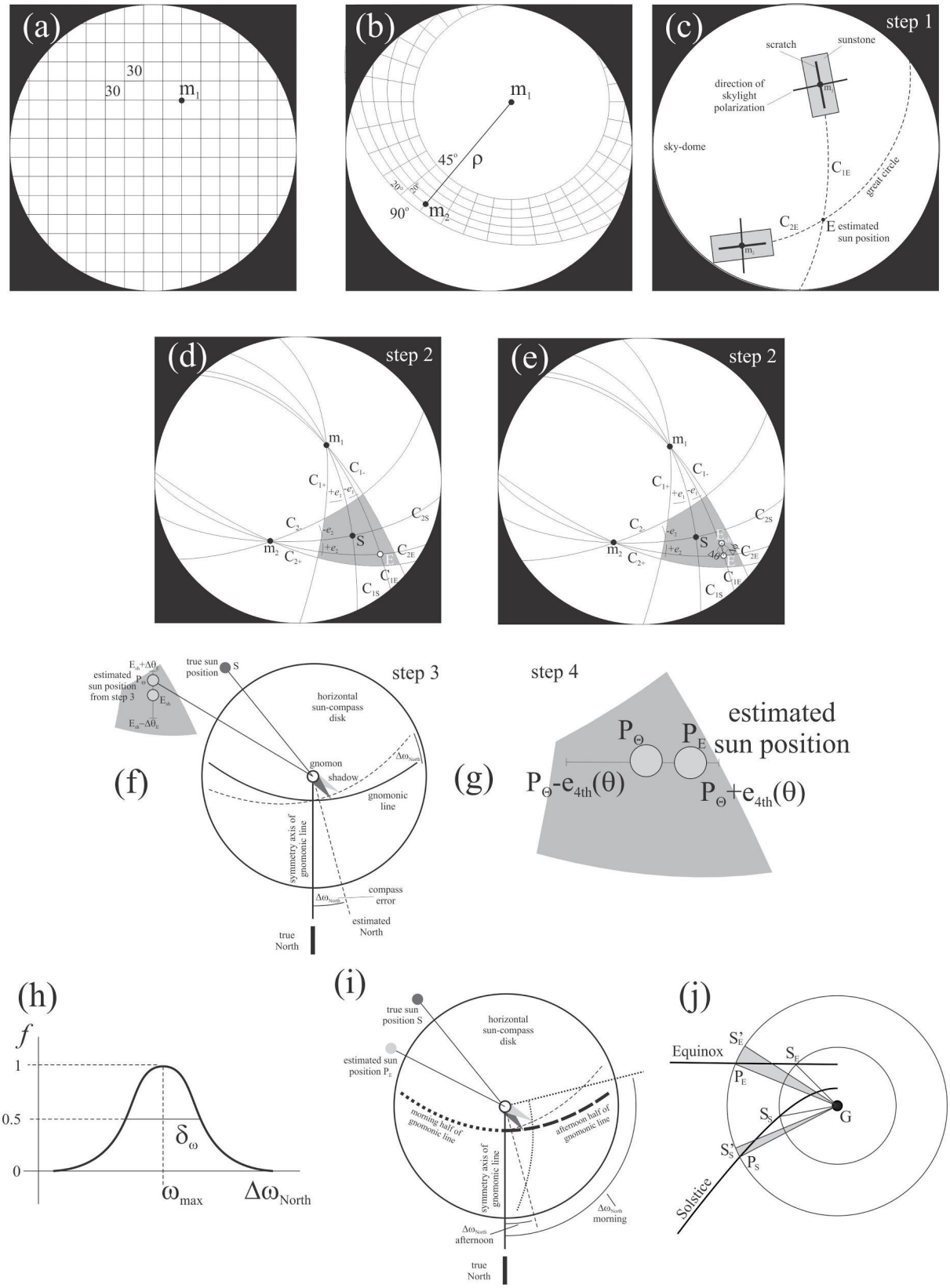

Figure 3.8: Steps of determination of the North uncertainty $\Delta\omega_N$. (a) Celestial square grid from which sky point m_1 is chosen, where the first sunstone is rotated. (b) Polar grid from which point m_2 is chosen, where the second sunstone is rotated at an angular distance γ from m_1. (c) The first step of sky-polarimetric Viking navigation. (d) Adjusting the orientation of

sunstones at sky points m_1 and m_2 has errors e_1 and e_2, which determine a spherical rectangle (grey) containing the real Sun position S and all possible estimated Sun positions E. (e) By finding the intersection of the great celestial circles where the estimated Sun positions E are located, the navigator commits elevation error $\Delta\theta$ and azimuth error $\Delta\varphi$, thus E has to be shifted with a vector ($\Delta\theta$, $\Delta\varphi$) getting the shifted estimated Sun position E_{sh}. (f) The third step of sky-polarimetric navigation with a North uncertainty $\Delta\omega_N$. The elevation of the Sun is estimated with an elevation error $\Delta\theta_E$, thus the estimated Sun position P_θ from the third step can be found in the inaccuracy interval between $E_{sh} - \Delta\theta_E$ and $E_{sh} + \Delta\theta_E$. (g) In the fourth step, the error of shadow-stick alignment parallel to the meridian of the invisible Sun was characterized by $e_{4th}(\theta)$ function and for each Sun position P_θ we got an interval between $\varphi_S(\theta) - e_{4th}(\theta)$ and $\varphi_S(\theta) + e_{4th}(\theta)$ that was devided into equal horizontal angular distances perpendicular to the meridian, where $\varphi_S(\theta)$ is the azimuth angle of point P_θ. Thus, the measured Sun position P_E can be found in this inaccuracy interval. (h) Distribution (frequency f) of the North error $\Delta\omega_N$ with a maximum at angle ω_{max} and half bandwidth δ_ω being the full width at half maximum. (i) The two possibilities to project the estimated sun position E onto the forenoon and afternoon half of the gnomonic line. (j) The gnomonic lines for the spring equinox (21 March) and the summer solstice (21 June), onto which the real and estimated sun positions were projected. The angular deviation from the gnomonic lines gives the navigation error. G: gnomon. S_E: real sun position projected onto the equinoctial line. S'_E: estimated erroneous Sun position projected onto the equinoctial line. P_E: point that we get after rotating S'_E to fit onto the equinoctial line. S_S: real sun position projected onto the solstice line. S'_S: estimated erroneous Sun position projected onto the solstice line. P_S: point that we get after rotating S'_S to fit onto the solstice line. Grey: angles $\Delta\omega_N$ with which S'_E and S'_S need to be rotated to fit onto the equinoctial and solstice line, respectively.

3.2.5.3. Calculations and data visualization

After the calculation of the error propagation, we got altogether 12 × 90 = 1080 North error $\Delta\omega_N$ values in the 90 (θ, ρ) parameter groups. For each solar elevation interval, we calculated the weighted mean

$$\langle \omega_{max} \rangle = \frac{\sum_{i-1}^{N} (\omega_{max})_i (\delta_\omega)_i^{-2}}{\sum_{i-1}^{N} (\delta_\omega)_i^{-2}} \tag{3.1}$$

and the standard deviation

$$\Delta\omega_{max} = \frac{\sum_{i=1}^{N} [(\omega_{max})_i - \overline{\omega_{max}}]^2}{N}, \ \omega_{max} = \frac{\sum_{i=1}^{N} (\omega_{max})_i}{N} \tag{3.2}$$

of the peaks ω_{max} of North errors. In Fig. 3.17, the range of these peaks is represented by rectangles with horizontal length $2\Delta\omega_{max}$ and uniform vertical length. These values were separately calculated both for forenoon and afternoon. We also studied the standard error

$$\delta\omega_{max} = \sqrt{\frac{1}{\sum_{i=1}^{N} (\delta_\omega)_i^{-2}}} \tag{3.3}$$

that was averaged for the 12 values of $\Delta\omega_N$ in the 90 different (θ, ρ) groups. Equations (3.1)-(3.3) were calculated for the three types of sunstone crystals and for the two specific dates (spring equinox and summer solstice).

The obtained data were visualized in a colour matrix (Figs. 3.18-3.20) in which each cell belongs to a given (θ, ρ) pair and contains the weighted mean $<\omega_{max}>$ of North errors that is coded with colours, where the blue and red hues mean negative and positive values, respectively. In each matrix cell, the standard error is represented with a square, the side length of which is proportional to $\delta\omega_{max}$. The data for forenoon and afternoon are visualized separately.

3.3. Results

3.3.1. Adjustment error of dichroic cordierite and tourmaline sunstones in the first step

In experiment 1 of the first step of sky-polarimetric Viking navigation, the mean μ and the median ε of the adjustment error of both cordierite and tourmaline sunstones approached zero as the degree of polarization d increased from 0 % to 100 % (Fig. 3.9). The difference of $|\mu|$ from zero was the smallest for cordierite in general: at N = 12 depolarizers (d = 5.5 %) the maximum of $|\mu|$ was 3° and 9.4° for codierite and tourmaline, respectively. The summed absolute values of the mean errors were $|\mu|_{sum}^{cordierite}$ = 12.9° and $|\mu|_{sum}^{tourmaline}$ = 20.9°, the

summed absolute values of the medians were $|\varepsilon|_{sum}^{cordierite} = 13°$ and $|\varepsilon|_{sum}^{tourmaline} = 24°$. We calculated these summed absolute values because after the evaluation of the 100 measurement series, we obtained 100 individual data for each d-value set in the experiment. To judge the general accuracy of a sunstone crystal, we introduced these sums that characterized the performance of a crystal better than the average of the corresponding data. The lower these values were, the more accurate the crystal was under the various circumstances in the experiment. Based on these quantitative values, cordierite was better than tourmaline.

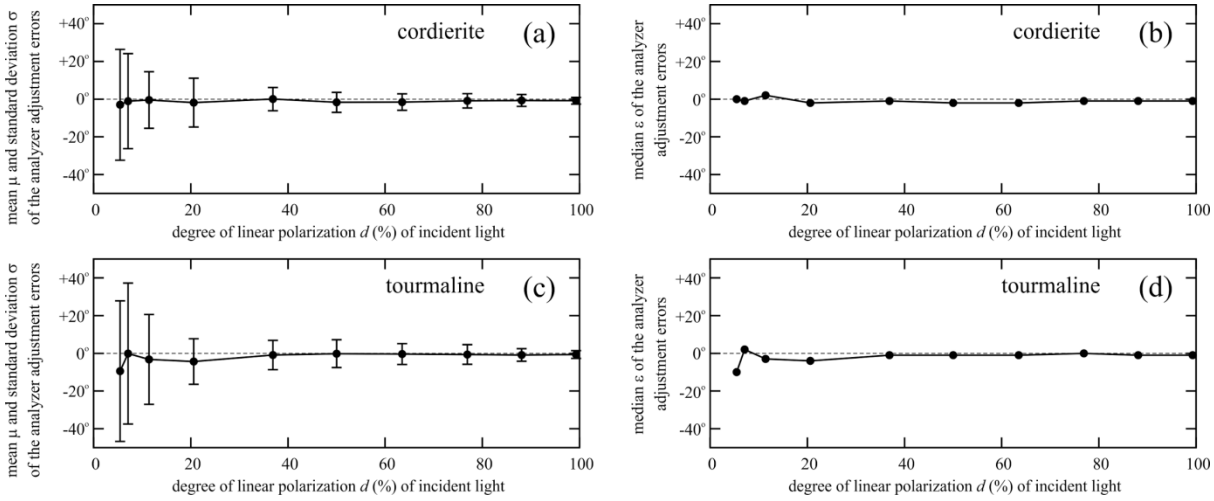

Figure 3.9: Mean μ with standard deviation Σ (a, c) and median ε (b, d) of the adjustment error angles measured for the cordierite (a, b) and tourmaline (c, d) sunstone crystals in experiment 1 as a function of the degree of linear polarization d (%) of incident light averaged for the 100 measurements performed with 10 test persons.

The standard deviations σ of adjustment errors increased with decreasing d of incident light (Fig. 3.10) for both crystals. We also determined the threshold d^*, below which the test persons could not perceive periodical intensity change of light transmitted through the crystals, independently of the test persons' declarations in the following way: if $d < d^*$, the test persons adjusted the orientation of the sunstones randomly (with equal probability). The standard deviation of such a situation is $\sigma \geq \sigma^* = 45°$ for both the tourmaline and cordierite crystals. In the cases of the tourmaline and cordierite, σ was always smaller than the threshold σ^*, thus the measured data series did not show a threshold, where the test persons could not see intensity changes through the crystals.

We also determined d^* by asking the test persons to signal whether they could or could not see intensity changes while rotating the crystals. When the number of depolarizers was $N \geq 9$ ($d^* \leq 11.4$ %), the test persons could not detect intensity changes at least in 10 % and 20 % of the total measurements for cordierite and tourmaline, respectively. At $N = 7$ ($d^* = 20.6$ %) depolarizers, only 3 % and 2 % of the measurements fell below the perceived d^* threshold of the test persons (Table 3.3).

number *N* of depolarizers	**0–5**	**7**	**9**	**11**	**12**
d_{green} (%)	99.3–36.9	20.6	11.4	7.1	5.5
f (cordierite)	0	0.03	0.10	0.31	0.39
f (tourmaline)	0	0.02	0.20	0.58	0.64

Table 3.3: Fraction f of the total number of cases when the test persons could not sense intensity changes seen through the rotating dichroic cordierite and tourmaline sunstones as functions of the number N of depolarizers and the degree of linear polarization d (%) of transmitted light in the green (550 nm) part of the spectrum in which the human eye is the most sensitive. Cases with $N = 6$, 8 and 10 did not occur, because in our experiment we used only 0, 1, 2, 3, 4, 5, 7, 9, 11 and 12 depolarizers between the polarizer and the sunstones.

We obtained the error function of the first step by fitting the following function to the values of $\mu+\sigma$ plotted with respect to d for cordierite and tourmaline, separately: $e_{1st}(d) = \frac{1^\circ}{ad+b} + c$, with $0 \leq d_{min} < d < d_{max} \leq 1$. The fitting parameters a, b, c, as well as p_{min} and p_{max} are given in Table 3.4.

sunstone crystal	**±Δ*a***	**±Δ*b***	**±Δ*c***	d_{min}	d_{max}
cordierite	0.000918	0.0048	0.001°	0.050	0.900
tourmaline	0.000686	0.00351	0.0173°	0.050	0.900
calcite 1 (equal intensity: task 1)	0.000044	0.0061	0.1329°	0.369	0.900
calcite 1 (maximal contrast: task 2)	0.00052	0.00198	0.0378°	0.050	0.900
calcite 2 (equal intensity: task 1)	0.0066	0.0046	0.1821°	0.071	0.900
calcite 2 (maximal contrast: task 2)	0.000394	0.00206	0.1826°	0.050	0.900
calcite 3 (equal intensity: task 1)	0.00154	0.00834	0.7082°	0.050	0.900
calcite 3	0.00125	0.00684	0.5455°	0.050	0.900

(maximal contrast: task 2)					
calcite 4 (equal intensity: task 1)	0.000966	0.00438	0.1532°	0.050	0.900
calcite 4 (maximal contrast: task 2)	0.000178	0.00676	0.3144°	0.050	0.900

Table 3.4: Numerical values of the standard deviations Δa, Δb and Δc of the fitting parameters a, b and c for the error function $e_{1st}(d) = \frac{1^\circ}{ad + b} + c$ with $d_{\min} < d < d_{\max}$ obtained for the adjustment of cordierite, tourmaline and four calcite sunstone crystals.

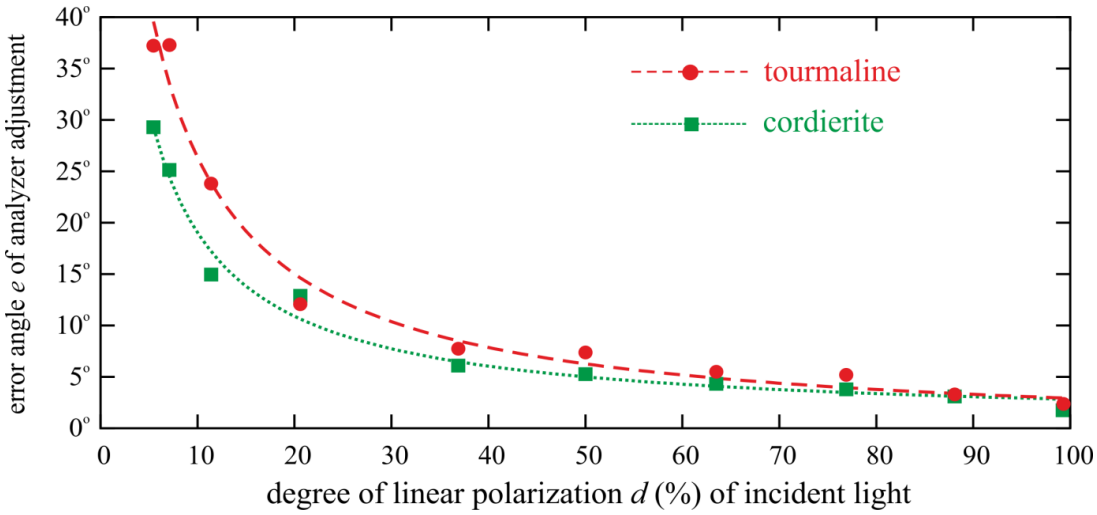

Figure 3.10: Error functions $e_{1st}(d)$ obtained for the dichroic cordierite and tourmaline sunstone crystals in our psychophysical experiment. d (%) is the degree of linear polarization of incident light, and e is equal to the standard deviation Σ of the error angles of sunstone adjustment. The continuous hyperbolic curves were fitted to the measured data points to obtain the continuous error functions of the first step of sky-polarimetric Viking navigation.

3.3.2. Adjustment error of birefringent calcite sunstones in the first step

In experiment 2 of the first step of sky-polarimetric Viking navigation, in accordance with exiperiment 1, the mean μ and the median ε of the adjustment errors of the four calcite crystals approached zero as the degree of polarization d of incident light increased from 0 to 100 % both in the equal intensity (task 1) and maximal contrast (task 2) tasks. The d^+ threshold, where contaminations made impossible to detect equal light intensities seen through the crystals, was 36.9 and 7.1 % for the most contaminated calcites 1 and 4, respectively. The standard deviation σ of calcite adjustment errors increased with decreasing

d of incident light in both adjustment tasks for all the four calcite crystals. This is also in accordance with the result obtained for dichroic cordierite and tourmaline sunstones.

	$\Sigma\lvert\mu\rvert$(°)		$\Sigma\lvert\varepsilon\rvert$ (°)	
sunstone	**equal intensity (task 1)**	**maximal contrast (task 2)**	**equal intensity (task 1)**	**maximal contrast (task 2)**
calcite 1	20.4	4.3	26.0	4.0
calcite 2	11.4	8.4	11.5	10.0
calcite 3	14.0	16.4	16.5	8.0
calcite 4	5.0	3.6	8.5	5.5

Table 3.5: Summed absolute values Σ|μ| and Σ|ε| of the mean μ and median ε of the adjustment errors cumulated for degrees of polarization 36.9 % < *d* < 100 % in the case of the four studied calcite crystals in task 1 (equal intensity adjustment) and in task 2 (maximal contrast adjustment).

We compared the summed absolute values $|\mu|_{sum}$ and $|\varepsilon|_{sum}$ of the adjustment errors in Table. 3.5. So that the crystals could remain comparable in spite of the contaminations of calcites 1 and 4, these values were calculated for 36.9 % ≤ *d* < 100 %. Considering the mean and median of adjustment errors, in task 1, calcite 1 was the best and calcite 4 was the worst, calcites 2 and 3 performed similarly, which is not surprising, since they were split from the same major crystal. In task 2, calcite 4 was the most and calcite 3 the least accurate and the $|\mu|_{sum}$- and $|\varepsilon|_{sum}$-values of calcites 1, 2 and 4 were were smaller than those in task 1. This suggests, that maximal contrast was easier to detect even at low *d*-values than equal intensity, in addition, the different contaminations in the two optical paths did not shift the angle of maximum contrast for different *d*-values. Surprisingly, calcite 3 with polished surfaces was slightly less accurate than the unpolished calcite 2.

The error functions of the four calcites (Fig. 3.11, Table 3.4) were determined for tasks 1 and 2 separately, the same way as in experiment 1.

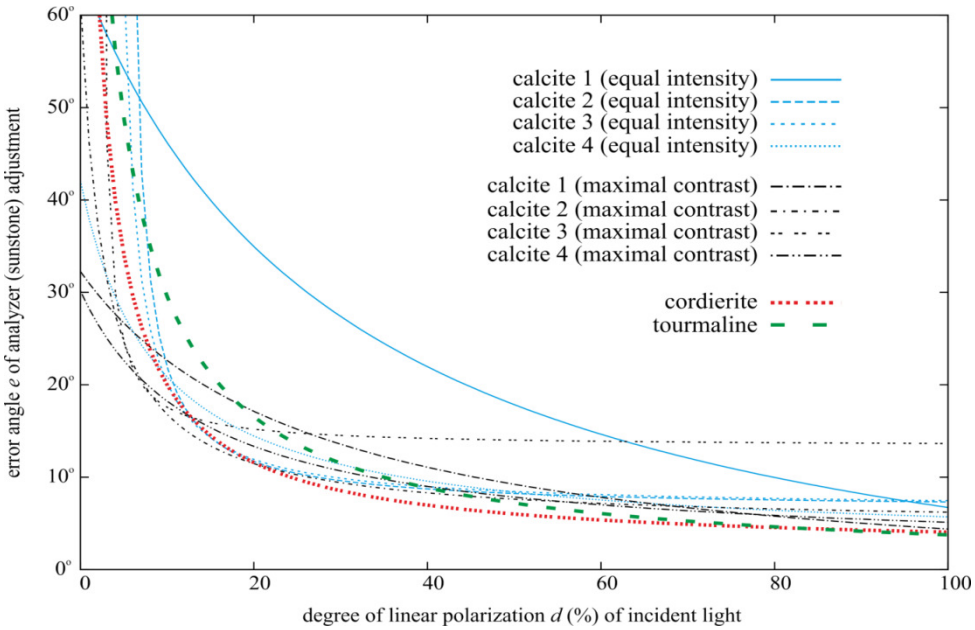

Figure 3.11: Error functions $e_{1st}(d)$ obtained for the four birefringent calcite crystals in our psychophysical experiment. d (%) is the degree of polarization of incident light, and e is the sum of the mean μ and standard deviation Σ of the error angles of calcite adjustment. The continuous hyperbolic curves were fitted to the measured data points to obtain the continuous error functions of the first step. For comparison, the error functions of dichroic cordierite and tourmaline crystals are also displayed.

We also studied the d^* threshold of intensity change perception of the test persons seen through the crystals. Such cases occurred only at d = 36.9, 20.6, 11.4, 7.1, 5.5 %. For higher d-values the test persons could always detect intensity changes while rotating the crystals. Altogether 1077 cases were counted when no intensity changes were detected (Fig. 3.12). Concerning the numbers of these cases, there was a difference between tasks 1 and 2: In task 1, by 240 more cases were marked than in task 2. This also suggests that the maximal contrast adjustment method was more comfortable for the test persons, and a navigator could use it more confidently. We determined a threshold line at which no intensity changes were detected in 10 % of the measurements at a given d-value. This threshold was d^* = 11.4 % for all calcites but for calcite 1 in task 1, for which d^* was 20.6 %. These cases took 35 % of all the 2200 measurements (10 d-values for 11 test persons repeated 10 times in 2 tasks, 10 × 11 × 10 × 2 = 2200). When the above threshold was set to 50 % of the measurements at a given d-value, d^* was less than 10 % for all calcites in both tasks with the exception of calcite 1 in task 1 where d^* = 20.6 %. These cases took 4 % of all the 2200 measurements (Fig. 3.12).

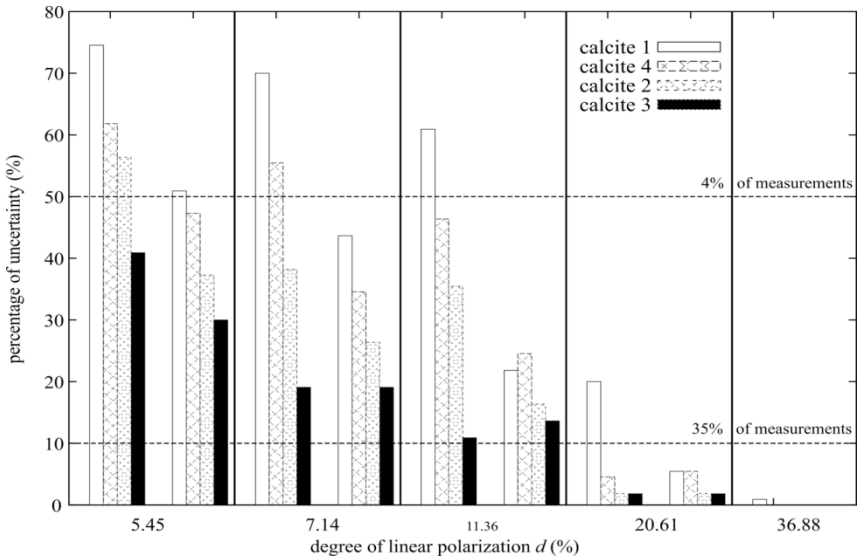

Figure 3.12: Percentage of uncertainty among the 110 measurements in experiment 2 for task 1 (equal intensity adjustment) and task 2 (maximal contrast adjustment) when the test persons could not sense intensity changes in the light spots of rotating calcite crystals as a function of the degree of polarization d (%) of incident white light. The horizontal dashed line marks the thresholds at 10 % and 50 % of uncertainty (the percentage of the measurements for a given crystal and a given d-value, when no intensity changes were detected), above which the sky-polarimetric Viking navigation could not be used. At the 10 % threshold 35 % of all the 2200 measurements was regarded as insecure, while at the 50 % threshold, only 4 % of all the 2200 measurements were insecure.

3.3.3. Error function of solar elevation estimation in the third step

The errors of the solar elevation estimation and their standard deviations were calculated according to the calibration for all the 10 test person individually. These results are seen in Figs. 3.13 and 3.14. The standard deviation of the calibration curves generally increased, although, some test persons (e.g. 5, 8 and 10) had a break in the monotonously growing calibration curve, the causes of which are described in detail in subchapter 3.4. The standard deviation of elevation errors also showed an increasing tendency as a function of the virtual solar elevation. For some test persons, clear overestimations (test person 7) and underestimations (test persons 4, 8 and 10) of the solar elevation could be observed. The cumulated elevation error Σ, according to which test persons 1, 7 and 10 were selected, is summarized in Table 3.6. Σ for the worst navigator (test person 10 with the highest Σ) was almost four times as much as that for the best navigator (test person 1 with the lowest Σ),

while test person 7 (with the highest standard deviation σ of μ) had 2.5 times higher errors than the best navigator.

test person	cumulated elevation error Σ (°)	rank
1	**79.28 (25.16 %)**	**1**
2	115.20 (36.56 %)	7
3	85.33 (27.08 %)	2
4	149.89 (47.57 %)	8
5	111.81 (35.48 %)	5
6	88.02 (27.93 %)	3
7	**193.83 (61.51 %)**	**9**
8	110.16 (34.96 %)	4
9	113.55 (36.04 %)	6
10	**315.10 (100 %)**	**10**

Table 3.6: The cumulated elevation error Σ for the 10 test persons and their rank (1 for the best and 10 for the worst navigator). The three selected persons with the lowest (test person 1), highest (test person 10) and second highest (test person 7) error values are marked in bold. The percentages in the brackets mean the relative error of the test persons compared to that of the worst navigator (test person 10).

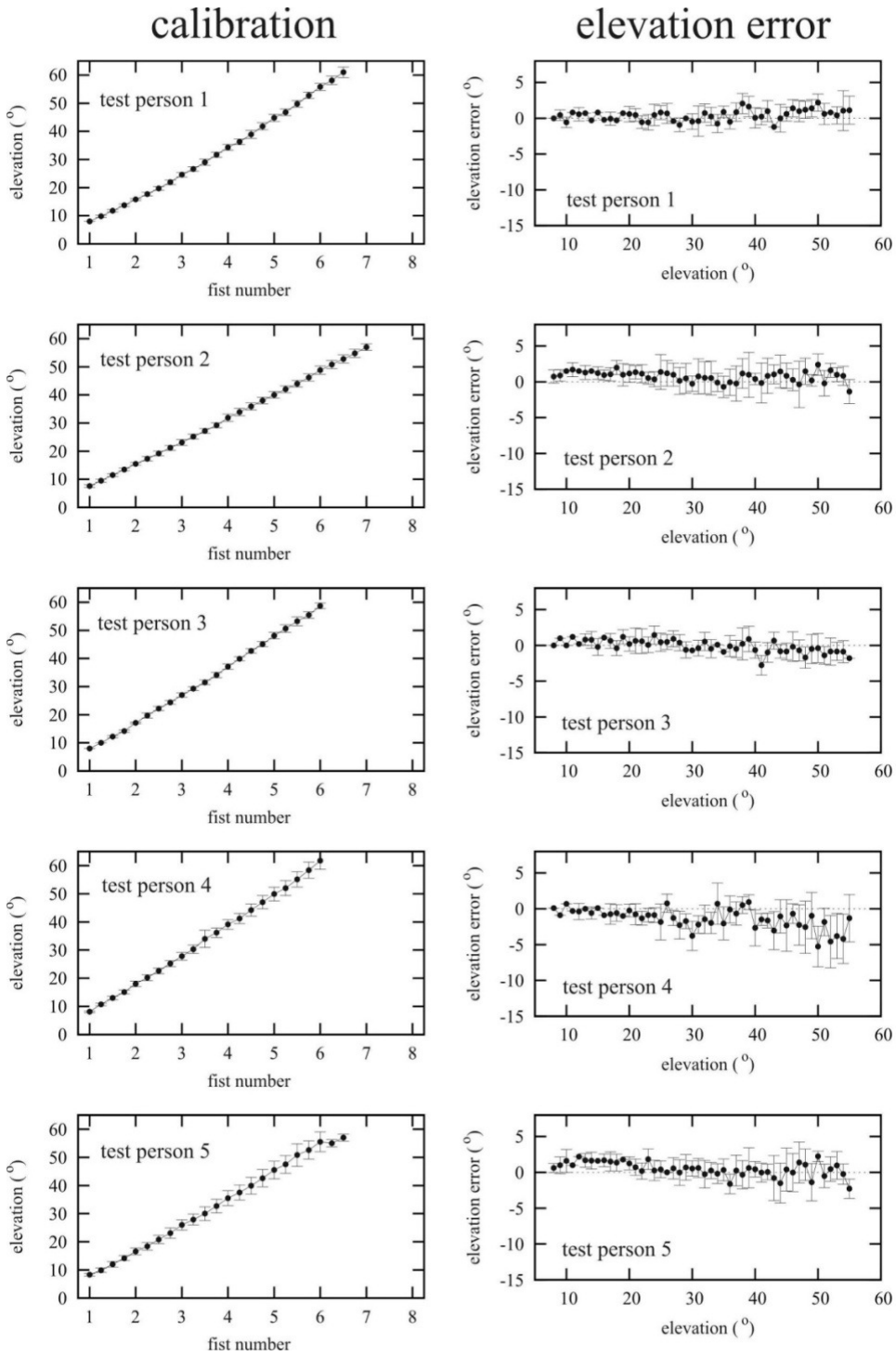

Figure 3.13: Calibration and elevation results for test persons 1-5 in the third step of sky-polarimetric Viking navigation.

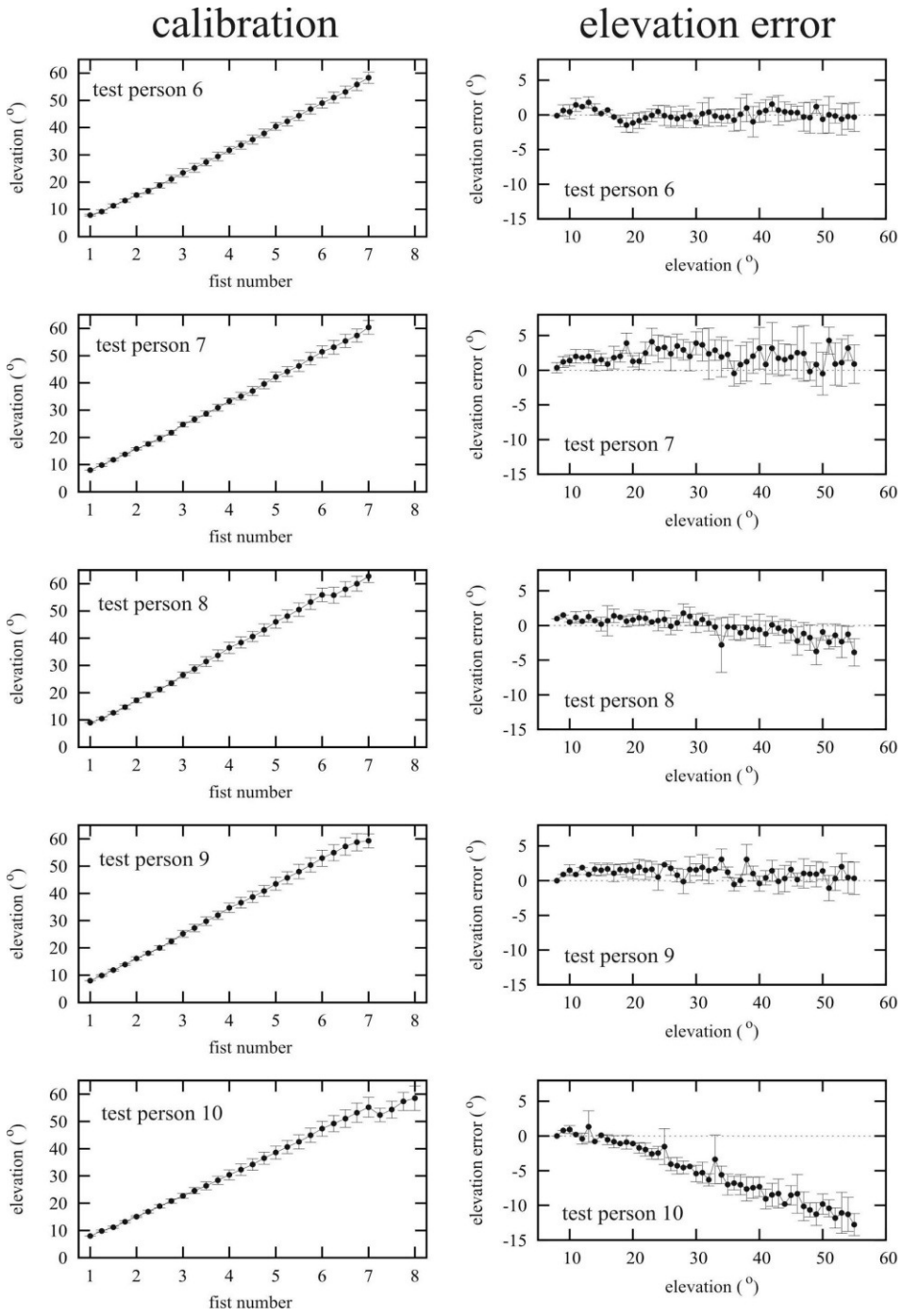

Figure 3.14: Calibration and elevation results for test persons 6-10 in the third step of sky-polarimetric Viking navigation.

The error function of the third step $e_{3rd}(\theta)$ was calculated for the three selected test persons by fitting the function $f(x) = ax^b$ to the values of $|\mu| + \sigma$ as a function of solar elevation θ (Fig. 3.15). The choice of the fitted function form was rather arbitrary and was motivated by catching the trend of the measured data to quantify a continuous curve for interpolation

between the data points. From the selected three test persons, the error function of test person 1 (having the lowest errors) was used for North error determination.

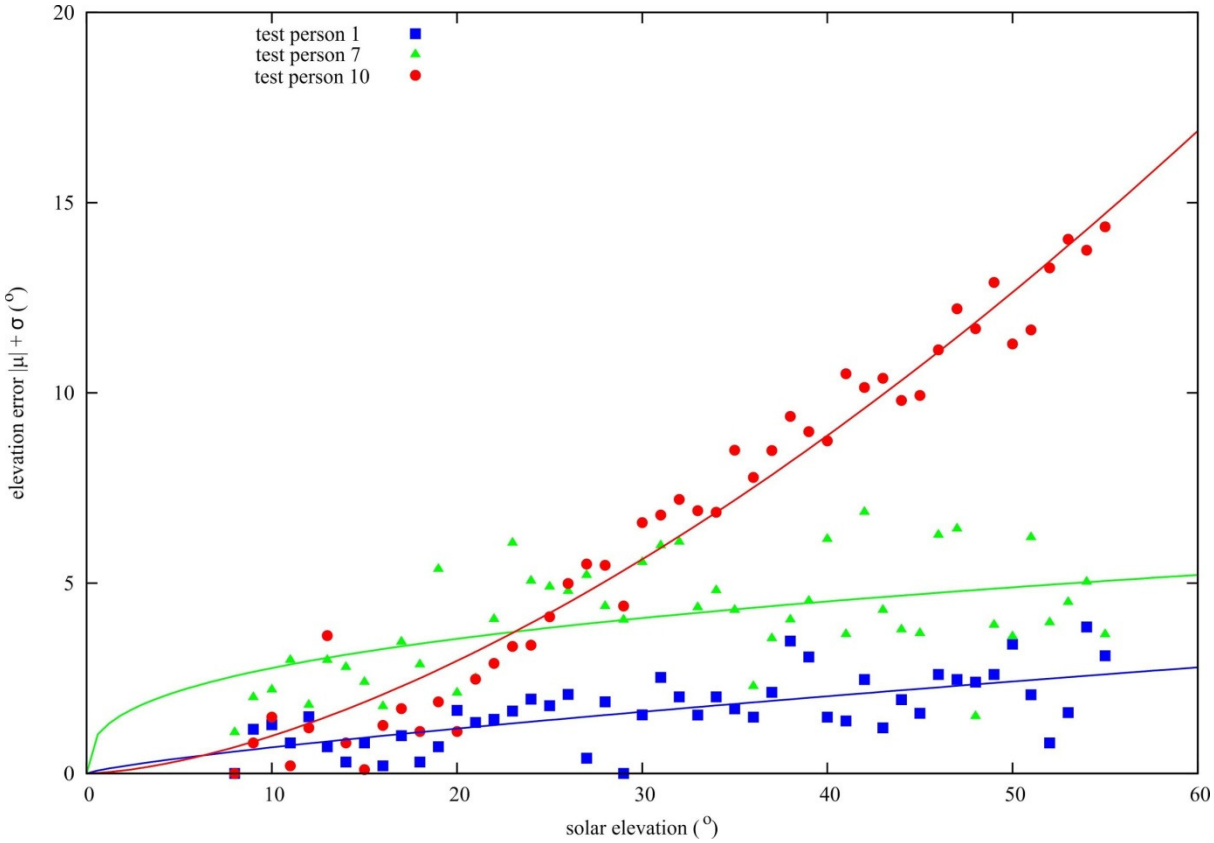

Figure 3.15: Error functions fitted in the form of $f(x) = ax^b$ to the elevation measurement results of the three selected test persons 1, 7 and 10. Table 3.2 contains the numerical values of the fitting parameters.

3.3.4. Error function of shadow-stick alignment in the fourth step

In the fourth step of sky-polarimetric Viking navigation, the difference $\Delta = \varphi_e - \varphi_r$ between the estimated and real azimuth angle of the projected dot was determined for all the 4800 measurements and from these the average difference $<\Delta>$ ± standard deviation σ_φ were calculated for each solar elevation θ. These values approached zero independently of θ, thus the error function of the fourth step was defined by fitting a parabola to the standard deviation of the data, to which we fitted the following function: $e_{4th}(\theta) = 0.0002 \cdot \theta^2 + 1.1829$ (Fig. 3.16). Based on these results, we can see that the fourth step gave the smallest contribution to the North error.

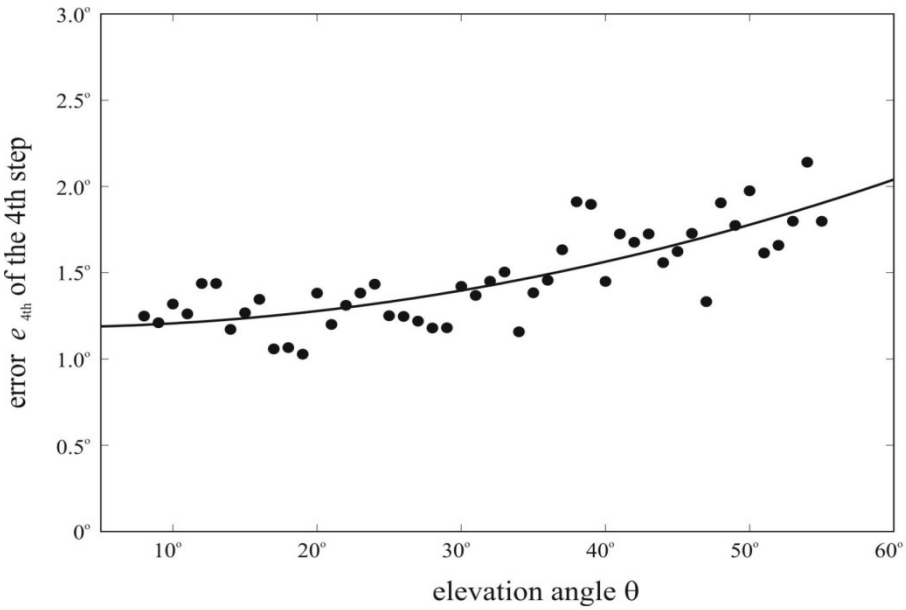

Figure 3.16: Error function $e_{4th}(\theta)$ of the fourth step of sky-polarimetric Viking navigation. The continuous curve is the parabola fitted to the measured values.

3.3.5. Navigation error under different sky conditions

3.3.5.1. Weighted mean and standard deviation of North error distribution peaks

We determined the peaks ω_{max} of the North error distribution for the 1080 selected sky situations and calculated the weighted mean $<\omega_{max}>$ and its standard deviation $\Delta\omega_{max}$ for each applied elevation range. In Fig. 31.7 and Tables 3.7-3.9, we can see that at summer solstice the smallest North errors occurred at solar elevations $35° \leq \theta \leq 40°$ with $|<\omega_{max}>| = 3.4°$ in the forenoon and $|<\omega_{max}>| = 1.8°$ in the afternoon for calcite, $|<\omega_{max}>| = 2.9°$ in the forenoon and $|<\omega_{max}>| = 1.6°$ in the afternoon for cordierite, $|<\omega_{max}>| = 1.2°$ in the forenoon and $|<\omega_{max}>| = 0.2°$ in the afternoon for tourmaline. At spring equinox, the smallest North errors occurred for solar elevations $15° \leq \theta \leq 25°$ with $|<\omega_{max}>| = 6.2°$ in the forenoon and $|<\omega_{max}>| = 3.7°$ in the afternoon for calcite, $|<\omega_{max}>| = 7.1°$ in the forenoon and $|<\omega_{max}>| = 3.0°$ in the afternoon for cordierite, $|<\omega_{max}>| = 5.4°$ in the forenoon and $|<\omega_{max}>| = 6.3°$ in the afternoon for tourmaline.

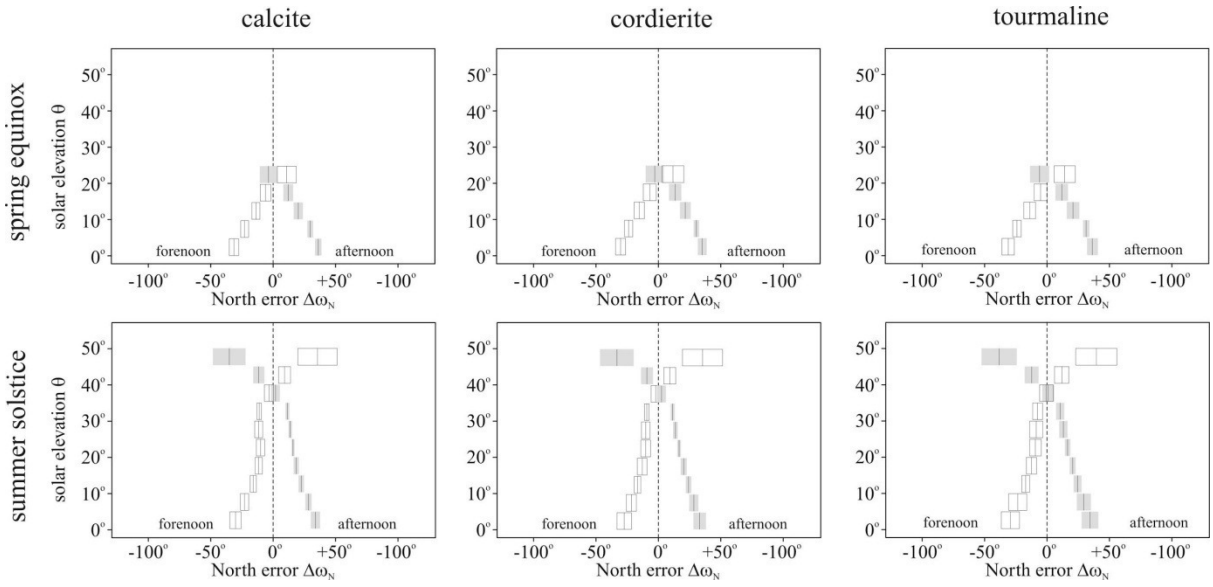

Figure 3.17: Weighted mean $<\omega_{max}>$ and standard deviation $\Delta\omega_{max}$ of peaks ω_{max} of North errors for each elevation interval marked with rectangles for the calcite, cordierite and tourmaline sunstone crystals for navigation in the forenoon and afternoon at spring equinox and summer solstice. The horizontal length of rectangles is $2\Delta\omega_{max}$ and the $<\omega_{max}>$ values are shown by the vertical bars in the centres of the rectangles. White and grey rectangles mean data for forenoon and afternoon, respectively. The vertical dashed line is at $\Delta\omega_N = 0°$.

Using any of the three investigated sunstone crystals, at summer solstice $\Delta\omega_{max}$ of peaks ω_{max} decreased with increasing solar elevation θ both for the forenoon and the afternoon navigation if $\theta < 35°$, then $\Delta\omega_{max}$ increased strongly with increasing θ. At spring equinox, however, $\Delta\omega_{max}$ tendentiously increased with increasing θ for all three sunstones in the forenoon and in the afternoon (Fig. 3.17).

The peaks ω_{max} of North errors changed sign (±) at $40° \leq \theta \leq 45°$ both in the forenoon and the afternoon at summer solstice and at $20° \leq \theta \leq 25°$ at spring equinox (Fig. 3.17).

Comparing the three sunstone crystals (Fig. 3.17, Tables 3.7-3.9), at spring equinox for solar elevations $\theta \leq 20°$, the smallest standard deviations $\Delta\omega_{max}$ of peaks ω_{max} of North errors occurred for calcite ($2.2° < \Delta\omega_{max} < 4.3°$), the largest $\Delta\omega_{max}$ values were found for tourmaline ($2.5° < \Delta\omega_{max} < 5.3°$) and the $\Delta\omega_{max}$-values of cordierite were inbetween ($2.1° < \Delta\omega_{max} < 5.2°$). At summer solstice for solar elevations $\theta \leq 35°$, the smallest standard deviations $\Delta\omega_{max}$ occurred for calcite ($1.1° < \Delta\omega_{max} < 4.5°$), the largest $\Delta\omega_{max}$-values were found for tourmaline ($2.1° < \Delta\omega_{max} < 7.3°$) and the $\Delta\omega_{max}$-values of cordierite were inbetween ($1.4° < \Delta\omega_{max} < 5.8°$).

θ (°)	spring equinox			
	forenoon		afternoon	
	weighted mean $\langle\omega_{max}\rangle$ (°)	standard deviation $\Delta\omega_{max}$ (°)	weighted mean $\langle\omega_{max}\rangle$ (°)	standard deviation $\Delta\omega_{max}$ (°)
0-5	-31.4	3.8	36.0	2.5
5-10	-22.8	3.2	29.6	2.2
10-15	-13.8	3.3	20.1	3.6
15-20	-6.2	4.3	12.0	3.8
20-25	10.9	7.6	-3.7	6.8
θ (°)	**summer solstice**			
	forenoon		**afternoon**	
	weighted mean $\langle\omega_{max}\rangle$ (°)	**standard deviation $\Delta\omega_{max}$ (°)**	**weighted mean $\langle\omega_{max}\rangle$ (°)**	**standard deviation $\Delta\omega_{max}$ (°)**
0-5	-30.1	4.5	33.8	3.6
5-10	-22.9	3.3	28.2	2.4
10-15	-15.9	2.4	22.4	2.1
15-20	-11.6	2.8	18.4	2.0
20-25	-10.1	3.3	15.9	1.1
25-30	-11.6	3.2	13.6	1.3
30-35	-11.3	1.8	11.4	1.5
35-40	-3.4	3.6	1.8	3.4
40-45	9.1	4.7	-11.5	4.3
45-50	35.4	15.7	-35.1	13.0

Table 3.7: Weighted mean $\langle\omega_{max}\rangle$ and standard deviation $\Delta\omega_{max}$ of peaks ω_{max} of North errors versus solar elevation θ for the calcite sunstone crystal for navigation in the forenoon and the afternoon at spring equinox and summer solstice. Note that at equinox θ is not larger than 25°.

θ (°)	spring equinox			
	forenoon		afternoon	
	weighted mean $\langle\omega_{max}\rangle$ (°)	standard deviation $\Delta\omega_{max}$ (°)	weighted mean $\langle\omega_{max}\rangle$ (°)	standard deviation $\Delta\omega_{max}$ (°)
0-5	-30.4	4.0	34.8	3.5
5-10	-23.9	3.3	30.2	2.1
10-15	-15.4	4.1	21.4	4.2
15-20	-7.1	5.2	13.3	4.8
20-25	11.5	8.7	-3.0	7.2
θ (°)	**summer solstice**			
	forenoon		**afternoon**	
	weighted mean $\langle\omega_{max}\rangle$ (°)	**standard deviation $\Delta\omega_{max}$ (°)**	**weighted mean $\langle\omega_{max}\rangle$ (°)**	**standard deviation $\Delta\omega_{max}$ (°)**
0-5	-28.2	5.8	32.2	4.9
5-10	-22.4	4.0	27.4	3.6
10-15	-17.5	2.7	23.2	2.2
15-20	-13.8	3.9	19.4	2.4
20-25	-11.0	3.9	15.7	1.4
25-30	-10.9	3.4	12.8	1.8
30-35	-10.1	1.8	10.6	1.5
35-40	-2.9	3.9	1.6	3.4
40-45	8.3	4.7	-10.0	4.7
45-50	34.4	16.0	-34.0	13.3

Table 3.8: Weighted mean $\langle\omega_{max}\rangle$ and standard deviation $\Delta\omega_{max}$ of peaks ω_{max} of North errors versus solar elevation θ for the cordierite sunstone crystal for navigation in the forenoon and the afternoon at spring equinox and summer solstice. Note that at equinox θ is not larger than 25°.

θ (°)	spring equinox			
	forenoon		afternoon	
	weighted mean $\langle\omega_{max}\rangle$ (°)	standard deviation $\Delta\omega_{max}$ (°)	weighted mean $\langle\omega_{max}\rangle$ (°)	standard deviation $\Delta\omega_{max}$ (°)
0-5	-31.4	4.9	36.0	4.2
5-10	-24.3	3.4	30.9	2.5
10-15	-14.1	4.7	20.5	4.9
15-20	-5.4	5.3	11.4	4.9
20-25	13.8	8.5	-6.3	7.5
θ (°)	**summer solstice**			
	forenoon		**afternoon**	
	weighted mean $\langle\omega_{max}\rangle$ (°)	**standard deviation $\Delta\omega_{max}$ (°)**	**weighted mean $\langle\omega_{max}\rangle$ (°)**	**standard deviation $\Delta\omega_{max}$ (°)**
0-5	-30.0	7.3	33.6	6.6
5-10	-24.1	7.3	28.7	5.5
10-15	-17.7	3.1	23.7	3.1
15-20	-13.1	4.1	19.8	2.4
20-25	-10.0	4.6	15.8	2.1
25-30	-9.3	5.3	12.4	3.3
30-35	-8.2	3.9	9.8	3.2
35-40	-1.2	5.4	0.2	4.6
40-45	11.1	5.8	-12.9	5.4
45-50	38.8	16.5	-38.8	14.0

Table 3.8: Weighted mean $\langle\omega_{max}\rangle$ and standard deviation $\Delta\omega_{max}$ of peaks ω_{max} of North errors versus solar elevation θ for the cordierite sunstone crystal for navigation in the forenoon and the afternoon at spring equinox and summer solstice. Note that at equinox θ is not larger than 25°.

3.3.5.2. θ-ρ matrix of North errors

We visualized the weighted mean $\langle\omega_{max}\rangle$ and the standard error $\delta\omega_{max}$ of the North error peaks ω_{max} for the 1080 selected sky situations in a colour matrix, where the horizontal and

vertical axis represented the cloudiness ρ in oktas and the solar elevation θ in degrees, respectively. The detailed results are seen in Figs. 3.18-3.20 and Tables 3.10-3.12.

At summer solstice, the most accurate navigation was at $35° \leq \theta \leq 40°$ for all the three sunstone crystals. In this solar elevation range, the most accurate navigation with minimal absolute weighted mean $|\omega_{max}|$ ($<\omega_{max}> = -1.4°$) was at $\rho = 2$ and 7 oktas in the forenoon and at $\rho = 7$ oktas ($<\omega_{max}> = -0.1°$) in the afternoon for calcite (Fig. 3.18), at $\rho = 7$ oktas ($<\omega_{max}> = -0.4°$) in the forenoon and at $\rho = 2$ oktas ($<\omega_{max}> = 0.0°$) in the afternoon for cordierite (Fig. 3.19), at $\rho = 3$ oktas ($<\omega_{max}> = -0.2°$) in the forenoon and at $\rho = 3$ oktas ($<\omega_{max}> = 0.3°$) in the afternoon for tourmaline (Fig. 3.20).

At spring equinox, the minimum $|\omega_{max}|$ values were at $15° \leq \theta \leq 20°$, $\rho = 8$ oktas ($<\omega_{max}> = -0.2°$) in the forenoon and at $20° \leq \theta \leq 25°$, $\rho = 1$ okta ($<\omega_{max}> = -0.4°$) in the afternoon for calcite (Fig. 3.18), at $15° \leq \theta \leq 20°$, $\rho = 8$ oktas ($<\omega_{max}> = 0.1°$) in the forenoon and at $20° \leq \theta \leq 25°$, $\rho = 0$ okta ($<\omega_{max}> = -0.1°$) in the afternoon for cordierite (Fig. 3.19) and at $15° \leq \theta \leq 20°$, $\rho = 8$ oktas ($<\omega_{max}> = 0.9°$) in the forenoon and at $20° \leq \theta \leq 25°$, $\rho = 1$ okta ($\omega_{max} = -1.1°$) in the afternoon for tourmaline (Fig. 3.20). For a given ρ, the absolute value of $<\omega_{max}>$ dramatically decreased with increasing θ until the sign (±) change of $<\omega_{max}>$. For a given θ, the trend of this absolute value did not show strong dependence on the cloud coverage ρ.

Based on these results, we found the following situations as the most disadvantageous for sky-polarimetric Viking navigation (Figs. 3.18-3.20): (i) High solar elevations of $45° \leq \theta \leq 50°$. In this elevation range, the weighted means of navigation errors were $27° < |<\omega_{max}>| < 47°$ for calcite, $23° < |<\omega_{max}>| < 47°$ for cordierite and $26° < |<\omega_{max}>| < 51°$ for tourmaline. Such high solar elevations occur only at summer solstice. (ii) Low solar elevations of $0° \leq \theta \leq 10°$ with high cloudiness 5 oktas $< \rho <$ 8 oktas. In this range, the weighted means of navigation errors were $21° < |<\omega_{max}>| < 38°$ for calcite, $21° < |<\omega_{max}>| < 39°$ for cordierite and $22° < |<\omega_{max}>| < 44°$ for cordierite.

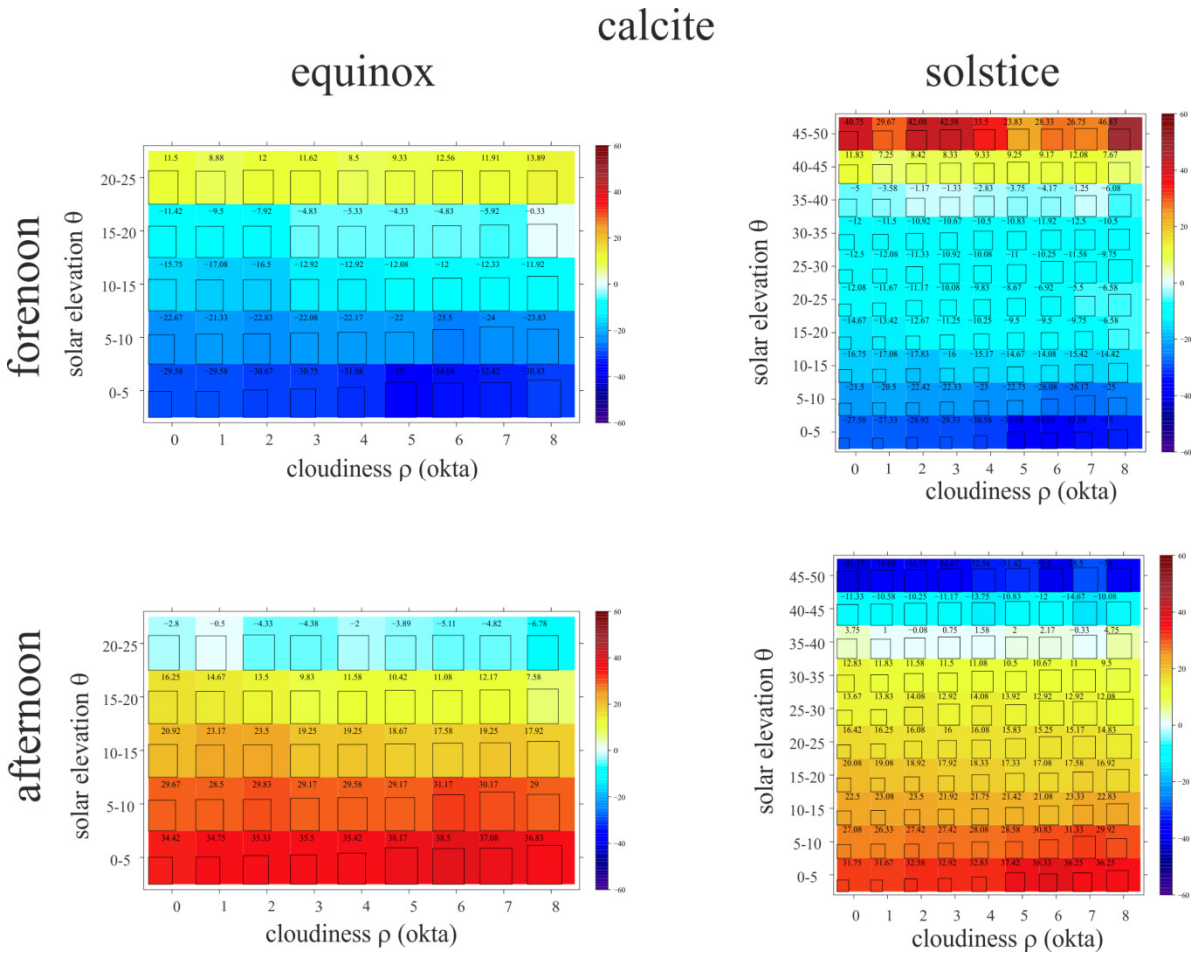

Figure 3.18: Colour matrix plot for the calcite sunstone crystal where each cell belongs to a given solar elevation-cloudiness (θ, ρ) pair and contains the weighted mean $<\omega_{max}>$ of North errors, the values of which are marked with a continuous colour transition from blue to red (blue meaning negative and red meaning positive values), and the relative standard error $\delta\omega_{max}/(\delta\omega_{max})_{max}$ in the given dataset is marked with squares in the cell, the side length of which is proportional to the $\delta\omega_{max}$-values. The data for forenoon and afternoon navigation at spring equinox and summer solstice are visualized separately.

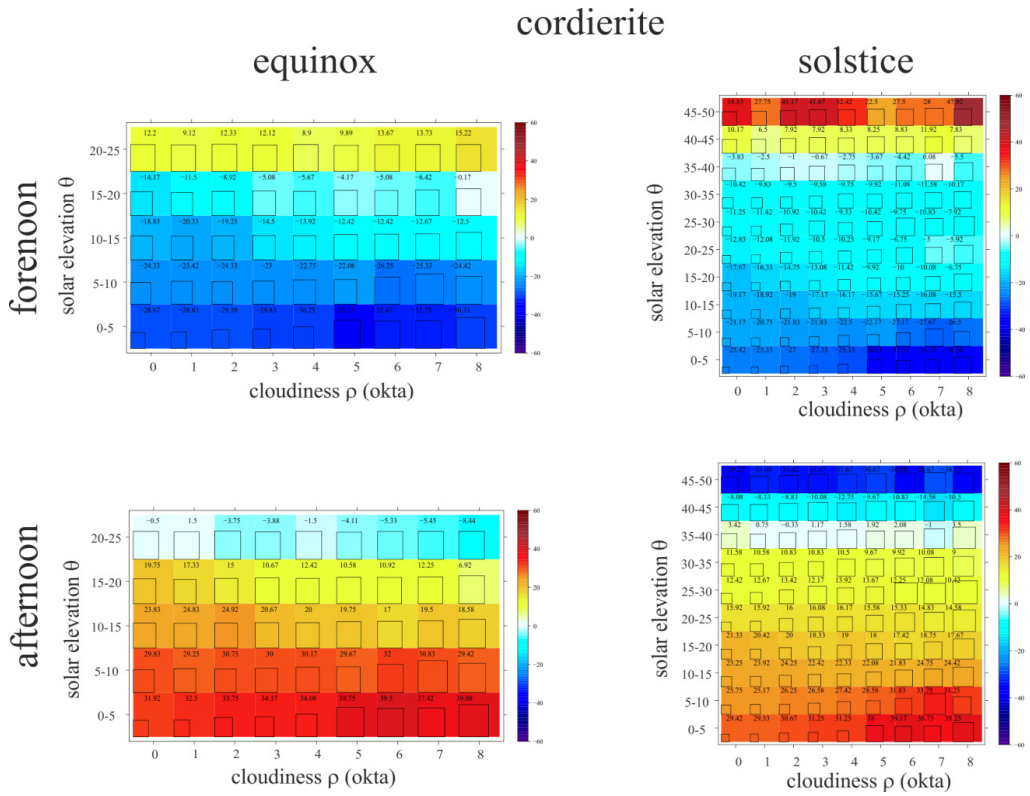

Figure 3.19: As Fig. 3.18 for the cordierite sunstone crystal.

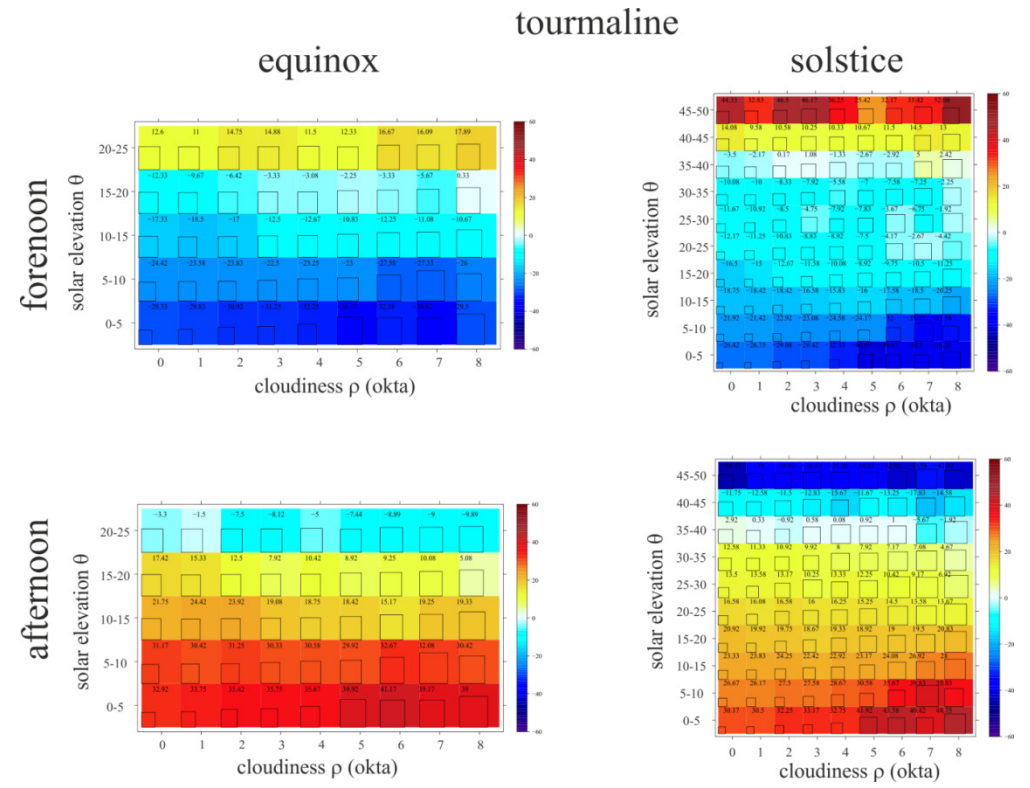

Figure 3.20: As Fig. 3.18 for the tourmaline sunstone crystal.

θ (°)	**ρ (okta)**	**spring equinox**			
		forenoon		**afternoon**	
		weighted mean $\langle\omega_{max}\rangle$ (°)	**standard error** $\delta\omega_{max}$ (°)	**weighted mean** $\langle\omega_{max}\rangle$ (°)	**standard error** $\delta\omega_{max}$ (°)
0-5	0	-29.8	10.3	34.5	10.8
	1	-29.7	10.4	34.8	11.1
	2	-30.9	10.8	35.4	11.4
	3	-31.0	11.2	35.6	11.5
	4	-31.3	11.9	35.5	11.5
	5	-35.0	13.6	38.2	13.2
	6	-33.9	13.3	38.2	13.1
	7	-32.3	13.7	37.0	12.9
	8	-30.9	14.8	36.8	13.8
5-10	0	-22.7	11.7	29.7	11.8
	1	-21.4	11.9	28.5	11.9
	2	-22.9	12.0	29.9	12.1
	3	-22.1	12.4	29.2	12.2
	4	-22.2	12.7	29.7	12.3
	5	-22.2	12.6	29.3	13.0
	6	-25.4	13.5	31.2	13.3
	7	-23.8	14.8	30.1	14.3
	8	-23.7	13.8	29.0	13.5
10-15	0	-15.8	12.5	20.9	12.1
	1	-17.1	12.2	23.2	12.1
	2	-16.5	12.4	23.5	12.3
	3	-12.9	12.5	19.1	12.4
	4	-13.0	12.5	19.3	12.7
	5	-12.1	12.8	18.7	12.7
	6	-11.9	12.9	17.7	13.3
	7	-12.4	13.1	19.2	13.1
	8	-11.9	13.6	17.9	13.6
15-20	0	-11.4	12.4	16.2	11.6
	1	-9.5	12.3	14.5	11.4

	2	-7.9	12.5	13.4	11.9
	3	-4.9	12.6	9.7	12.0
	4	-5.4	12.4	11.6	12.3
	5	-4.3	12.8	10.4	12.5
	6	-4.9	12.7	10.9	12.6
	7	-5.9	12.9	12.1	12.8
	8	-0.2	13.2	7.4	12.9
20-25	0	10.8	14.5	-2.7	11.8
	1	8.6	16.0	-0.4	13.5
	2	11.7	13.5	-4.7	11.7
	3	11.1	16.2	-4.7	14.3
	4	8.5	14.5	-2.2	13.0
	5	9.1	15.1	-3.8	14.1
	6	12.1	15.4	-4.7	14.1
	7	11.8	13.8	-4.9	12.9
	8	13.7	15.3	-6.4	14.7

θ (°)	**ρ (okta)**	**summer solstice**			
		forenoon		**afternoon**	
		weighted mean $\langle\omega_{max}\rangle$ (°)	**standard error** $\delta\omega_{max}$ (°)	**weighted mean** $\langle\omega_{max}\rangle$ (°)	**standard error** $\delta\omega_{max}$ (°)
0-5	0	-27.7	8.1	31.8	8.6
	1	-27.4	8.0	31.7	8.7
	2	-29.0	8.6	32.6	9.1
	3	-29.5	9.0	32.9	9.2
	4	-30.9	9.9	32.9	9.2
	5	-35.3	12.3	37.4	11.5
	6	-33.9	11.6	37.5	11.5
	7	-33.4	12.7	36.1	11.2
	8	-33.2	14.5	36.3	13.0
5-10	0	-21.6	9.5	27.1	9.1
	1	-20.6	9.9	26.4	9.1
	2	-22.5	9.9	27.4	9.3

	3	-22.4	10.4	27.4	9.6
	4	-23.1	11.3	28.2	9.8
	5	-23.1	11.5	28.8	10.9
	6	-25.7	12.4	30.7	11.5
	7	-26.0	15.2	31.3	13.7
	8	-24.9	13.4	29.8	12.3
10-15	0	-16.7	9.8	22.5	9.2
	1	-17.1	10.1	23.1	9.5
	2	-17.8	10.6	23.6	9.8
	3	-15.9	10.9	22.0	10.3
	4	-15.2	11.4	21.7	10.8
	5	-14.7	11.9	21.5	10.9
	6	-14.2	12.8	21.2	12.1
	7	-15.5	13.1	23.0	12.1
	8	-14.6	14.4	22.6	13.3
15-20	0	-14.7	9.5	20.1	9.3
	1	-13.4	9.5	19.1	9.4
	2	-12.7	10.3	18.9	10.2
	3	-11.3	10.9	17.9	10.8
	4	-10.6	11.6	18.4	10.9
	5	-9.9	12.5	17.6	11.8
	6	-9.6	12.8	17.2	12.2
	7	-9.8	13.3	17.5	12.5
	8	-6.6	15.2	16.8	13.5
20-25	0	-12.1	9.3	16.4	9.3
	1	-11.7	10.1	16.2	9.3
	2	-11.2	11.8	16.0	10.2
	3	-10.5	12.3	16.0	10.8
	4	-10.3	12.5	16.1	11.1
	5	-9.3	13.2	15.9	11.8
	6	-7.4	14.5	15.4	11.7
	7	-5.8	15.2	15.2	12.7
	8	-6.7	16.4	14.9	13.7

25-30	0	-12.5	10.2	13.7	9.3
	1	-12.1	10.7	13.9	9.9
	2	-11.4	12.4	14.1	11.1
	3	-11.0	13.9	13.1	11.9
	4	-11.1	12.6	14.2	11.2
	5	-11.5	13.7	14.0	11.9
	6	-10.7	16.5	13.0	12.9
	7	-11.9	16.2	13.0	12.9
	8	-10.0	17.9	12.3	14.6
30-35	0	-12.0	11.7	12.9	10.7
	1	-11.6	11.9	11.9	10.9
	2	-11.0	12.6	11.6	11.7
	3	-10.6	13.0	11.6	12.6
	4	-10.4	14.3	11.1	13.6
	5	-10.8	14.1	10.5	13.5
	6	-11.7	15.0	10.6	13.8
	7	-12.4	15.3	11.1	14.0
	8	-10.6	15.9	9.6	14.4
35-40	0	-5.0	13.7	3.8	13.8
	1	-3.9	13.5	1.3	13.2
	2	-1.4	14.2	0.2	14.1
	3	-1.7	14.8	0.7	14.4
	4	-3.0	15.6	1.7	14.9
	5	-4.0	14.9	2.0	14.6
	6	-4.2	14.9	2.3	15.0
	7	-1.4	16.1	-0.1	15.5
	8	-6.1	17.1	4.9	15.8
40-45	0	11.8	14.5	-11.2	14.3
	1	7.2	14.8	-10.5	15.1
	2	8.3	15.3	-10.2	15.1
	3	7.9	15.7	-11.0	15.4
	4	8.7	15.6	-13.5	15.6
	5	9.2	16.5	-10.5	15.4

	6	8.9	16.3	-11.8	15.6
	7	12.0	16.3	-14.7	15.8
	8	7.6	16.3	-10.0	16.1
45-50	0	41.0	14.5	-41.2	14.6
	1	30.1	15.1	-35.1	14.8
	2	43.7	15.4	-34.5	15.3
	3	41.9	15.9	-34.5	15.8
	4	33.3	16.1	-31.9	15.7
	5	23.9	16.4	-31.2	16.0
	6	28.4	16.4	-39.2	15.6
	7	26.7	16.9	-28.5	16.0
	8	46.5	16.3	-38.2	15.3

Table 3.10: Numerical data of the weighted mean $<\omega_{max}>$ and standard error $\delta\omega_{max}$ of North errors in the forenoon and the afternoon at spring equinox and summer solstice for the calcite sunstone crystal where each cell belongs to a given solar elevation-cloudiness (θ, ρ) pair.

θ (°)	**ρ (okta)**	**spring equinox**			
		forenoon		**afternoon**	
		weighted mean $<\omega_{max}>$ (°)	**standard error $\delta\omega_{max}$ (°)**	**weighted mean $<\omega_{max}>$ (°)**	**standard error $\delta\omega_{max}$ (°)**
0-5	0	-29.0	8.1	31.9	9.7
	1	-29.0	8.4	32.5	10.0
	2	-29.8	9.4	33.7	10.5
	3	-30.1	9.8	34.2	10.8
	4	-30.5	11.2	34.1	10.9
	5	-35.2	14.0	38.6	13.7
	6	-32.7	13.5	38.9	13.4
	7	-32.6	14.2	37.3	13.3
	8	-30.6	16.0	39.1	14.9
5-10	0	-24.5	11.3	29.9	11.1
	1	-23.5	11.9	29.3	11.3
	2	-24.4	11.6	30.8	11.5
	3	-23.1	12.1	30.0	11.9

	4	-22.8	12.6	30.3	11.9
	5	-22.5	12.7	29.8	13.0
	6	-26.0	13.7	31.9	13.8
	7	-25.2	15.8	30.7	15.5
	8	-24.3	14.4	29.4	14.0
10-15	0	-18.8	12.5	23.8	11.3
	1	-20.4	12.3	24.8	11.6
	2	-19.3	12.5	24.9	12.2
	3	-14.5	12.7	20.6	12.3
	4	-13.9	12.7	20.0	12.8
	5	-12.5	13.1	19.7	12.7
	6	-12.3	13.2	17.2	13.6
	7	-12.8	13.5	19.5	13.5
	8	-12.5	14.3	18.6	14.3
15-20	0	-14.2	12.4	19.7	11.0
	1	-11.5	12.1	17.1	10.8
	2	-8.9	12.6	15.0	11.8
	3	-5.2	12.9	10.5	11.9
	4	-5.8	12.6	12.6	12.3
	5	-4.2	13.1	10.7	12.7
	6	-5.2	13.0	10.7	12.9
	7	-6.4	13.3	12.2	13.2
	8	0.1	13.9	6.7	13.4
20-25	0	11.2	15.2	-0.1	11.0
	1	8.5	16.8	1.8	13.1
	2	12.0	14.1	-4.0	11.7
	3	11.7	16.6	-4.2	14.5
	4	8.8	15.3	-1.7	13.1
	5	9.6	15.6	-4.1	14.4
	6	13.2	15.9	-4.6	14.3
	7	13.4	14.5	-5.5	13.4
	8	14.9	16.0	-8.1	15.4

θ (°)	ρ (okta)	summer solstice			
		forenoon		afternoon	
		weighted mean $\langle\omega_{max}\rangle$ (°)	standard error $\delta\omega_{max}$ (°)	weighted mean $\langle\omega_{max}\rangle$ (°)	standard error $\delta\omega_{max}$ (°)
0-5	0	-25.6	6.6	29.4	8.1
	1	-25.4	6.7	29.3	8.2
	2	-27.0	7.4	30.6	8.7
	3	-27.4	8.0	31.2	8.8
	4	-29.4	9.3	31.3	9.0
	5	-35.5	12.7	37.7	12.3
	6	-33.4	12.1	37.5	12.0
	7	-34.1	13.4	36.3	11.8
	8	-34.9	16.4	38.1	14.7
5-10	0	-21.2	7.9	25.8	8.4
	1	-20.8	8.4	25.2	8.3
	2	-21.8	8.6	26.3	8.6
	3	-21.8	9.5	26.6	9.0
	4	-22.5	10.8	27.5	9.4
	5	-22.7	11.1	28.8	10.9
	6	-25.9	12.4	31.2	12.0
	7	-27.4	17.3	33.5	15.6
	8	-26.2	14.6	30.7	13.2
10-15	0	-19.2	8.6	23.3	8.5
	1	-18.9	8.8	23.9	8.9
	2	-19.0	9.8	24.3	9.2
	3	-17.1	10.4	22.5	9.7
	4	-16.3	11.1	22.3	10.5
	5	-15.7	11.8	22.2	10.7
	6	-15.4	13.3	21.8	12.7
	7	-16.0	13.7	24.1	12.6
	8	-15.5	16.0	24.0	14.5
15-20	0	-17.7	8.4	21.3	8.6
	1	-16.3	8.6	20.4	8.7

	2	-14.8	9.8	20.0	9.5
	3	-13.2	10.5	18.3	10.4
	4	-11.9	11.5	19.2	10.7
	5	-10.8	12.8	18.5	11.8
	6	-10.4	13.3	17.7	12.5
	7	-10.2	14.1	18.6	13.0
	8	-6.7	17.0	17.4	14.5
20-25	0	-12.8	8.1	15.9	8.8
	1	-12.2	8.8	15.8	8.9
	2	-12.0	10.8	15.9	9.9
	3	-11.1	11.8	16.1	10.6
	4	-11.0	12.0	16.2	11.0
	5	-10.3	13.1	15.6	12.0
	6	-7.9	14.9	15.5	11.9
	7	-5.6	16.2	14.9	13.2
	8	-6.5	17.6	14.6	14.8
25-30	0	-11.2	8.9	12.4	8.3
	1	-11.5	9.6	12.6	9.1
	2	-10.9	11.7	13.4	10.5
	3	-10.5	13.5	12.4	11.8
	4	-10.7	12.0	14.0	11.0
	5	-11.1	13.7	13.8	12.0
	6	-10.4	17.5	12.4	13.5
	7	-11.3	17.2	12.2	13.3
	8	-8.2	19.7	10.9	15.9
30-35	0	-10.4	10.6	11.6	9.7
	1	-9.9	10.7	10.7	9.8
	2	-9.6	11.6	10.8	10.9
	3	-9.6	12.5	11.1	12.3
	4	-9.7	14.3	10.6	13.9
	5	-9.8	14.1	9.6	13.5
	6	-10.8	15.2	9.8	14.2
	7	-11.4	15.9	10.2	14.5

	8	-10.3	16.8	9.1	15.2
35-40	0	-3.8	12.9	3.4	13.2
	1	-2.7	12.4	1.1	12.1
	2	-1.4	13.5	0.0	13.3
	3	-1.4	14.4	1.0	14.0
	4	-3.0	16.0	1.9	14.8
	5	-3.9	14.9	1.9	14.4
	6	-4.5	15.0	2.3	14.9
	7	-0.4	16.7	-0.5	15.8
	8	-5.4	18.4	3.8	16.6
40-45	0	10.1	14.1	-7.9	13.8
	1	6.4	14.3	-8.2	14.6
	2	7.7	15.1	-8.7	14.9
	3	7.2	15.7	-9.8	15.4
	4	7.3	15.4	-12.4	15.8
	5	8.1	16.8	-9.0	15.2
	6	8.4	16.7	-10.4	15.7
	7	11.9	16.7	-14.6	16.2
	8	7.7	17.0	-10.3	16.6
45-50	0	39.1	14.2	-39.4	14.6
	1	28.0	14.8	-33.1	14.7
	2	42.8	15.4	-33.2	15.5
	3	40.4	16.3	-33.4	16.3
	4	32.0	16.4	-30.6	16.0
	5	22.6	16.7	-30.1	16.4
	6	27.3	16.8	-37.6	16.0
	7	27.8	17.6	-28.6	16.5
	8	47.1	17.1	-38.5	15.6

Table 3.11: Numerical data of the weighted mean $<\omega_{max}>$ and standard error $\delta\omega_{max}$ of North errors in the forenoon and the afternoon at spring equinox and summer solstice for the cordierite sunstone crystal where each cell belongs to a given solar elevation-cloudiness (θ, ρ) pair.

θ (°)	**ρ (okta)**	**spring equinox**			
		forenoon		**afternoon**	
		weighted mean $\langle\omega_{max}\rangle$ (°)	**standard error** $\delta\omega_{max}$ (°)	**weighted mean** $\langle\omega_{max}\rangle$ (°)	**standard error** $\delta\omega_{max}$ (°)
0-5	0	-29.7	8.8	32.9	10.2
	1	-30.0	9.4	33.7	10.5
	2	-31.0	10.5	35.4	11.2
	3	-31.4	11.0	35.8	11.5
	4	-32.3	12.5	35.7	11.6
	5	-36.2	16.2	40.0	15.8
	6	-33.3	15.5	40.3	15.2
	7	-34.7	16.2	39.0	15.3
	8	-29.6	18.7	39.2	18.0
5-10	0	-24.5	11.5	31.2	11.5
	1	-23.6	11.9	30.5	11.6
	2	-23.9	12.1	31.3	11.8
	3	-22.6	12.6	30.4	12.2
	4	-23.1	13.5	30.7	12.5
	5	-23.6	13.8	30.2	14.1
	6	-27.3	15.2	32.7	15.3
	7	-27.3	18.6	31.8	18.5
	8	-26.0	16.6	30.5	16.1
10-15	0	-17.4	12.9	21.8	11.9
	1	-18.5	12.5	24.4	12.2
	2	-17.0	12.8	24.0	12.6
	3	-12.4	13.1	19.2	12.9
	4	-12.7	13.3	18.8	13.5
	5	-11.1	13.8	18.4	13.6
	6	-12.3	14.7	16.0	15.2
	7	-11.9	14.9	19.3	15.0
	8	-10.7	16.7	19.4	16.4
15-20	0	-12.4	13.1	17.4	11.5
	1	-9.7	12.8	15.2	11.5

	2	-6.5	13.1	12.5	12.6
	3	-3.6	13.3	7.8	13.1
	4	-3.3	13.2	10.6	13.1
	5	-2.6	14.0	9.3	13.6
	6	-3.4	14.3	9.2	14.2
	7	-5.4	14.7	10.2	14.4
	8	0.9	15.7	4.9	15.4
20-25	0	11.9	15.6	-2.7	12.4
	1	10.6	17.3	-1.1	14.7
	2	14.6	14.2	-7.7	12.8
	3	14.8	17.4	-8.3	16.0
	4	11.5	15.9	-5.1	14.6
	5	12.2	16.3	-7.3	15.8
	6	16.2	17.3	-8.4	15.9
	7	15.6	15.9	-9.1	14.8
	8	17.7	17.9	-9.8	17.8

θ (°)	**ρ (okta)**	**summer solstice**			
		forenoon		**afternoon**	
		weighted mean $\langle\omega_{max}\rangle$ (°)	**standard error** $\delta\omega_{max}$ (°)	**weighted mean** $\langle\omega_{max}\rangle$ (°)	**standard error** $\delta\omega_{max}$ (°)
0-5	0	-26.6	7.2	30.2	8.4
	1	-26.8	7.4	30.5	8.6
	2	-28.7	8.6	32.1	9.2
	3	-29.4	9.2	33.1	9.4
	4	-32.2	10.9	32.8	9.9
	5	-39.0	15.5	40.9	14.9
	6	-36.9	15.0	40.8	14.4
	7	-38.7	16.2	39.6	14.4
	8	-40.4	20.7	44.1	19.1
5-10	0	-22.0	8.7	26.7	8.7
	1	-21.5	9.1	26.2	8.6
	2	-22.8	9.6	27.5	9.1

	3	-23.0	10.7	27.6	9.8
	4	-24.4	12.4	28.7	10.4
	5	-24.8	12.9	30.7	12.7
	6	-29.3	14.7	34.1	14.2
	7	-37.1	22.0	39.6	19.9
	8	-32.1	18.3	34.6	16.4
10-15	0	-18.7	9.5	23.3	8.9
	1	-18.5	9.8	23.8	9.3
	2	-18.4	10.9	24.3	9.8
	3	-16.4	12.0	22.6	11.1
	4	-16.0	13.1	22.9	12.4
	5	-15.7	13.9	22.7	12.4
	6	-16.8	16.3	23.6	15.5
	7	-17.6	16.8	25.8	15.0
	8	-19.8	20.1	27.1	17.9
15-20	0	-16.5	9.3	20.9	9.1
	1	-15.0	9.4	19.9	9.4
	2	-12.9	11.5	19.7	10.7
	3	-11.9	12.6	18.6	12.3
	4	-10.6	14.1	19.4	12.3
	5	-10.0	15.8	19.4	14.1
	6	-10.3	16.7	19.2	15.3
	7	-10.2	17.9	19.1	15.8
	8	-10.5	21.6	20.5	18.3
20-25	0	-12.3	9.7	16.5	9.6
	1	-11.6	10.8	16.0	9.8
	2	-11.1	13.6	16.5	11.6
	3	-9.9	14.7	16.1	13.0
	4	-10.1	15.1	16.3	13.1
	5	-9.0	16.1	15.4	14.8
	6	-5.5	18.8	14.8	14.5
	7	-3.3	19.8	13.6	16.3
	8	-4.8	21.5	13.7	18.9

25-30	0	-11.7	10.6	13.4	9.7
	1	-11.2	11.9	13.7	10.8
	2	-9.1	14.7	13.4	13.1
	3	-7.3	16.5	11.0	14.5
	4	-9.9	15.0	13.6	13.7
	5	-9.1	17.2	12.6	15.1
	6	-4.4	21.8	10.8	16.7
	7	-7.2	21.5	9.6	16.8
	8	-2.1	23.6	7.3	19.8
30-35	0	-10.2	13.0	12.6	11.9
	1	-10.1	13.0	11.4	11.9
	2	-8.5	14.2	11.0	13.4
	3	-8.1	15.5	10.3	15.3
	4	-6.4	17.6	8.3	17.2
	5	-7.6	17.6	8.3	16.7
	6	-7.8	19.4	7.6	17.4
	7	-7.4	20.2	7.5	17.9
	8	-2.3	21.5	4.7	18.9
35-40	0	-3.5	14.7	2.9	14.8
	1	-2.4	13.7	0.7	13.3
	2	-0.3	14.9	-0.6	14.8
	3	-0.2	16.3	0.3	16.0
	4	-1.3	19.1	0.6	17.3
	5	-2.8	17.7	0.9	16.6
	6	-3.0	18.2	1.2	17.6
	7	3.9	20.1	-4.2	18.4
	8	2.4	22.9	-1.6	19.9
40-45	0	14.0	15.0	-11.5	14.3
	1	9.5	15.0	-12.4	15.4
	2	10.3	16.3	-11.3	16.0
	3	9.3	17.1	-12.5	16.9
	4	8.9	16.8	-15.1	17.1
	5	10.6	18.8	-10.8	17.0

	6	10.7	18.9	-12.8	17.8
	7	14.6	19.1	-17.8	18.3
	8	12.1	20.1	-13.9	19.2
45-50	0	44.4	15.0	-45.4	15.2
	1	33.2	15.8	-39.0	15.3
	2	48.1	16.5	-38.7	16.2
	3	44.4	17.9	-37.9	17.8
	4	35.3	17.8	-33.4	17.2
	5	25.6	18.2	-34.2	17.9
	6	31.6	18.4	-42.0	17.6
	7	32.8	20.3	-33.1	19.0
	8	50.5	19.3	-42.9	17.7

Table 3.12: Numerical data of the weighted mean $<\omega_{max}>$ and standard error $\delta\omega_{max}$ of North errors in the forenoon and the afternoon at spring equinox and summer solstice for the tourmaline sunstone crystal where each cell belongs to a given solar elevation-cloudiness (θ, ρ) pair.

3.4. Discussion

When the Sun was occluded in the sky, the keystone of Viking navigation was the application of sunstones to detect the hidden Sun. Viking navigators went through several-years training and acquired many years of navigational experience to fulfill this task. During our psychophysical experiments measuring the error function of the first step, we have also seen the effect of experience, since three of our test persons had participated earlier in field experiments with sunstones (Bernáth et al. 2013) and generally performed better in these experiments, as well. Since the majority of the test persons in our experiments were inexperienced and it is rather trivial that an experienced navigator could have used the sunstones more accurately, the error of sunstone adjustment might have been overestimated. On the other hand, using polarization-optically ideal sunstone crystals in our experiments, the error of sunstone adjustment might have been underestimated, because the sunstones might have used by Viking navigators were far from ideal and they used these crystals under the harsh conditions of voyages. These over- and underestimations of the error of sunstone

adjustment weaken each other, and nobody knows which effect is stronger. For North error determination, we could only rely on our actual measurements.

We found for calcite crystals, that based on the summed absolute values of the mean errors, calcite 3 with a polished surface performed worse than calcite 2 with an unpolished one, although both crystals were split out from the same major calcite. The explanation for this is the following: As polishing made the crystal more transparent, it could be assumed to be easier to detect intensity differences between the two light spots. However, due to the increased transparency, the internal crystal defects also became more visible, which could confuse and mislead the test persons and resulted in adjusting the sunstone to a wrong orientation. On the other hand, when a calcite with dull surfaces was used, the test person could see the average intensity of the polarized light transmitted through the crystal, while the local contaminations remained blurred. Calcite crystals found in nature are always contaminated, full of inner and superficial scratches, impurities and defects. Hence, according to our findings, it is advisable not to polish the surface of calcite sunstones.

The test persons marked by 240 less cases when they did not see intensity changes through the calcite crystals while rotation for the maximal contrast adjustment than for the equal intensity adjustment. We expected the results to be similar due to the same settings applied in the two adjustment tasks. We assume that the test persons also marked the cases in equal intensity adjustment when they could not find equal intensity, since there was no such angles due to different contaminations in the two optical paths. The detailed description of this phenomenon is seen in subchapter 3.2.1.3. These false markings coming from the misinterpretation of the task could not be excluded. This did not occur at the maximal contrast adjustment, which underlines that finding the maximal contrast is a more reliable method to use calcite sunstones than the equal intensity adjustment.

For North error determination, we used the error function of the best performing calcite (calcite 4) besides that of the two dichroic sunstones. This assumes, that the Viking navigator used two identical crystals to locate the direction of the Sun in two celestial points. However, the Vikings possibly used two calcite sunstones that could have been of different qualities. To simulate this possibility, we should have applied all possible combinations of two calcites that could have increased the computation time dramatically. Thus, we applied only the error function of the best calcite, since it is logical to assume that Viking navigators kept only the best-performing sunstones as navigation tools.

In the planetarium experiment of the third step of sky-polarimetric Viking navigation, we observed a tendency that the standard deviations of the elevation error were larger for

higher solar elevations. This trend occurred both in the calibration and measurement parts. This was expected due to the navigator's cumulative estimation process. Since estimation was based on sequential fist-finger steps, the error itself was cumulative, as seen from our results, and was probably facilitated by the tiring of arm muscles. The test persons had to stretch out their arms and measure the elevation with their fists and fingers by putting the two fists above each other. At low solar elevations ($\theta < 16°$), this task was easy because the test person had to use maximal two fists, but at higher elevations, the fists could accidentally move downwards, owing to gravitation and the tiring of arm muscles, causing an elevation error. The more times a test person had to put his fists on the top of each other, the stronger this effect could became. The same effect could be elicited by the gradual tiring of the test person's arms, as well. Since, this effect occurred randomly during the measurements, it was different in the five sessions and caused the increasing standard deviation of the elevation errors.

The systematic overestimation of some test persons can also be explained by the same effect and was also observed by Bernáth et al. (2013b; 2014) and Farkas et al. (2014). When the fists of the test person moved downwards, he systematically reported a higher elevation than the true one, as seen for test person 7 in Fig. 3.14, for example. Unfortunately, this effect could not be eliminated from the experiment, however, it surely occurred in a real-life situation on the board of a moving Viking ship, as well. In a real-life scenario of Viking navigation, when the ship, and thus the horizon, was continuously swinging due to undulation, it would have been difficult to use any device that could help the navigators in reducing estimation errors caused by muscle stress and/or an occasional slip of their arms and fists.

The systematic underestimation of certain test persons, however, can have a different explanation. When a test person at higher elevations raised his arms, he did not keep them outstretched straight but instead bent them in slightly to compensate for the tiring of arm muscles. This reaction could be unintentional. When the arms were bent in, the fists were closer to the eyes and thus they seemed optically bigger than when the arms were outstretched. A bigger fist referred to a higher elevation, thus the test person reported systematically lower fist-finger values. Since the calibration procedure was shorter than the measurements, this effect happened only rarely or did not occur at all during that part and thus, this effect could not have been compensated. Based on this, according to the calibration, the given fist-finger value belonged to a lower solar elevation than the true one. This effect can be observed for test persons 4, 8 and 10 in Figs. 3.13-3.14.

Some test persons had a break in the monotonously growing calibration curve. This could be caused by tiring of the arm muscles during calibration. When the test person got tired, his hands could accidentally move downwards, or he might have put his hands down for a moment. These are unintentional natural reactions induced by tiring that the test persons could not eliminate during the measurements. This effect also increased the elevation error. Consequently, a navigator who got tired less easily could measure more accurately.

Problems of tiring did not occur for the measurement of the error function of the fourth navigation step, since the device applied for measuring the adjustment error of the azimuth direction of the detected Sun stood still on a tripod stand. We assumed here, that the sun-compass was also fixed and balanced on some kind of a portable stand that might have been used by the Vikings. The error of the parallel alignment of the sun-compass to the azimuth direction of the solar meridian showed a slight dependence on the solar elevation. This can be explained by the following: Human perception can handle abstract projections, such as projecting along a celestial great circle, only with difficulty as found by Farkas et al. (2014), as well. Since, the detected Sun had to be mentally projected first to the horizon, it was easier to perform (with less error) when the Sun was at low solar elevations.

After we determined the navigation error using the earlier measured error functions of the four navigation steps for birefringent calcite and dichroic cordierite and tourmaline sunstone crystals for 1080 different sky situations characterized by the solar elevation θ and cloudiness ρ, we obtained that both in the forenoon and afternoon and for all three sunstones, the standard deviation of North error peaks $\Delta\omega_{\max}$ tendentiously increased with increasing θ at spring equinox, while at summer solstice, the standard deviation $\Delta\omega_{\max}$ decreased with increasing solar elevation θ if $\theta < 35°$, then $\Delta\omega_{\max}$ increased strongly with increasing θ (Fig. 3.17). The net North error was the result of the complex interaction of the θ-dependent error functions of the four steps of sky-polarimetric navigation during the error propagation. The errors from the first step contributed considerably to the net navigation error when the degree of polarization d of skylight was low. The errors of the second step were the most dominant at low solar elevations ($\theta < 35°$ for summer solstice and $\theta < 20°$ for spring equinox), while the errors of the third step became dominant at high solar elevations. The fourth step with errors less than 2.5° had only a slight contribution to the net North error that was is the largest for the highest solar elevations $\theta > 45°$ at summer solstice.

The sign change of the North errors observed both in the forenoon and in the afternoon (Fig. 3.17) can partly be explained by the characteristics of the elevation error in the third navigation step: The contribution of the underestimated solar elevation increased

with increasing θ, thus, the North errors were shifted in the opposite direction. At low solar elevations, the navigator could practically only overestimate the elevation θ, because underestimations would have caused the Sun to be positioned below the horizon that did not occur in our situations. In such cases (when the Sun was position below the horizon), there was no gnomon shadow that could have reached the gnomonic line on the horizontal surface of the sun-compass, thus the measurement had to be repeated. However, elevation errors for low solar elevations were much smaller than for high elevations. Nevertheless, the extent of the third step errors could not explain the sign change alone. The error vector of the second navigation step (Table 3.1) also had an elevation error component which was rather large ($|\Delta\theta| < 21°$) for low solar elevations ($5° \leq \theta \leq 25°$) and was dominantly positive, meaning overestimations, while for high elevations ($35° \leq \theta \leq 55°$), these errors were small ($|\Delta\theta| < 6°$) and their positive and negative values distributed equally, meaning that they did not have a significant contribution to the resulting elevation error. At higher θ-values, the overestimations of the solar elevation became less dominant as θ increased, and for $35° \leq \theta \leq 40°$ at summer solstice and for $20° \leq \theta \leq 25°$ at spring equinox, over- and underestimations of θ occurred with similar frequency. At high solar elevations, around the daily maximum of θ, dominantly underestimations of θ could occur, because if the estimated Sun had been above the possible daily maximum, the tip of the gnomon shadow could not have reached the gnomonic line. In such cases, the Viking navigator had to re-measure the solar elevation, because he could not use it for North estimation. These underestimated solar elevations around noon gave North errors with the opposite sign relative to the overestimated elevations around sunset or sunrise. In Fig. 3.17, it is also clearly seen that the sign of North errors in the forenoon was the opposite of the sign in the afternoon, because the sun-compass had to be rotated in the opposite direction, so that the shadow tip could reach the gnomonic line.

In the θ-ρ matrix of North errors (Figs. 3.18-3.20), we found the most accurate region of sky-polarimetric Viking navigation at solar elevations $35° \leq \theta \leq 40°$ and $15° \leq \theta \leq 15°$ at summer solstice and spring equinox, respectively. As expected, we obtained that the majority of the less overcast situations were the most suitable (with the smallest North errors) for navigation at a given solar elevation. However, we cannot exclude the possibility that this navigation method was also usable under strongly cloudy circumstances, because in some sky situations the minimum of the weighted mean $|<\omega_{max}>|$ of North errors was found at cloudiness ρ = 7–8 oktas. The most advantageous sky situations for this navigation method were at summer solstice when the solar elevation and cloudiness were $35° \leq \theta \leq 40°$ and 1 okta $\leq \rho \leq$ 7 oktas. Although there is no archaeological evidence of increased Viking

seafaring during summertime (around summer solstice) compared to springtime (around spring equinox), our findings show that the sky-polarimetric navigation was more accurate in summer than in spring.

The most unsuitable sky situations (with the largest North errors) for sky-polarimetric Viking navigation could be found more obviously. These occurred generally at low solar elevations ($0° \leq \theta \leq 10°$) with high cloudiness (ρ = 5–8 oktas) when the navigation errors were the highest for all three sunstone crystals and both for summer solstice and spring equinox. At summer solstice, very high solar elevations ($45° \leq \theta \leq 50°$) could also be disadvantageous due to the high North errors.

In the forenoon and in the afternoon, the sign of the North errors were opposite for the corresponding situations. This has the following consequence: If the navigator measured and corrected his orientation several times a day with equal temporal distribution in the forenoon and afternoon, the North errors averaged for the whole day were relatively small due to the opposite sign of forenoon and afternoon North erros (Figs. 3.17-3.20). This is in accordance with the earlier findings of Thirslund (2001) that in sunshine (when the Viking sun-compass was easy to use in direct sunlight), it was worthwhile for the Vikings to orient themselves regularly, several times a day during their sailing routes.

Comparing the different sunstone crystal types, the use of birefringent calcite resulted in a more accurate navigation on average, because the weighted mean and standard error of North errors were smaller than those for dichroic tourmaline and cordierite crystals. Despite we used the error function of the best calcite for North error determination, in some special sky situations (generally at $35° \leq \theta \leq 40°$, 1 okta $\leq \rho \leq$ 6 oktas for summer solstice, and at $20° \leq \theta \leq 25°$, 0 okta $\leq \rho \leq$ 4 oktas for spring equinox), tourmaline and cordierite crystals performed better, respectively, resulting in smaller North errors, meaning a more accurate navigation. The extraordinary performance of the calcite sunstone can be explained by the fact that we selected the best-performing calcite crystal from the four possible ones. Our results corroborated experimentally the widespread belief that calcite could be a better sunstone than tourmaline and cordierite. But, in the above-mentioned special sky situations, it was worth choosing cordierite or tourmaline instead.

Interestingly, we found that the weather conditions at the 61° North latitude sailing route may not have been as severe a hindrance to sky-polarimetric navigation as one would naively have assumed, because North errors dramatically increase for solar elevations $\theta >$ 40°. Since the navigation error tendentiously increased with increasing θ, a navigator at the Equator with much larger θ-values may have had quite a difficult time using this technique.

In our studies (psychophysical laboratory and planetarium experiments), the circumstances were ideal. In a real-life situation, the continuous swaying and rolling of the ship, blowing and cold weather necessarily affect the accuracy of sky-polarimetric navigation. Under these real circumstances the alignment of the shadow-stick and/or the sunstones would have been more problematic. Narrow vessels like those the Vikings used were prone to rocking and bobbing even in smooth seas, but could somewhat be stabilized by hoisting a sail. Thus, our results obviously underestimate the real-life North errors of this navigation method.

Throughout this work, we used the geographical North as a reference direction, from which the navigation error was measured. As mentioned in subchapter 3.1., the Vikings possibly did not use the notion of North in the sense as we do today. Originally and most frequently, they determined the West-East direction. The navigation error, however, was determined generally and could be applied to the deviation from any reference direction.

3.5. Further Studies

The third chapter of my PhD work focused on the measurement of the error functions in the first, third and fourth steps, and we defined an error vector for the second step, the errors of which were measured in a psychophysical planetarium study by Farkas et al. (2014), in which experiment I also participated. Although, the detailed introduction of this experiment is out of the scope of my thesis, we used these errors and calculated the error propagation through the four subsequent measurement steps and determined the net North errors for 1080 weather situations.

We obtained the North error for many possible weather circumstances that may have occurred during a Viking sailing route, but this is only the momentary error of one orientation. Since these weather situations could vary frequently during a voyage, based on our results, we cannot determine, whether the Viking ships reached the coasts of Greenland. To determine the chance of reaching Greenland, using the North error results, we simulated 1000 three-week-long routes from Norway (Bergen) to Greenland (Hvarf). The detailed description of this study is described by Száz et al. (2018).

Acknowledgements

First and foremost I wish to express my deepest gratitude to my two supervisors: Dr. Gábor Horváth, the head of the Environmental Optics Laboratory (Department of Biological Physics, Eötvös University) and Dr. György Kriska (Biological Institute, Eötvös University). They continuously provided assistance during my doctoral researches with high level of competence and enthusiasm both in the fields of physics and biology.

I am very grateful to the co-authors of my publications for their work and assistance in the experiments. I am also grateful for the valuable comments of the anonymous reviewers of my publications.

I am grateful to Dr. András Barta (Estrato Research and Development Ltd., Budapest), who helped in the design and construction of the measurement equipments, which were necessary for the experiments. I also thank Sándor Hopp (Mechanical Workshop, Physical Institute, Eötvös University) for constructing the mechanical device of the rotatable analyzers.

We are grateful to the Department of Mineralogy of Eötvös University (Budapest) for the cordierite and tourmaline crystals used in our experiment.

I express my thanks to Prof. Kristóf Petrovay (Head of the Department of Astronomy) for permitting our psychophysical measurements in the planetarium of the Eötvös University. I thank Dóra Tarczai-Nehéz for her help in astronomical calculations and logistic help with the planetarium.

I thank the test persons for their participation in the laboratory and planetarium experiments.

Many thanks to Csaba Viski (Szokolya, Hungary), who allowed to perform our experiments with matte and shiny test surfaces on his horse farm.

My work was supported by the grants OTKA K-105054 (Full-Sky Imaging Polarimetry to Detect Clouds and to Study the Meteorological Conditions Favourable for Polarimetric Viking Navigation) received by my supervisor, Gábor Horváth from the Hungarian Science Foundation and NKFIH PD115451 (Studying the polarotaxis of aquatic arthropods and complex optical ecological traps in the aspect of conservation biology) received by my co-author, Ádám Egri from the Hungarian National Research, Development and Innovation Office.

I am also grateful to Prof. Jenő Kürti (Department of Biological Physics, Physical Institute, Eötvös University) for his leading in the doctoral programme.

Finally, many thanks to my friends and family for their support during the years of my doctoral studies and researches.

References

Barta A, Horváth G, Meyer-Rochow VB. 2005. Psychophysical study of the visual sun location in pictures of cloudy and twilight skies inspired by Viking navigation. *Journal of the Optical Society of America A* 22: 1023-1034

Barta A, Horváth G, Horváth Á, Egri Á, Blahó M, Barta P, Bumke K, Macke A. 2015. Testing a polarimetric cloud imager aboard research vessel polarstern: comparison of color-based and polarimetric cloud detection algorithms. *Applied Optics*, 54, 1065–1077.

Ball P. 2011. Material witness: a light compass? *Nature Materials*, 10, article no. 909.

Behringer W. 2010. A klíma kultúrtörténete. A jégkorszaktól a globális felmelegedésig. *Corvina Kiadó, Budapest*.

Bernáth B, Szedenics G, Molnár G, Kriska G, Horváth G. 2001a. Visual ecological impact of "shiny black anthropogenic products" on aquatic insects: oil reservoirs and plastic sheets as polarized traps for insects associated with water. *Archives of Nature Conservation and Landscape Research* 40: 89–109.

Bernáth B, Szedenics G, Molnár G, Kriska G, Horváth G. 2001b. Visual ecological impact of a peculiar waste oil lake on the avifauna: dual-choice field experiments with water-seeking birds using huge shiny black and white plastic sheets. *Archives of Nature Conservation and Landscape Research* 40: 1–28.

Bernáth B, Kriska G, Suhai B, and Horváth G. 2008. Wagtails (Aves: Motacillidae) as insect indicators on plastic sheets attracting polarotactic aquatic insects. *Acta Zoologica Academiae Scientiarum Hungaricae* H 54: 145–155.

Bernáth B, Horváth G, Meyer-Rochow VB. 2012 Polarotaxis in egg-laying yellow fever mosquitoes Aedes (Stegomyia) aegypti is masked due to infochemicals. *Journal of Insect Physiology* 58: 1000-1006.

Bernáth B, Blahó M, Egri Á, Barta A, Kriska G, Horváth G. 2013. Orientation with a Viking sun-compass, a shadow-stick, and two calcite sunstones under various weather conditions. *Applied optics*, 52 (25): 6185-6194.

Bernáth B, Farkas A, Horváth G. 2015. Navigáció égre néző vikingekkel. 1. rész. Alkonyfény-iránytű. *Élet és Tudomány* 70 (10): 307-309.

Bij de Vaate A, Klink A, Oosterbroek F. 1992. The mayfly, Ephoron virgo (Olivier), back in the dutch parts of the rivers Rhine and Meuse. *Hydrobiological Bulletin* 25: 237–240.

Blahó M, Herczeg T, Kriska G, Egri Á, Száz D, Farkas A, Tarjányi N, Czinke L, Barta A, Horváth G. 2014. Unexpected attraction of polarotactic water-leaving insects to matt black car surfaces: mattness of paintwork cannot eliminate the polarized light pollution of black cars. *Public Library of Science One* 9 (7): e103339 (doi:10.1371/journal.pone.0103339).

Boda P, Horváth G, Kriska G, Blahó M, Csabai Z. 2014 Phototaxis and polarotaxis hand in hand: Night dispersal flight of aquatic insects distracted synergistically by light intensity and reflection polarization. *Naturwissenschaften* 101: 385-395.

Boxwell M. 2012: Solar Electricity Handbook. A simple, practical guide to solar energy – designing and installing photovoltaic solar electric systems. *Greenstream Publishing. Warwickshire.*

Boyle G. 2012. Renewable energy. Power for a sustainable future. *Oxford University Press. Oxford.*

Bowden J. 1981. The relationship between light- and suction-trap catches of Chrysoperla carnea (Stephens) (Neuroptera: Chrysopidae), and the adjustment of light-trap catches to allow for variation in moonlight. *Bulletin of Entomological Research* 71: 621–629.

Bowden J. 1982. An analysis of factors affecting catches of insects in light-traps. *Bulletin of Entomological Research* 72: 535–556.

Bradley RS, Hughes MK, Diaz HF. 2003. Climate in medieval time. *Science*, 302(5644): 404-405.

Briscoe AD, Chittka L. 2001. The evolution of color vision in insects. *Annual Review of Entomology* 46: 471–510

Broecker WS. 2001. Was the Medieval Warm Period Global? *Science*, 291 (5508): 1497–1499.

Brøndsted J. 1983. A vikingek. *Corvina Kiadó. Budapest.*

Cazorla A, Olmo FJ, Alados-Arboledas L. 2008. Development of a sky imager for cloud cover assessment. *Journal of the Optical Society of America A* 25: 29–39.

Cid N, Ibanez C, Prat N. 2008. Life history and production of the burrowing mayfly Ephoron virgo (Olivier, 1791) (Ephemeroptera: Polymitarcyidae) in the lower Ebro river: a comparison after 18 years. *Aquatic Insects* 30: 163–178.

Coulson KL. 1988. Polarization and intensity of light in the atmosphere. *Hampton, VA: A Deepak Publishing*.

Crowley TJ, Zielinski G, Vinther B, Udisti R, Kreutz K, Cole-Dai J, Castellano E. 2008. Volcanism and the little ice age. *PAGES news* 16 (2): 22-23.

Csabai Z, Boda P, Bernáth B, Kriska G, Horváth G. 2006. A 'polarisation sun-dial' dictates the optimal time of day for dispersal by flying aquatic insects. *Freshwater Biology* 51: 1341–1350.

Dacke M, Nilsson ED, Scholtz CH, *et al*. 2003. Insect orientation to polarized moonlight. *Nature* 424: 33.

Danthanarayana W, Dashper S. 1986. Response of some nightflying insects to polarized light. *In: Danthanarayana W (Ed). Insect flight: dispersal and migration. Berlin, Germany: Springer-Verlag*.

Diamond J. (2007): Összeomlás. Tanulságok a társadalmak továbbéléséhez. *Typotex Kiadó, Budapest*.

Dugmore AJ, Church MJ, Mairs K, McGovern TH, Perdikaris S, Vésteinsson O. 2007. Abandoned Farms, Volcanic Impacts, and Woodland Management: Revisiting Þjórsárdalur, the "Pompeii of Iceland. *Arctic Anthropology* 44: 1-11.

Egri Á, Blahó M, Sándor A, Kriska G, Gyurkovszky M, Farkas R, Horváth G. 2012a. New kind of polarotaxis governed by degree of polarization: attraction of tabanid flies to differently polarizing host animals and water surfaces. *Naturwissenschaften* 99: 407-416.

Egri Á, Blahó M, Kriska G, Farkas R, Gyurkovszky M, Akesson S, Horváth G. 2012b. Polarotactic tabanids find striped patterns with brightness and/or polarization modulation least attractive: An advantage of zebra stripes. *Journal of Experimental Biology* 215: 736–745.

Egri Á, Blahó M, Száz D, Barta A, Kriska G, Antoni G, Horváth G. 2013. A new tabanid trap applying a modified concept of the old flypaper: Linearly polarising sticky black surfaces as an effective tool to catch polarotactic horseflies. *International Journal for Parasitology* 43: 555-563.

Egri Á, Száz D, Farkas A, Pereszlényi Á, Horváth G, Kriska Gy. 2017. Method to improve the survival of night-swarming mayflies near bridges in areas of distracting light pollution. *Royal Society Open Science* 4: 171166.

Eisenbeis G. 2001. Künstliches Licht und Insekten: eine vergleichende Studie in Rheinhessen. *Schriftenreihe für Landschaftspflege und Naturschutz* 67: 75–100.

Eisenbeis G. 2006. Artificial night lighting and insects: attraction of insects to streetlamps in a rural setting in Germany. In: Rich C, Longcore T, editors. Ecological consequences of artificial night lighting. *Washington—Covelo—London: Island Press,* Chapter 12, pp. 281–304.

Encalada AC, Peckarsky BL. 2007. A comparative study of the cost of alternative mayfly oviposition behaviors. *Behavioral Ecology and Sociobiology* 61: 1437–1448.

Fairbairn MB. 2001. Physical models of Haidinger's brush. *The Journal of the Royal Astronomical Society of Canada* 95: 248–251.

Farkas A, Száz D, Egri Á, Blahó M, Barta A, Nehéz D, Bernáth B, Horváth G. 2014. Accuracy of sun localization in the second step of sky-polarimetric Viking navigation for north determination: a planetarium experiment. *Journal of the Optical Society of America A*, 31: 1645-1656.

Farkas A, Száz D, Egri Á, Barta A, Mészáros Á, Hegedüs R, Horváth G, Kriska Gy. 2016. Mayflies are least attracted to vertical polarization: A polarotactic reaction helping to avoid unsuitable habitats. *Physiology and Behavior* 163 (2016): 219-227.

Fletcher RJ Jr, Orrock JL, Robertson BA. 2012. How the type of anthropogenic change alters consequences of ecological traps. *Proceedings of the Royal Society B* 279: 2546–2552.

Foote PG. 1956. Icelandic sólarsteinn and the Medieval Background. Arv. *Journal of Scandinavian Folklore* 12: 26–40.

Forster HWJ. 1954. The clinical use of the Haidinger's brushes phenomenon. *American Journal of Ophthalmology* 38: 661–665.

Foster R, Ghassemi M, Cota A. 2010. Solar Energy. Renewable Energy and the Environment. *CRC Press. Boca Raton.*

Frank KD. 1998. Impact of outdoor lighting on moths: an assessment. *Journal of Lepidopteran Society* 42: 63–93.

Frisch von K. 1967. The dance language and orientation of bees. *Cambridge, MA: Belknap Press/Harvard University Press.*

Gaston KJ, Bennie J, Davies TW, Hopkins J. 2013. The ecological impacts of nighttime light pollution: a mechanistic appraisal. *Biological Reviews* 88: 912–927.

Gál J, Horváth G, Pomozi I, Wehner R. 1998. Az égbolt polarizálatlan pontjai, avagy amit már Arago, Babinet és Brewster is ismert, de eddig közvetlenül még senki sem látott. *Természet Világa* 129: 151-154, 212-215.

Gál J, Horváth G, Meyer-Rochow VB. 2001. Measurement of the reflection-polarization pattern of the flat water surface under a clear sky at sunset. *Remote Sensing of Environment* 76: 103–111.

Grove JM. 2001. The Initation of the „Little Ice Age" in Regions Round the North Atlantic. *Climatic Change* 48 (1): 53–82.

Hammer CU, Clausen HB, Dansgaard W. 1981. Past volcanism and climate revealed by Greenland ice cores. *Journal of Volcanology and Geothermal Research* 11 (1): 3-10.

Hawthorne CF, Dirlam DM. 2011. Tourmaline the indicator mineral: from atomic arrangement to Viking navigation. *Elements*, 7: 307–312.

Hegedüs R, Åkesson S, Horváth G. 2007a. Polarization patterns of thick clouds: overcast skies have distribution of the angle of polarization similar to that of clear skies. *Journal of the Optical Society of America A* 24 (8): 2347-2356.

Hegedüs R, Åkesson S, Wehner R, Horváth G. 2007b. Could Vikings have navigated under foggy and cloudy conditions by skylight polarization? On the atmospheric optical prerequisites of polarimetric Viking navigation under foggy and cloudy skies. *Proceedings of the Royal Society of London A* 463 (2080): 1081-1095.

Hegedüs R, Farkas A, Horváth G. 2015. Navigáció égre néző vikingekkel 6. rész: A napkőhasználat légköroptikai feltételei. *Élet és Tudomány* 70 (36): 1142-1144.

Henze MJ and Labhart T. 2007. Haze, clouds and limited sky visibility: polarotactic orientation of crickets under difficult stimulus conditions. *Journal of Experimental Biology* 210: 3266–3276.

Herczeg T, Blahó M, Száz D, Kriska G, Gyurkovszky M, Farkas R, Horváth G. 2014. Seasonality and daily activity of male and female tabanid flies monitored in a Hungarian hill-country pasture by new polarization traps and traditional canopy traps. *Parasitological Research* 113: 4251–4260.

Herczeg T, Száz D, Blahó M, Barta A, Gyurkovszky M, Farkas R, Horváth G. 2015. The effect of weather variables on the flight activity of horseflies (Diptera: Tabanidae) in the continental climate of Hungary. *Parasitological Research* 114: 1087–1097.

Horridge GA, Marcelja L, Jahnke L. 1982. Light guides in the dorsal eye of the male mayfly. *Proceedings of the Royal Society B* 216: 25–51.

Horváth G, Zeil J. 1996. Kuwait oil lakes as insect traps. *Nature* 379: 303–304.

Horváth G, Pomozi I. 1997. How celestial polarization changes due to reflection from the deflector panels used in deflector loft and mirror experiments studying avian navigation. *Journal of Theoretical Biology* 184: 291–300.

Horváth G, Bernáth B, and Molnár G. 1998. Dragonflies find crude oil visually more attractive than water: multiple-choice experiments on dragonfly polarotaxis. *Naturwissenschaften* 85: 292–297.

Horváth G, Varjú D. 1997. Polarization pattern of freshwater habitats recorded by video polarimetry in red, green and blue spectral ranges and its relevance for water detection by aquatic insects. *Journal of Experimental Biology* 200: 1155–1163.

Horváth G, Gál J, Pomozi I, Wehner R. 1999. Sarkított világ. Az égboltpolarizáció és az állatok. *Élet és Tudomány* 54: 235-237.

Horváth G, Varjú D. 2004. Polarized light in animal vision–polarization patterns in nature. *Berlin, Germany: Springer-Verlag*.

Horváth G, Malik P, Kriska G, and Wildermuth H. 2007. Ecological traps for dragonflies in a cemetery: the attraction of Sympetrum species (Odonata: Libellulidae) by horizontally polarizing black gravestones. *Freshwater Biology* 52: 1700–1709.

Horváth G, Majer J, Horváth L, *et al*. 2008a. Ventral polarization vision in tabanids: horseflies and deerflies (Diptera: Tabanidae) are attracted to horizontally polarized light. *Naturwissenschaften* 95: 1093–1100.

Horváth G, Barta A, Hegedüs R, Pomozi I, Suhai B, Åkesson S, Meyer-Rochow B, Wehner R. 2008b. Sarkított fénnyel a vikingek nyomában az Északi-sarkvidéken: A polarimetrikus viking navigáció légköroptikai feltételeinek kísérleti vizsgálata. *Fizikai Szemle* 58: 131-140.

Horváth G, Kriska G. 2008. Polarization vision in aquatic insects and ecological traps for polarotactic insects. *In: Lancaster J and Briers RA (Eds). Aquatic insects: challenges to populations. Wallingford, UK: CAB International Publishing*.

Horváth G, Kriska G, Malik P, Robertson B. 2009 Polarized light pollution: a new kind of ecological photopollution. *Frontiers in Ecology and the Environment* 7: 317-325.

Horváth G, Blahó M, Egri Á, Kriska G, Seres, I, Robertson B. 2010a. Reducing the maladaptive attractiveness of solar panels to polarotactic insects. *Conservation Biology* 24 (6): 1644-1653.

Horváth G, Blahó M, Kriska G, Hegedüs R, Gerics B, Farkas R, Akesson S. 2010b. An unexpected advantage of whiteness in horses: The most horsefly–proof horse has a depolarizing white coat. *Proceedings of the Royal Society B* 277: 1643–1650.

Horváth G, Kriska G, Malik P, Hegedűs R, Neumann L, Akesson S, Robertson B. 2010c. Asphalt surfaces as ecological traps for water-seeking polarotactic insects: how can the polarized light pollution of asphalt surfaces be reduced? Series: Environmental Remediation Technologies, Regulations and Safety. *Nova Science Publishers, Inc.*, Hauppauge, p. 47. ISBN: 978-1-61668-863-9

Horváth G, Kriska G. 2010. A napelem evolúciós csapdája. *Interpress Magazin* 30 (1): 106–110.

Horváth G, Barta A, Pomozi I, Suhai B, Hegedüs R, Akesson S, Meyer-Rochow B, Wehner R. 2011a. On the trail of Vikings with polarized skylight: Experimental study of the atmospheric optical prerequisites allowing polarimetric navigation by Viking seafarers. *Philosophical Transactions of the Royal Society B* 366: 772-782.

Horváth G, Móra A, Bernáth B, Kriska G. 2011b Polarotaxis in non-biting midges: female chironomids are attracted to horizontally polarized light. *Physiology and Behavior* 104: 1010-1015.

Horváth G, editor. 2014. Polarized light and polarization vision in animal sciences. *Heidelberg—Berlin—New York: Springer-Verlag* (Springer Series in Vision Research, vol. 2, Collin S, Marshall J, series editors).

Horváth G, Farkas A, Bernáth B. 2014a. Chapter 25. Sky-polarimetric Viking navigation. In: Horváth G. (ed.) 2014. Polarized Light and Polarization Vision in Animal Sciences (2nd edition) *Springer Series in Vision Research, Volume 2. Springer: Heidelberg, Berlin, Dordrecht, London, New York. pp. 603–635.*

Horváth G, Kriska G, Robertson B. 2014b. Chapter 20. Anthropogenic Polarization and Polarized Light Pollution Inducing Polarized Light Traps. In: Horváth G. 2014. Polarized Light and Polarization Vision in Animal Sciences (2nd edition). *Springer Series in Vision Research, Volume 2. Springer: Heidelberg, Berlin, Dordrecht, London, New York. pp. 443–513.*

Horváth G, Takács P, Kretzer B, Szilasi Sz, Száz D, Farkas A, Barta A. 2017. Celestial polarization patterns sufficient for Viking navigation with the naked eye: Detectability of Haidinger's brushes on the sky versus meteorological conditions. *Royal Society Open Science* 4: 160688.

Hough TP. 2007. Recent Developments in Solar Energy. *Nova Science Publishers. New York.*

Hughes MK, Diaz HF. 1994. Was there a 'Medieval Warm Period', and if so, Where and When? *Climatic Change* 26: 109–142.

Ibanez C, Escosa R, Munoz I, Prat N. 1991. Life cycle and production of Ephoron virgo (Ephemeroptera: Polymitarcidae) in the lower river Ebro (NE Spain). In: Aba-Tercr J, Sanchez-Ortega A, editors. *Overview and strategies of Ephemeroptera and Plecoptera. Sandhill Crane Press*; pp. 483–492.

Ingstad H. 1972. Vikingek az Újvilágban. *Gondolat Kiadó. Budapest.*

Kammann R. 1967. The overestimation of vertical distance and slope and its role in the moon illusion. *Perception and Psychophysics* 2: 585–589.

Hershenson M. 1989. The Moon Illusion, *Erlbaum* (1989).

Kang TS, Smith AP, Taylor BE, Durstock MF. 2009. Fabrication of highly-ordered TiO2 nanotube arrays and their use in dye-sensitized solar cells. *Nano Letters* 9 (2): 601-606.

Karlsen LK. 2003. Secrets of the Viking Navigators. *One Earth Press: Seattle, USA.*

Karman SB, Diah SZM, Gebeshuber IC. 2012. Bio-inspired polarized skylight-based navigation sensors: A review. *Sensors* 12 (11): 14232-14261.

Kazanci N. 2013. The swarm of Ephoron virgo (Olivier, 1791) (Ephemeroptera: Polymitarcyidae) as nuptial behaviour in Sakarya River (Turkey). *Review of Hydrobiology* 6: 69–80.

Kovarov BG, Monchadskiy AS. 1963. About the application of polarized light in light-traps to catch insects. *Entomologicheskow Obozrenie* 42: 49–55.

Krcmar S, Lajos P. 2011. Response of horse flies to aged equine urine (Diptera: Tabanidae). *Entomologia Generalis* 33: 245–250.

Krcmar S. 2013. Comparison of the efficiency of the olfactory and visual traps in the collection of horseflies (Diptera: Tabanidae). *Entomologia Generalis* 34: 261–267.

Kreithen ML, Keeton WT. 1974. Detection of polarized light by the homing pigeon, Columba livia. *Journal of Comparative Physiology* 89 (1): 83–92.

Kriska G, Horváth G, Andrikovics S. 1998. Why do mayflies lay their eggs en masse on dry asphalt roads? Water-imitating polarized light reflected from asphalt attracts Ephemeroptera. *Journal of Experimental Biology* 201: 2273–2286.

Kriska G. 2000. Polarotaxis a rovarvilágban. *Állattani Közlemények* 85: 17–27.

Kriska G, Csabai Z, Boda P, Malik P, Horváth G. 2006a. Why do red and dark-coloured cars lure aquatic insects? The attraction of water insects to car paintwork explained by reflection–polarisation signals. *Proceedings of the Royal Society B* 273: 1667–1671.

Kriska G, Malik P, Csabai Z, Horváth G. 2006b. Why do highly polarizing black burnt-up stubble-fields not attract aquatic insects? An exception proving the rule. *Visual Research* 46: 4382–4386.

Kriska G, Bernáth B, Horváth G. 2007. Positive polarotaxis in a mayfly that never leaves the water surface: polarotactic water detection in Palingenia longicauda (Ephemeroptera). *Naturwissenschaften* 94: 148–154.

Kriska G, Malik P, Szivák I, and Horváth G. 2008. Glass buildings on river banks as "polarized light traps" for mass-swarming polarotactic caddis flies. *Naturwissenschaften* 95: 461–467.

Kriska G, Bernáth B, Farkas R, Horváth G. 2009 Degrees of polarization of reflected light eliciting polarotaxis in dragonflies (Odonata), mayflies (Ephemeroptera) and tabanid flies (Tabanidae). *Journal of Insect Physiology* 55: 1167-1173.

Kokko H, Sutherland WJ. 2001. Ecological traps in changing environments: ecological and evolutionary consequences of a behaviourally mediated Allee effect. *Evolutionary Ecology Research* 3: 537–551.

Können GP. 1985. Polarized light in nature. *Cambridge, UK: Cambridge University Press*.

Kuo ML, Poxson DJ, Kim YS, Mont FW, Kim JK, Schubert EF, Lin SY. 2008. Realization of a near-perfect antireflection coating for silicon solar energy utilization. *Optics Letters* 33 (21): 2527-2529.

Kureck A. 1992. Das Massenschwärmen der Eintagsfliegen am Rhein: Zur Rückkehr von Ephoron virgo (Olivier 1791). *Natur und Landschaft* 67: 407–409.

Kureck A, Fontes RJ. 1996. The life cycle and emergence of Ephoron virgo, a large potamal mayfly that has returned to the river Rhine. *Archiv für Hydrobiologie* (Supplement) 113: 319–323.

Labhart T, Meyer EP. 2002. Neural mechanisms in insect navigation: polarization compass and odometer. *Current Opinion in Neurobiology* 12: 707–14.

Lamb HH. 1965. The early Medieval Warm Epoch and its sequel. *Palaeogeography, Palaeoclimatology, Palaeoecology* 1: 13–37.

Langevelde van F, Ettema JA, Donners M, Wallis De Vrises MF, Groenendijk D. 2011. Effect of spectral composition of artificial light on the attraction of moths. *Biological Conservation* 144: 2274–2281.

Le Floch A, Ropars G, Lucas J, Wright S, Davenport T, Corfield M, Harrisson M. 2013. The sixteenth century Alderney crystal: a calcite as an efficient reference optical compass?. *Proceedings of the Royal Society A* 469 (2153): 20120651.

Lehn WH, Schroeder II. 1979. Polar Mirages as Aids to Norse Navigation. *Polarforschung*, 49 (2): 173–187.

Lester G. 1970. Haidinger's brushes and the perception of polarization: the history to the present of an on-going problem. *Acta Psychologica* 34: 106–114.

Longcore T, Rich C. 2004. Ecological light pollution. *Frontiers of Ecology and Environment* 2: 191–98.

Lythgoe JN, Hemmings CC. 1967. Polarized light and underwater vision. *Nature* 213: 893–894.

Malaise R. 1937. A new insect–trap. *Entomologisk Tidskrift Stockholm* 58: 148–160.

Malik P, Hegedüs R, Kriska G, and Horváth G. 2008. Imaging polarimetry of glass buildings: why do vertical glass surfaces attract polarotactic insects? *Applied Optics* 47: 4361–4374.

Málnás K, Polyák L, Prill É, Hegedüs R, Kriska G, Dévai G, Horváth G, Lengyel S. 2011. Bridges as optical barriers and population disruptors for the mayfly Palingenia longicauda: An overlooked threat to freshwater biodiversity? *Journal of Insect Conservation* 15: 823-832.

Marshall J, Cronin TW, Shashar N, and Land M. 1999. Behavioural evidence for polarisation vision in stomatopods reveals a potential channel for communication. *Current Biology* 9: 755–758.

McGhee R. 1984. Contact between native North Americans and the medieval Norse: a review of the evidence. *American Antiquity* 49 (1): 4–26.

McGovern TH. 1991. Climate, correlation, and causation in Norse Greenland. *Arctic Anthropology* 28 (2): 77–100.

McGovern TH. 1997. Death in Norse Greenland. *Science* 275 (5302): 924–926.

McGovern TH, Vésteinsson O, Friðriksson A, Church M, Lawson I, Simpson IA, Einarsson A, Dugmore A, Cook G, Perdikaris S, Edwards KJ, Thomson AM, Adderley WP, Newton A, Lucas G, Edvardsson R, Aldred O, Dunbar E. 2007. Landscapes of Settlement in Northern Iceland: Historical Ecology of Human Impact and Climate Fluctuation on the Millennial Scale. *American Anthropologist* 109: 27–51.

McGregor J, Temple S, Horváth G. 2014. Human polarization sensitivity. In Polarized light and polarization vision in animal sciences (ed. G Horváth), ch. 14, pp. 303–315. *Berlin, Germany: Springer.*

Menzel R. 1979. Spectral sensitivity and color vision in invertebrates. In: Autrum H, editor. *Handbook of sensory physiology*. Berlin: Springer-Verlag; pp. 503–580.

Metcalf NB, Valdimarsson SK, Fraser NHC. 1997. Habitat profitability and choice in a sit-and-wait predator: juvenile salmon prefer slower currents on darker nights. *Journal of Animal Ecology* 66: 866–875.

Mihályi D. 2015. Mennyire „zöld" a napelem? A matt napelemek használata megoldás lehet a poláros fényszennyezés csökkentésére. *Tudományos diákköri dolgozat. Eötvös Loránd Tudományegyetem, Természettudományi Kar, Biológiai Fizika Tanszék. Budapest.*

Minnaert MGJ. 1993. Light and Color in the Outdoors. *Springer-Verlag. New York.*

Moore TR, Slosser JE, Cocke J, Newton WH. 1996. Effect of trap design and color in evaluating activity of Tabanus abactor Philip in Texas rolling plains habitat. *Southwestern Entomologist* 21: 1–11.

Moore MV, Kohler SJ, Cheers MS. 2006. Artificial light at night in freshwater habitats and its potential ecological effects. In: Rich C, Longcore T, editors. Ecological consequences of artificial night lighting. *Washington—Covelo—London: Island Press*; Chapter 15, pp. 365–384.

Muirhead–Thomson RC. 1991. Trap Responses of Flying Insects: The Influence of Trap Design on Capture Efficiency. *Academic Press, Harcourt Brace Jovanovich Publishers, London – New York.*

Novales FI, Browman HI. 2001. Foraging and preysearch behaviour of small juvenile rainbow trout (Oncorhynchus mykiss) under polarized light. *Journal of Experimental Biology* 204: 2415–2422.

Ogilvie AE, Barlow LK, Jennings AE. 2000. North Atlantic climate c. AD 1000: Millennial reflections on the Viking discoveries of Iceland, Greenland and North America. *Weather* 55 (2): 34-45.

Ogilvie AE, Woollett JM, Smiarowski K, Arneborg J, Troelstra S, Kuijpers A, McGovern TH. 2009. Seals and sea ice in medieval Greenland. *Journal of the North Atlantic* 2: 60-80.

Olsen O, Crumlin-Pedersen O. 1978. Five Viking Ships from Roskilde Fjord. *National Museum* 136.

Orlove B. 2005. Human adaptation to climate change: a review of three historical cases and some general perspectives. *Environmental Science and Policy* 8: 589–600.

Ovcharenko AP, Yegorenkov VD. 2002. Teaching students to observe Haidinger brushes. *European Journal of Physics* 23 (2): 123.

Pasini A. 2005. From observations to simulations. A conceptual introduction to weather and climate modelling. *Singapore: World Scientific Publishing.*

Paulescu M, Paulescu E, Gravila P, Badescu V. 2013. Weather modeling and forecasting of PV systems operation. *Springer-Verlag. London.*

Perkin EK, Hölker F, Richardson JS, Sadler JP, Wolter C. 2011. The influence of artificial light on stream and riparian ecosystems: questions, challenges, and perspectives. *Ecosphere* 2: 1–16.

Pomozi I, Horváth G, Wehner R. 2001. How the clear-sky angle of polarization pattern continues underneath clouds: full-sky measurements and implications for animal orientation. *Journal of Experimental Biology* 204 (17): 2933-2942.

Pörtner R. 1983. A viking kaland. *Kossuth Kiadó.*

Ramskou T. 1967. Solstenen. *Skalk* 2: 16–17.

Ribeiro S, Moros M, Ellegaard M, Kuijpers A. 2012. Climate variability in West Greenland during the past 1500 years: evidence from a high-resolution marine palynological record from Disko Bay. *Boreas* 41 (1): 68-83.

Robertson B, Hutto RL. 2006. A framework for understanding ecological traps and an evaluation of existing evidence. *Ecology* 87: 1075–1085.

Robertson BA. 2012. Investigating targets of avian habitat management to eliminate an ecological trap. *Avian Conservation and Ecology* 7 (2): 2

Robertson BA, Rehage J, Sih A. 2013. Ecological novelty and the emergence of evolutionary traps. *TREE* 28: 552–560.

Ropars G, Gorre G, Le Floch A, Enoch J, Lakshminarayanan V. 2012. A depolarizer as a possible precise sunstone for Viking navigation by polarized skylight. *Proceedings of the Royal Society A* 468 (2139): 671-684.

Roslund C, Beckman C. 1994. Disputing Viking navigation by polarized skylight. *Applied Optics* 33 (21): 4754–4755.

Schlaepfer MA, Runge MC, Sherman PW. 2002. Ecological and evolutionary traps. *TREE* 17: 478–480.

Schnoemund E. 1930. Eintagsfliegen oder Ephemeroptera. *Die Tierwelt Deutschlands* (Jena) 19: 1–106.

Sawatzky HL, Lehn WH. 1976. The Arctic Mirage and the Early North Atlantic. *Science*, 192 (4246): 1300–1305.

Schaefer BE. 1997. Vikings and Polarization Sundials. *Sky and Telescope* 93 (5): 91–94.

Schwind R. 1985. Sehen unter und über Wasser, sehen von Wasser. *Naturwissenschaften* 72: 343–352.

Schwind R. 1991. Polarization vision in water insects and insects living on a moist substrate. *Journal of Comparative Physiology A* 169: 531–540.

Schwind R. 1995. Spectral regions in which aquatic insects see reflected polarized light. *Journal of Comparative Physiology* 177: 439–448.

Sharpe LT, Stockman A, Jagla W, Jagle H. 2005. A luminous efficiency function, V*(λ), for daylight adaptation. *Journal of Vision* 5: 948–968.

Shashar N, Hanlon RT, and Petz AM. 1998. Polarization vision helps detect transparent prey. *Nature* 393: 222–223.

Sloan LL, Naquin HA. 1955. A quantitative test for determining the visibility of the Haidinger brushes: clinical applications. *American Journal of Ophthalmology* 40: 393–406.

Sølver CV. 1953. The Discovery of an Early Bearing-Dial. *Journal of Navigation* 6 (3): 294–296.

Sølver CV. 1954. Vestervejen. Om Vikingernes Sejlads. *Weilbach Co. Copenhagen.*

Suzuki S, Abe K. 1985. Topological structural analysis of digitized binary images by border following. *Computer Vision in Graphics and Image Processing* 30: 32–46.

Száz D, Herzeg T. 2013. A bögölyök (tabanidae) polarotaktikus viselkedésével kapcsolatos tudományos ismeretek összefoglalása. *Tájökológiai Lapok* 11 (1): 183-192.

Száz D, Horváth G, Barta A, Robertson B, Farkas A, Egri Á, Tarjányi N, Rácz G, Kriska Gy. 2015. Lamp-lit bridges as dual light-traps for the night-swarming mayfly, Ephoron virgo: Interaction

of polarized and unpolarized light pollution. *Public Library of Science ONE* 10 (3): e0121194 (doi: 10.1371/journal.pone.0121194)

Száz D, Farkas A, Blahó M, Barta A, Egri Á, Kretzer B, Hegedüs T, Jäger Z, Horváth G. 2016a. Adjustment errors of sunstones in the first step of sky-polarimetric Viking navigation: studies with dichroic cordierite/tourmaline and birefringent calcite crystals. *Royal Society Open Science* 3: 150406.

Száz D, Mihályi D, Farkas A, Egri Á, Barta A, Kriska Gy, Robertson B, Horváth G. 2016b. Polarized light pollution of matte solar panels: Anti-reflective photovoltaics reduce polarized light pollution but benefit only some aquatic insects. *Journal of Insect Conservation* 20 (4): 663-675 (doi: 10.1007/s10841-016-9897-3)

Száz D, Farkas A, Barta A, Kretzer B, Egri Á, Horváth G. 2016. North error estimation based on solar elevation errors in the third step of sky-polarimetric Viking navigation. *Proceedings of the Royal Society A* 472: 20160171 (pp. 1-15, doi: 10.1098/rspa.2016.0171)

Száz D, Farkas A, Barta A, Kretzer B, Blahó M, Egri Á, Szabó Gy, Horváth G. 2017. Accuracy of the hypothetical sky-polarimetric Viking navigation versus sky conditions: revealing solar elevations and cloudinesses favourable for this navigation method. *Proceedings of the Royal Society A* 473: 20170358 (18 pages, doi: 10.1098/rspa.2017.0358)

Száz D, Horváth G. 2018. Success of sky-polarimetric Viking navigation: revealing the chance Viking sailors could reach Greenland from Norway. *Royal Society Open Science* 5: 172187 (doi: 10.1098/rsos.172187)

Teague MR. 1980. Image analysis via the general theory of moments. *Journal of Optical Society of America* 70: 920–930.

Temple SE, McGregor JE, Miles C, Graham L, Miller J, Buck J, Scott-Samuel NE, Roberts NW. 2015. Perceiving polarization with the naked eye: characterization of human polarization sensitivity. *Proceedings of the Royal Society B* 282: 20150338.

Thirslund S. 1991. A presumed sun compass from Narsarsuaq. In: Vebæk, C. L.: The Church Topography of the Eastern Settlement and the Excavation of the Benedictine Convent at Narsarsuaq in the Uunartoq Fjord. Meddelelser om Grønland. *Bioscience. Geoscience. Man and Society.* 14. *The Commission for Scientific Research. Grönland.* 65–71.

Thirslund S. 1993. The Discovery of an Early Bearing-Dial. Further Investigations. *Journal of Navigation* 46 (1): 33–48.

Thirslund S. 1997. Sailing Directions of the North Atlantic Viking Age (from about the year 860 to 1400). *Journal of Navigation* 50 (1): 55–64.

Thirslund S. 2001. Viking navigation: sun-compass guided Norsemen first to America. *Humlebaek, Denmark: Gullanders Bogtrykkeri a-s, Skjern.*

Tobias W. 1996. Sommernächtliches ”Schneetreiben” am Main: zum Phänomen des Massenfluges von Eintagsfliegen. *Natur und Museum* 126 (2): 37–54.

Tomar A, Jain L, Batra P. 2013. Solar Energy – Finding New Ways. *International Journal of Research in Advent Technology* 1 (4): 1–6.

Umow N. 1905. Chromatische depolarisation durch Lichtzerstreuung. *Physikalische Zeitschrift* 6: 674–676.

Vésteinsson O, McGovern TH, Keller C. 2002. Enduring impacts: social and environmental aspects of Viking Age settlement in Iceland and Greenland. *Archaeologia Islandica* 2: 98-136.

Vilhjálmsson Þ. 1997. Time and Travel in the Old Norse Society. In: Poster C and Utz R. (ed.) Disputatio. An International Transdisciplinary Journal of the Late Middle Ages. Vol. 2. Constructions of Time in the Late Middle Ages. *Northwestern University Press. Evanston. Illinois*. 89–114.

Vilhjálmsson Þ. 1999. The Navigation and Vínland. Approaches to Vínland: a conference on the written and archaeological sources for the Norse settlements in the North-Atlantic region and exploration of America. *Reykjavík*. 9–11. August 1999.

Walker J. 1978. The Amateur Scientist: More about polarizers and how to use them, particularly for studying polarized sky light. *Scientific American* 238 (1): 132–136.

Waterman TH. 2006. Reviving a neglected celestial underwater polarization compass for aquatic animals. *Biological Reviews* 81: 111–115.

Wehner R. 1976. Polarized-light navigation by insects. *Scientific American* 235 (7): 106–115.

Wehner R. 2001. Polarization vision – a uniform sensory capacity? *Journal of Experimental Biology* 204: 2589–2596.

Wehner R, Labhart T. 2006. Polarization vision. *In: Warrant EJ and Nilsson DE (Eds). Invertebrate vision. Cambridge, UK: Cambridge University Press*.

Wild W, Fromme B. 2007. Der Sonnenstein der Wikinger. Navigation mit polarisiertem Himmelslicht. *Praxis der Naturwissenschaften* 56 (3): 33–38.

Wildermuth H. 1998. Dragonflies recognize the water of rendezvous and oviposition sites by horizontally polarized light: a behavioural field test. *Naturwissenschaften* 85: 297–302.

Young S, Watt PJ. 1996. Daily and seasonal vertical migration rhythms in Daphnia. *Freshwater Biology* 36: 17–22.

Zar JH. 2010. Biostatistical analysis. *Pearson Prentice Hall, New Jersey.*

Zhevandrov ND. 1995. Polarisation physiological optics. *Physics Uspekhi* 38: 1147–1166.

Summary

In my Ph.D. thesis, light polarization played a central role to experimentally study the polarized light pollution of matte solar panels, the polarization-driven behaviour and the complex ecological trap of compensatory-flying *Ephoron virgo* mayflies and the accuracy of sky-polarimetric Viking navigation. My results facilitate the better understanding of the polarization light pollution and complex ecological traps, which led to new methods and solutions in the field of environmental protection. Through the study of sky-polarimetric Viking navigation, we got a better picture of its usage and accuracy under different weather situations that has never been measured before.

In Chapter 1, I studied the extent of polarized light pollution of matte and shiny black solar panels depending on the site of the experiment and the attracted polarotactic species. In experiment 1, matte black solar panels attracted significantly less polarotactic tabanids that the shiny one, however, in experiment 2, matte black solar panels attracted more polarotactic mayflies than the shiny one. The reason for the latter, determined by measuring the polarization characteristics of the surfaces, was that matte black surfaces mimicked calm water being the natural habitat of these mayflies.

In Chapter 2, I described the attraction of the night-swarming *Ephoron virgo* mayflies to a complex ecological trap formed at illuminated bridges. I studied the swarming behaviour of the mayflies in the vicinity of the trap, in which phototaxis and polarotaxis strengthen each other. I showed in a field experiment that horizontally polarized light attracted 5-10 times more *Ephoron virgo* mayflies than unpolarized light of the same intensity. Based on these results, I introduced a method with which night-swarming mayflies could be prevented from dying at complex light traps formed at illuminated bridges.

Ramskou (1967) hypothesized that Vikings might have used birefringent or dichroic crystals to measure the polarization of the sky to navigate on the open ocean in cloudy weather. This theory has been accepted and cited for decades without knowing its accuracy. In Chapter 3, I studied the accuracy of the sky-polarimetric Viking navigation. In psychophysical experiments, I measured the error functions of the first, third and fourth steps of this method and then, I determined the resulting net North error in an error propagation process for 1080 weather situations, 3 sunstone crystals (calcite, cordierite, tourmaline) and 2 specific dates (spring equinox and summer solstice).

Összefoglalás

Doktori disszertációmban központi szerepet játszik a fénypolarizáció a matt napelemek poláros fényszennyezésének terepkísérleti vizsgálatában, a kompenzációs repülésüket végző dunavirág (*Ephoron virgo*) viselkedésének és az őket érintő összetett ökológiai csapda vizsgálatában, valamint az égbolt-polarimetrikus viking navigáció pontosságának meghatározásában. Eredményeim hozzájárultak a poláros fényszennyezés és az érintett ökológiai csapda mélyebb megértéséhez, ami új természetvédelmi módszerek és megoldások kidolgozásához vezetett. Az égbolt-polarimetrikus viking navigáció vizsgálata során elsőként határoztuk meg a módszer pontosságát különböző meteorológiai helyzetekben.

Az 1. fejezetben bemutattam a matt és fényes fekete napelemek poláros fényszennyezésének terepkísérleti vizsgálatát. Az 1. terepkísérletben a matt tesztfelületek szignifikánsan kevesebb polarotaktikus bögölyt vonzottak, mint a fényesek, míg a 2. terepkísérlet során a matt felületek több polarotaktikus kérészt vonzottak, mint a fényesek. Ez utóbbinak az oka, hogy bár a matt felületekről visszavert fény polarizációfoka alacsonyabb volt, azok nyugodt vizet utánoztak, ami a vizsgált kérészek természetes élőhelye.

A 2. fejezetben az éjjel rajzó dunavirágra (*Ephoron virgo*) ható, kivilágított hidaknál kialakuló összetett ökológiai csapdát mutattam be. Vizsgáltam a kérészek viselkedését a csapda közelében a rajzás során, melynek létrejöttében a foto- és polarotaxis egymás hatását erősítve játszik szerepet. Terepkísérletben megmutattam, hogy a dunavirág 5-10-szer erősebben vonzódik a vízszintesen poláros fényhez, mint az azonos intenzitású polarizálatlanhoz. Kidolgoztunk egy módszert, mellyel megakadályozható a dunavirág pusztulása a kivilágított hidaknál kialakuló összetett ökológiai csapdáknál.

Ramskou (1967) elmélete szerint a vikingek kettőstörő vagy dikroikus kristályokkal mérték az égbolt polarizációját, és ezzel tájékozódtak felhős időben a nyílt tengeren. Az elméletet évtizedeken át idézték, a módszer pontosságának ismerete nélkül. A 3. fejezetben megvizsgáltam az égbolt-polarimetrikus viking navigáció pontosságát. Pszichofizikai kísérletek során mértem az első, harmadik és negyedik lépés hibafüggvényét, majd hibaterjedéssel meghatároztam az eredő északi hibát 1080 meteorológiai helyzetben, 2 napkő kristályra (kalcit, kordierit, turmalin) és 2 kitüntetett dátumra (tavaszi napéjegyenlőség, nyári napforduló). Ezt követően elemeztem, mely helyzetek kedveztek leginkább a navigációnak.

ADATLAP

a doktori értekezés nyilvánosságra hozatalához*

I. A doktori értekezés adatai

A szerző neve: Száz Dénes

MTMT-azonosító: 10044398

A doktori értekezés címe és alcíme: Significance of light polarization in solar panels, Ephoron virgo mayflies and Viking navigation

DOI-azonosító[46]: 10.15476/ELTE.2018.064

A doktori iskola neve: Fizika Doktori Iskola

A doktori iskolán belüli doktori program neve: Statisztikus fizika, biológiai fizika és kvantumrendszerek fizikája doktori program

A témavezető neve és tudományos fokozata: 1: Dr. habil. Horváth Gábor (D.Sc., egyetemi docens), 2: Dr. habil. Kriska György (egyetemi docens)

A témavezető munkahelye: 1: Biológiai Fizika Tanszék, Fizikai Intézet, Eötvös Loránd Tudományegyetem, 2: Biológiai Szakmódszertani Csoport, Biológiai Intézet, Eötvös Loránd Tudományegyetem

II. Nyilatkozatok

1. A doktori értekezés szerzőjeként

a) hozzájárulok, hogy a doktori fokozat megszerzését követően a doktori értekezésem és a tézisek nyilvánosságra kerüljenek az ELTE Digitális Intézményi Tudástárban. Felhatalmazom a Természettudományi kar Dékáni Hivatal Doktori, Habilitációs és Nemzetközi Ügyek Csoportjának ügyintézőjét, hogy az értekezést és a téziseket feltöltse az ELTE Digitális Intézményi Tudástárba, és ennek során kitöltse a feltöltéshez szükséges nyilatkozatokat.

b) kérem, hogy a mellékelt kérelemben részletezett szabadalmi, illetőleg oltalmi bejelentés közzétételéig a doktori értekezést ne bocsássák nyilvánosságra az Egyetemi Könyvtárban és az ELTE Digitális Intézményi Tudástárban;

c) kérem, hogy a nemzetbiztonsági okból minősített adatot tartalmazó doktori értekezést a minősítés (*dátum*)-ig tartó időtartama alatt ne bocsássák nyilvánosságra az Egyetemi Könyvtárban és az ELTE Digitális Intézményi Tudástárban;

d) kérem, hogy a mű kiadására vonatkozó mellékelt kiadó szerződésre tekintettel a doktori értekezést a könyv megjelenéséig ne bocsássák nyilvánosságra az Egyetemi Könyvtárban, és az ELTE Digitális Intézményi Tudástárban csak a könyv bibliográfiai adatait tegyék közzé. Ha a könyv a fokozatszerzést követőn egy évig nem jelenik meg, hozzájárulok, hogy a doktori értekezésem és a tézisek nyilvánosságra kerüljenek az Egyetemi Könyvtárban és az ELTE Digitális Intézményi Tudástárban.

2. A doktori értekezés szerzőjeként kijelentem, hogy

a) az ELTE Digitális Intézményi Tudástárba feltöltendő doktori értekezés és a tézisek saját eredeti, önálló szellemi munkám és legjobb tudomásom szerint nem sértem vele senki szerzői jogait;

b) a doktori értekezés és a tézisek nyomtatott változatai és az elektronikus adathordozón benyújtott tartalmak (szöveg és ábrák) mindenben megegyeznek.

3. A doktori értekezés szerzőjeként hozzájárulok a doktori értekezés és a tézisek szövegének plágiumkereső adatbázisba helyezéséhez és plágiumellenőrző vizsgálatok lefuttatásához.

Kelt: Budapest, 2018.03.27.

……
a doktori értekezés szerzőjének aláírása

**ELTE SZMSZ SZMR 12. sz. melléklet*